

JOURNAL OF NEW ENERGY

An International Journal of New Energy Systems

Vol. 1, No. 4, 1996

Published by the
Fusion Information Center
P.O. Box 58639
Salt Lake City, Utah 84158-0639

A Quarterly Journal
Subscription: \$150 for 4 issues
Single issues: \$45



Winter 1996

ISSN 1092-0250

EDITORIAL COMMENTS

EWe welcome new authors to this issue of the *Journal of New Energy*. We also are pleased to invite others to present professional papers on new energy topics. Occasionally, we will publish a student paper on new energy topics. We recognize that today's students will be among those who will develop the energy systems of the next century.

There are many who, knowing that there will be new energy sources, wish to invest in new energy companies. We get several queries a month from persons who want to know where to invest in the coming energy revolution. These questions elicited a discussion with a friend who is a securities attorney. Here are some things to think about:

◆ Any securities to be offered for sale must first be registered with either the federal or state (or both) securities exchange agencies. These agencies were established to help protect unskilled investors from being bilked by irresponsible entrepreneurs. As with most government agencies, there has been an attempt to protect unskilled investors from being swindled by writing new regulations in response to the latest ingenious financial gimmicks by the dishonest promoter. The laws are not written to protect the wealthy (the term used is "accredited investors"). Accredited investors are exempted.

◆ The laws and regulations of both federal and state are now so numerous that it requires hiring an attorney skilled in securities law before one can offer a security for sale. The definition of a security is so broad that one presidential candidate was even jailed for borrowing money to finance his campaign. The end result is that we have essentially denied the right of a small investor to "get in on the ground floor" (defined as before the company has filed its securities with the appropriate federal and state agencies). Therefore, only the wealthy are left to take advantage of ground-floor investment opportunities. This is an excellent example of the laws that were intended to protect, end up prohibiting or penalizing the group to be protected.

◆ It has been suggested that we should form investment clubs. Previously, any corporation, including an investment club, was treated as a "sophisticated investor" and was exempt. The concept was that the laws were not provided to protect corporations. However, due to unethical promoters who took advantage of "investment clubs", the regulations have now been changed so that the members of the investment club or closely-held corporation must be "accredited investors" in order to be exempt from SEC regulations.

◆ There have been a number of suggestions for the formation of mutual fund corporations which would have a qualified expert to select appropriate new-energy stocks to purchase. Some of the requirements for a mutual fund are an initial investment by the founders of a minimum of \$100,000 and the mutual fund cannot own more than 5% of the stock of any one company. Many other regulations must be followed by the mutual fund company.

If you are a small investor and wish to invest in a new-energy company, it is suggested that you join with others and start your own company. The "others" should include a knowledgeable broker-dealer who will help get your company's shares sold and traded OTC (Over The Counter). Then file in your own state to raise up to one million dollars under the federal exemption from federal regulation (rule 504, I believe, but check with your securities attorney). Hire an excellent marketing manager and set up a company to sell and install new-energy systems. By the time you get your company set up and your stock sold, there should be some good new-energy products ready to market.

Happy New-Energy Year from the editor.

JOURNAL OF NEW ENERGY

Volume 1, Number 4

Page

- 1 **EDITORIAL** Hal Fox
- 5 **CHARACTERISTICS OF HIGH-DENSITY CHARGE CLUSTERS: A THEORETICAL MODEL**
Shang-Xian Jin and Hal Fox
- 21 **NUCLEAR TRANSMUTATION IN COLD FUSION EXPERIMENTS**
Hideo Kozima, Masahiro Nomura,, Katsuhiko Hiroe and Masayuki Ohta
- 26 **HYDROGEN REDISTRIBUTION BY CATASTROPHIC DESORPTION IN SELECT
TRANSITION METALS**
Mitchell R. Swartz
- 34 **EXCESS HEAT MEASUREMENT IN GAS-LOADING D/Pd SYSTEM**
Xing Zhong Li et al.
- 40 **NUCLEAR REACTION CAUSED BY ELECTROLYSIS IN LIGHT AND HEAVY WATER
SOLUTIONS**
Reiko Notoya, Toshiyuki Ohnishi and Yohichi Noya
- 44 **A NEW APPROACH TOWARDS FUSION ENERGY WITH NO STRONG NUCLEAR
RADIATION**
Xing Zhong Li
- 55 **CARBON PRODUCTION ON PALLADIUM POINT ELECTRODE WITH NEUTRON BURST
UNDER DC GLOW DISCHARGE IN PRESSURIZED DEUTERIUM GAS**
H. Yamada, H. Nonaka, A. Dohi, H. Hirahara, T. Fujiwara, X. Li and A. Chiba
- 59 **EXPERIMENTAL EVIDENCE FAVORING BRIGHTSEN'S NUCLEON CLUSTER MODEL**
Robert W. Bass
- 62 **ELECTRON CHARGE CLUSTER SPARKING IN AQUEOUS SOLUTIONS**
Atul Bhadkamkar and Hal Fox
- 69 **SOME FEATURES OF H₂O LOW-PRESSURE DISCHARGE IN PULSE MODE**
E.E. Antonov, V.G. Dresvyannikov, V.I. Popovich
- 76 **ANTI-GRAVITY IMPLIES INFINITE FREE ENERGY**
Robert Bass
- EDITOR'S CHOICE*
- 79 **EXPERIMENTS OF UNDERWATER SPARK DISCHARGES WITH PINCHED ELECTRODES**
Takaaki Matsumoto

- 93 AN ALTERNATIVE SOLAR ENERGY SOURCE**
David R. Criswell and Philip R. Harris (Originally appearing in *Earth Space Review*, vol 2, no 2, 1993)
- 98 IN SEARCH OF A WARP DRIVE**
Norman Silliman
- 105 LETTER TO THE EDITOR**
Letter from Wingate A. Lambertson, Ph.D.
 “Unemployment Gives One Time To Think”
Letter from Ernest Criddle
- 107 FUSION FACTS ABSTRACTS**
Abstracts from *Fusion Technology*, *Cold Fusion* and other sources

CHARACTERISTICS OF HIGH-DENSITY CHARGE CLUSTERS: A THEORETICAL MODEL

Shang-Xian Jin and Hal Fox

ABSTRACT

The self-confined equilibrium properties of a moving EV are investigated and a necessary condition or criteria for which the EV could exist is deduced by macroscopic electron plasma fluid description. We conclude that an EV is a toroidal electron vortex and could exist at various combinations of the electron density, the directional velocity, and the size of the EV in accordance with the derived criteria. The electromagnetic field strength, kinetic and electrostatic potential energy of the EV are also computed with respect to the stated assumptions. A close agreement with experimental data is presented.

A. INTRODUCTION

A highly organized, micron-sized cluster of electrons having soliton behavior, along with number densities equal to Avagadro's number, have been investigated by Kenneth Shoulders since 1980 [1,2,3]. A short Latin acronym has been adopted as suggested by Shoulders, and the collective plasma state of self-contained negatively charged bundle of electrons is called EV, for *strong electrons*.

An explosive electron emission has been shown to involve not individual electrons but electron bunches or avalanches, as also recently described by G.T. Mesyats [4]. The name of "ectons" was adopted by Mesyats to describe these charged particle avalanches. The important arguments for the existence of the entity (EV in the following paragraphs) are cathode craters, sharp oscillations of the explosive electron emission current density with period of 10^{-9} - 10^{-8} s, discontinuity of the glow in the cathode spots of the vacuum sparks and arc, etc. [4].

The EVs have been reported to be generally spherical with diameters on the order of 1.0 to 10 μm , but may be toric, to travel at speeds on the order of 0.1 c, to have electron densities approaching that of a solid, $\sim 6.6 \times 10^{29} \text{ m}^{-3}$, with the total number of electrons in a 1 μm diameter EV is $\sim 10^{11}$, and with negligible ion content of about one ion per 10^6 electrons. EVs tend to propagate in straight lines for distance of 1.0 to 100 mm and to exhibit a tendency to form other quasi-stable structures, such as linking up like beads in a necklace, etc. [2].

Ziolkowski and Tippett [5] examined theoretically the possibility of the existence of an essentially single-species plasma state represented by a stable packet of charged particles moving collectively through space-time. It is, however, not clear physically how the localized electromagnetic fields, excited by a very short initiation process, provide the mechanism which can overcome the Coulomb force and lead to the possible existence of the collective state represented by the "free"-electron cluster. Beckmann [6] studied the organizational properties of electron clusters theoretically based on the force of the oscillating Faraday field surrounding moving electrons. We know from the electrodynamics, however, that the electric field established by a moving point charge is composed of an electrostatic part (Coulomb field) and voltaic part (Faraday field). The voltaic part is produced by the acceleration of the charge. The two parts of the field will never be balanced with each other. In addition, the physical nature of the EV is collective and cannot be treated with single particle model.

We present here some preliminary estimations on some parameters of the EV as a self-contained, non-neutral plasma; on the electric and magnetic fields established by the EV; on the kinetic and potential energy; on the possible mechanism which overcomes the strong Coulomb force and leads to the existence of the electron cluster; and on the electromagnetic radiation from the EV.

B. ESTIMATIONS OF SOME OF THE PARAMETERS OF AN EV AS A SELF-CONTAINED ELECTRON PLASMA

Following K. Shoulders' data, we assume in the following treatment that the dimension of the EV is $d = 1.0 \mu m$, i.e. in the spherical model the radius is $r_0 = 0.5 \mu m$; the electron densities in the EV is $n = 6.6 \times 10^{29} m^{-3}$ [3]. In this case the total number of electrons in the spherical EV is

$$N_e = (4/3) \pi r_0^3 n = 3.5 \times 10^{11} \text{ per EV}, \quad (1)$$

the total charge is

$$q = N_e e = -5.6 \times 10^{-8} \text{ Coulomb per EV}, \quad (2)$$

and the mean electron distance is

$$a_e = 2(3/4 \pi n)^{1/3} = 1.4 \times 10^{-4} \mu m = 1.4 \text{ \AA}. \quad (3)$$

Meanwhile, we take the velocity of the EV, as $v = 0.1 c = 3 \times 10^7 m/sec$. This corresponds to the electron kinetic energy of $\sim 2.5 KeV$, or the EV-creating pulse voltage $\sim 2.5 KV$.

In this case the electron plasma frequency in the EV is

$$\omega_{pe} = (ne^2/\epsilon_0 m_e)^{1/2} = 56.4 n^{1/2} = 4.6 \times 10^{16} \text{ rad/sec.}, \quad (4)$$

where m_e is electron mass and ϵ_0 is permittivity of free space. The ω_{pe} is a measure of space-charge force (or defocusing) in the electron plasma. The characteristic time scale of any change in the EV, therefore, is $1/\omega_{pe} \sim 10^{-17} s$.

The electron gyrofrequency on the surface of the EV in the magnetic field (see section C) established by the moving EV is

$$\omega_{ce} = eB/m_e = 1.76 \times 10^{11} B \text{ rad/sec} \sim 1.2 \times 10^{17} \text{ rad/sec}. \quad (5)$$

In the self-confinement of an electron cluster, the ω_{ce} is a measure of the self-focusing magnetic force on an electron fluid element.

The electron gyroradius is

$$\rho_e = v/\omega_{ce} = 2.38 \times 10^6 T^{1/2} (eV) B^{-1} m, \quad (6)$$

where T_e is the electron temperature. We assume two temperatures: $T_e = 10 eV$ and $T_e = 2.5 KeV$. The $T_e = 10 eV$ is initial temperature at which the EVs are formed, and possibly the temperature does not change much during the life time of the EV. The $T_e = 2.5 KeV$ is an assumed final temperatures in which we suppose that the thermal equilibrium in the EV is reached instantaneously with the increase of the directional kinetic energy of the electrons. Substituting both values for T_e in Eq. (6), we have

$$\begin{aligned} \rho_e &= 1.1 \times 10^{-5} \mu m & (T_e = 10 eV), \\ &= 1.7 \times 10^{-4} \mu m & (T_e = 2.5 KeV). \end{aligned} \quad (6a)$$

The electron *DeBroglie length* in the EV is

$$\lambda = \hbar/m_e k_B T_e^{-1/2} = 2.76 \times 10^{-10} T_e^{-1/2} (eV) m, \quad (7)$$

where \hbar is Planck constant ($h/2\pi$), k_B is Boltzman constant. Substituting the T_e to Eq. (7) and comparing the resultant λ with the mean electron distance in the EV, we have

$$\begin{aligned} \lambda &= 0.87 \text{ \AA} \leq a_e & (T_e = 10 \text{ eV}), \\ &= 5.5 \times 10^{-2} \text{ \AA} \ll a_e & (T_e = 2.5 \text{ KeV}). \end{aligned} \quad (7a)$$

This means that the quantum effect needs to be considered in the low temperature situation, but at higher temperatures ($T_e > 100 \text{ eV}$) the quantum effect can be neglected.

The thermal kinetic pressure corresponding to these temperatures in the EV are respectively

$$\begin{aligned} p_e &= nk_B T_e = 1.0 \times 10^{12} \text{ Pascal} = 1.0 \times 10^7 \text{ atm pressure}, & (T_e = 10 \text{ eV}), \\ &= 2.6 \times 10^{14} \text{ Pascal} = 2.6 \times 10^9 \text{ atm pressure}, & (T_e = 2.5 \text{ KeV}). \end{aligned} \quad (8)$$

The electron collision rate [7] in the EV may be estimated by

$$\nu_e = \frac{ne^4 \ln \Lambda}{16 \sqrt{\pi} \epsilon_0^2 m_e^{1/2} T^{3/2}} = 2.91 \times 10^{-12} n \ln \Lambda T_e^{-3/2} (eV) \text{ sec}^{-1}. \quad (9)$$

Here we assumed the electron velocity distribution in the EV is Maxwellian, and $\ln \Lambda$ is the Coulomb logarithm. Substituting the n and T_e and comparing the ν_e with the electron plasma frequency ω_{pe} , we have

$$\begin{aligned} \nu_e &= 1.2 \times 10^{18} / \text{Sec} \gg \omega_{pe} & (T_e = 10 \text{ eV}), \\ &= 3.1 \times 10^{14} / \text{Sec} \ll \omega_{pe} & (T_e = 2.5 \text{ KeV}), \end{aligned} \quad (10)$$

where we assumed $\ln \Lambda = 20$. This means that at the $T_e = 10 \text{ eV}$ the electron plasma in the EV is collision dominant, but at $T_e = 2.5 \text{ KeV}$ it behaves like a collisionless plasma.

The energy relaxation time of the electron in the EV, the $\tau_e^{(E)}$, may be roughly approximated by $1/\nu_e$:

$$\tau_e^{(E)} \sim 1/\nu_e. \quad (11)$$

Then from Eq. (9) we have

$$\begin{aligned} \tau_e^{(E)} &\sim 8.2 \times 10^{-19} \text{ sec} & (T_e = 10 \text{ eV}), \\ &\sim 3.2 \times 10^{-15} \text{ sec} & (T_e = 2.5 \text{ KeV}), \end{aligned}$$

i.e., both values are far less than the life time of the EV (on the order of a nanosecond, 10^9 sec). This means the kinetic energy attained by the electron in the EV from the external field will be quickly thermalized and the electron plasma in the EV can be seen as near Maxwellian.

The coupling parameter Γ of a plasma defined by the ratio of nearest-neighbor Coulomb energy ($e^2/4\pi\epsilon_0 a$) to the characteristic thermal energy of a particle ($k_B T_e$) is

$$\Gamma \equiv \frac{e^2}{4\pi\epsilon_0 k_B T_e a_e} = 1.86 \times 10^{-9} n^{1/3} T_e^{-1} (eV). \quad (12)$$

For the EV we have

$$\begin{aligned} \Gamma &\sim 1.5 && (T_e = 10 eV), \\ &\sim 6 \times 10^{-3} \ll 1 && (T_e = 2.5 KeV), \end{aligned} \quad (13)$$

i.e., at $T_e = 10 eV$ the electron plasma in the EV is strongly coupled and at $T_e = 2.5 KeV$ it is weakly coupled.

In brief, we see that with $T_e = 10 eV$ the electron plasma in the EV is a strongly coupled, collision-dominant quantum plasma, and with $T_e = 2.5 KeV$ it is a weakly coupled collisionless classical plasma.

In the following we regard the EV as a weakly coupled collisionless classical plasma and treat the EV using classical electrodynamics and plasma fluid descriptions.

C. THE ELECTRIC AND MAGNETIC FIELDS

We consider a spherical model of the EV. In view of the spherical symmetry, in this case the electromagnetic fields of the EV can be approximated by a moving point charge model. From the well-known general equations of the fields established by a moving point charge [8], the electric and magnetic field of the moving EV may be expressed by

$$\mathbf{E} = \frac{q}{4\pi\epsilon_0 r_0^3} \left[r \mathbf{e}_r + \frac{3}{c} r ((\mathbf{v} \cdot \mathbf{e}_r) \mathbf{e}_r - \mathbf{v}) + \frac{r^2}{c^2} \mathbf{e}_r \times (\mathbf{e}_r \times \dot{\mathbf{v}}) \right], \quad (r < r_0) \quad (14)$$

$$\mathbf{B} = \frac{q}{4\pi\epsilon_0 r_0^3} \left[\frac{r}{c^2} \mathbf{v} \times \mathbf{e}_r + \frac{r^2}{c^3} \dot{\mathbf{v}} \times \mathbf{e}_r \right], \quad (r < r_0) \quad (15)$$

and

$$\mathbf{E} = \frac{q}{4\pi\epsilon_0} \left[\frac{\mathbf{e}_r}{r^2} + \frac{3(\mathbf{v} \cdot \mathbf{e}_r) \mathbf{e}_r - \mathbf{v}}{c r^2} + \frac{\mathbf{e}_r \times (\mathbf{e}_r \times \dot{\mathbf{v}})}{c^2 r} \right], \quad (r > r_0) \quad (16)$$

$$\mathbf{B} = \frac{q}{4\pi\epsilon_0} \left[\frac{\mathbf{v} \times \mathbf{e}_r}{c^2 r^2} + \frac{\dot{\mathbf{v}} \times \mathbf{e}_r}{c^3 r} \right], \quad (r > r_0), \quad (17)$$

where $r^2 = x^2 + y^2 + z^2$, $\mathbf{e}_r = \mathbf{r}/|\mathbf{r}|$ is unit vector, r_0 is the radius of the spherical EV, $\dot{\mathbf{v}} = \partial \mathbf{v} / \partial t$ is the acceleration, and uniform electron charge distribution in the EV is assumed. We see clearly that the electric fields are composed of both electrostatic and voltaic parts, and usually the latter is much smaller than former.

For simplicity, we assume the EV moves along the straight line, axis Z-direction, then the above equations can be reduced to

$$\mathbf{E} = \frac{q}{4\pi\epsilon_0 r_0^3} \left[\left(\left(1 + \frac{3v}{c} \cos \theta \right) r + \frac{\dot{v} r^2}{c^2} \cos \theta \right) \mathbf{e}_r - \left(\frac{3v}{c} r + \frac{\dot{v}}{c^2} r^2 \right) \mathbf{e}_z \right], \quad (r < r_0) \quad (18)$$

$$\mathbf{B} = \frac{q v r}{4\pi\epsilon_0 c^2 r_0^3} \left[1 + \frac{\dot{v}}{c v} r \right] \sin \theta \mathbf{e}_z \times \mathbf{e}_r, \quad (r < r_0) \quad (19)$$

$$\mathbf{E} = \frac{q}{4\pi\epsilon_0 r^2} \left[\left(1 + \frac{3v}{c} \cos\theta + \frac{\dot{v}r}{c^2} \cos\theta\right) \mathbf{e}_r - \left(\frac{3v}{c} + \frac{\dot{v}r}{c^2}\right) \mathbf{e}_z \right], \quad (r > r_0) \quad (20)$$

$$\mathbf{B} = \frac{qv}{4\pi\epsilon_0 c^2 r^2} \left[1 + \frac{\dot{v}r}{cV} \right] \sin\theta \mathbf{e}_z \times \mathbf{e}_r, \quad (r > r_0) \quad (21)$$

where θ is the angle between r and Z -axis (in the direction of v).

As a typical case, we now assume that the distance between an EV launcher and the target is $l = 10.0$ mm and the applied pulse voltage is $V = 2.5$ KV. Then the acceleration of the EV is

$$\dot{v} = eV/m_e l = 4.4 \times 10^{16} \text{ m/sec}^2. \quad (22)$$

In this case we have $\dot{v}r/c^2 \sim \dot{v}r/cv \lesssim 10^{-7} \ll 1$ in the near surface and inside of the EV, i.e. the effect of acceleration on the \mathbf{E} and \mathbf{B} fields are negligible and Eqs. (18) - (21) can be reduced to

$$\mathbf{E} = \frac{qr}{4\pi\epsilon_0 r_0^3} \left[\left(1 + \frac{3v}{c} \cos\theta\right) \mathbf{e}_r - \frac{3v}{c} \mathbf{e}_z \right], \quad (r < r_0) \quad (23)$$

$$\mathbf{B} = \frac{qvr}{4\pi\epsilon_0 c^2 r_0^3} \sin\theta \mathbf{e}_z \times \mathbf{e}_r, \quad (r < r_0) \quad (24)$$

and

$$\mathbf{E} = \frac{q}{4\pi\epsilon_0 r^2} \left[\left(1 + \frac{3v}{c} \cos\theta\right) \mathbf{e}_r - \frac{3v}{c} \mathbf{e}_z \right], \quad (r > r_0) \quad (25)$$

$$\mathbf{B} = \frac{qv}{4\pi\epsilon_0 c^2 r^2} \sin\theta \mathbf{e}_z \times \mathbf{e}_r, \quad (r > r_0). \quad (26)$$

The fields on the surface of the EV are given by

$$\mathbf{E} = \frac{q}{4\pi\epsilon_0 r_0^2} \left[\left(1 + \frac{3v}{c} \cos\theta\right) \mathbf{e}_r - \frac{3v}{c} \mathbf{e}_z \right], \quad (27)$$

$$\mathbf{B} = \frac{qv}{4\pi\epsilon_0 c^2 r_0^2} \sin\theta \mathbf{e}_z \times \mathbf{e}_r. \quad (28)$$

Substituting $r_0 = 0.5 \mu\text{m}$, $v = 0.1 c$, and Eq. (2) for q we have

$$\mathbf{E} = -2.0 \times 10^{15} \left[\left(1 + 0.3 \cos\theta\right) \mathbf{e}_r - \frac{3v}{c} \mathbf{e}_z \right] \text{ V/m}, \quad (r = r_0) \quad (29)$$

$$\mathbf{B} = 6.7 \times 10^5 \sin\theta \mathbf{e}_r \times \mathbf{e}_z \text{ Tesla}. \quad (r = r_0) \quad (30)$$

We see that the local fields established by the EV are very strong and beyond any present laboratory upper limit. The magnetic field ($\sim 10^6$ Tesla) of the EV exceeds the highest laboratory field ($\sim 10^4$ Tesla) produced by

explosive techniques and approaches the field strength on the surface of some neutron star ($\sim 10^7 - 10^8$ Tesla). The super strong electric fields on the EV will ionize any materials on its path.

D. KINETIC ENERGY

The kinetic energy of an electron EV is

$$W_{EV} = N_e eV = 8.8 \times 10^{14} eV = 1.4 \times 10^4 J, \quad (31)$$

where the applied voltage $V = 2.5$ KV is assumed.

For a nuclear EV (capable of causing a nuclear reaction) where the ion number $N_i \sim 10^{-6} N_e$, the kinetic energy is almost the same as the electron EV without positive ions:

$$W_{NEV} = (N_e + Z N_i) eV \approx N_e eV = W_{EV}, \quad N_i/N_e \sim 10^{-6} \ll 1, \quad (32)$$

where Z is atomic number of the ion. The ions in the EV will be attracted or drawn by the overwhelming majority of electrons in the EV and attain the same velocity as electrons. The kinetic energy attained by the ion in the EV then is

$$W_{EV}^{(i)} = \frac{1}{2} M_i v_e^2 = \frac{M_i}{m_e} \left(\frac{1}{2} m_e v_e^2 \right) = \frac{M_i}{m_e} eV \quad (33)$$

where m_e , M_i is the mass of electron and the ion, v_e is the electron velocity attained due to the applied voltage V . The energy attained by a single ion using the same voltage is

$$W^{(i)} = Z eV \quad (34)$$

Comparing Eqs. (33) and (34) we have

$$W_{EV}^{(i)}/W^{(i)} = \frac{M_i}{Z m_e} = \frac{m_p M_i}{Z m_e m_p} = 1836 \frac{A}{Z} \quad (35)$$

where A is atomic weight of the ion and m_p is proton mass.

This means the EV could act as a relatively simple mini-accelerator for accelerating positive ions. For example, in the $V = 2.5$ KV applied voltage, a proton (deuteron) will attain 2.5 KeV energy. However, the proton (deuteron) in the EV could get 4.6 MeV (9.2 MeV)! This kinetic energy imparted to the positive ions is now sufficient to overcome the Coulomb barrier of the nucleus and produce nuclear reactions. When a large number of EVs are produced and strike a target, the nuclear reactions rate can be quite high. Shoulders et al. [3] and Hal Fox et al. [9] have proposed this nuclear acceleration mechanism as a possible explanation of the anomalous nuclear transmutation phenomena [10, 11, 12].

E. ELECTROSTATIC POTENTIAL ENERGY

How much energy is required to produce an electron cluster - EV? Also, what is the electrostatic potential energy of the EV? We consider a spherical EV with uniform electron density n . From Eqs. (23), (25) the electrostatic field established by the EV is

$$\mathbf{E} = \frac{qr}{4\pi\epsilon_0 r^3} \mathbf{e}_r = \frac{n e r}{3\epsilon_0} \mathbf{e}_r, \quad (r < r_0) \quad (36a)$$

$$= \frac{q}{4\pi\epsilon_0 r^2} \mathbf{e}_r = \frac{n e r_0^3}{3\epsilon_0 r^2} \mathbf{e}_r, \quad (r > r_0). \quad (36b)$$

The potential is

$$V = -\int_{\infty}^r \mathbf{E} \cdot d\mathbf{r} = \frac{n e r_0^2}{2\epsilon_0} - \frac{n e r^2}{6\epsilon_0}, \quad (r < r_0) \quad (37a)$$

$$= \frac{n e r_0^3}{3\epsilon_0 r}, \quad (r > r_0). \quad (37b)$$

Thus the potential difference from center to surface of the EV is

$$\Delta V = V(r=0) - V(r=r_0) = \frac{n e r_0^2}{6\epsilon_0} = -5.0 \times 10^8 \text{ V} \quad (38)$$

with $r_0 = 0.5 \mu\text{m}$ and $n = 6.6 \times 10^{29} / \text{m}^3$.

The electrostatic potential energy is

$$\begin{aligned} W_{ES} &= \frac{1}{2} \iiint \rho V d\tau = \frac{1}{2} \int_0^{2\pi} \int_0^{\pi} \int_0^{r_0} n^2 e^2 \left(\frac{r_0^2}{2\epsilon_0} - \frac{r^2}{6\epsilon_0} \right) r^2 \sin\theta dr d\theta d\phi \\ &= \frac{4\pi n^2 e^2 r_0^5}{15\epsilon_0} = \frac{3q^2}{20\pi\epsilon_0 r_0}. \end{aligned} \quad (39)$$

Substituting the given data of r_0 and n to Eq. (39), we have

$$W_{ES} = 33.0 \text{ J} = 2.1 \times 10^{14} \text{ MeV}.$$

Or the corresponding potential energy density is

$$w_{ES} = W_{ES} / \frac{4\pi}{3} \pi r_0^3 = \frac{9q^2}{80\pi^2 \epsilon_0 r_0^4} = 6.4 \times 10^{19} \text{ J/m}^3. \quad (40)$$

This is an incredible, unimaginable energy combination. If the EV were “blasted” and this potential energy were completely transformed to kinetic energy, then each electron in the EV would have

$$W_e = W_{ES} / N_e = n e^2 r_0^2 / 5 \epsilon_0 = 9.6 \times 10^{-11} \text{ J} = 6.0 \times 10^2 \text{ MeV} \quad (41)$$

which corresponding to electron temperature $\sim 10^{12} \text{ K}$. That would be $\sim 10^2$ to 10^3 times higher than the temperature in the core of the hydrogen bomb explosion, a supernova explosion or in a “white dwarf.”

For a nuclear EV in which $N_i/N_e \sim 10^6$, the electrostatic potential energy is almost the same as the expression Eq. (39) (assuming ion distribution in the EV is uniform). If the nuclear EV were “blasted” (such as blasting a target anode), each electron would have almost the same amount of energy, as shown by Eq. (41), and each ion would have

$$W_i = M_i v_e^2 / 2 = M_i W_e / m_e = 1836 A W_e = 1.1 \times 10^6 A \text{ MeV} \quad (42)$$

where A is the atomic weight of positive ions and assuming the ions would be carried or drawn by the expanding electrons. Even if the EV with 1 μm diameter expands to only a 10% increase in diameter of the EV (on impacting the target), according to Eq. (39) about 9% of the potential energy will transform to kinetic energy of the electrons and ions, and each ion would receive an average kinetic energy of $W_i \sim 10^5 A \text{ MeV}$. This may be the main source of the nuclear effects of the EV.

The electrostatic expansion force in the EV, from Eq. (39), could be estimated by

$$f_{ES} = -\frac{\partial W_{ES}}{\partial r} = \frac{3q^2}{20\pi\epsilon_0 r^2}, \quad (43)$$

and the expansion pressure on the surface is

$$P_{ES} = f_{ES} / 4\pi r_0^2 = \frac{3q^2}{80\pi^2\epsilon_0 r_0^4} = \frac{n^2 e^2 r_0^2}{15\epsilon_0} \quad (44)$$

$$= 2.1 \times 10^{19} \text{ pascal} = 2.0 \times 10^{14} \text{ atm pressure.}$$

This is higher than any known pressure created in scientific laboratories.

We see from above that, in some respect, the EV can be seen as a mini super-projectile. When it arrives at a target, it will be exploded, and produce nuclear reactions (nuclear EV case), and release a large amount of potential energy to the target.

F. IS EV SPHERICAL OR TOROIDAL?

How can the super strong electric repulsive force in the EV be balanced by another force? And which model is the most likely to explain this phenomena, the spherical or the toroidal model?

To solve the problem, we begin with the non-neutral plasma macroscopic fluid equations [13]:

the *continuity equation*

$$\frac{\partial}{\partial t} n + \nabla \cdot (n \mathbf{u}) = 0 \quad (45)$$

and the *momentum equation* (or force balance equation)

$$n \left(\frac{\partial}{\partial t} + \mathbf{u} \cdot \nabla \right) \mathbf{p} = -\nabla \cdot \hat{\mathbf{P}} + n e (\mathbf{E} + \mathbf{u} \times \mathbf{B}), \quad (46)$$

where n is electron density, \mathbf{u} electron fluid velocity, \mathbf{p} mean momentum, and $\hat{\mathbf{P}}$ thermal pressure tensor. The Eqs. (44) and (45) are to be supplemented by *Maxwell's equations* for the self-consistent evolution of \mathbf{E} and \mathbf{B} .

$$\nabla \cdot \mathbf{E} = \frac{n e}{\epsilon_0}, \quad \nabla \times \mathbf{E} = - \frac{\partial \mathbf{B}}{\partial t}, \quad (47a)$$

$$\nabla \times \mathbf{B} = \mu_0 e n \mathbf{u} + \frac{1}{c^2} \frac{\partial \mathbf{E}}{\partial t}, \quad \nabla \cdot \mathbf{B} = 0. \quad (47b)$$

We are mainly interested in the possibility of the existence of collective state of the electron cluster. For this task we need an equilibrium solution to the Eqs. (45) - (47). Carrying out an equilibrium analysis of the equations by setting $\partial/\partial t = 0$, we have

$$\nabla \cdot (n_0 \mathbf{u}_0) = 0, \quad (48)$$

$$(\mathbf{u}_0 \cdot \nabla) \mathbf{p}_0 = n_0 e (\mathbf{E}_0 + \mathbf{u}_0 \times \mathbf{B}_0), \quad (49)$$

and

$$\nabla \cdot \mathbf{E}_0 = \frac{n_0 e}{\epsilon_0}, \quad \nabla \times \mathbf{E}_0 = 0, \quad (50a)$$

$$\nabla \times \mathbf{B}_0 = \mu_0 e n_0 \mathbf{u}_0, \quad \nabla \cdot \mathbf{B}_0 = 0, \quad (50b)$$

where $n_0 = n_0(\mathbf{r})$, $\mathbf{u}_0 = \mathbf{u}_0(\mathbf{r})$, $\mathbf{p}_0 = \mathbf{p}_0(\mathbf{r})$, $\mathbf{E}_0 = \mathbf{E}_0(\mathbf{r})$, and $\mathbf{B}_0 = \mathbf{B}_0(\mathbf{r})$ are the macroscopic equilibrium quantities. Notice that we dropped the thermal pressure-gradient term $\nabla \cdot \hat{\mathbf{p}}$ in the force balance equation (46). The reason is that the thermal kinetic pressure (Eq. 8) is negligibly smaller than the electrostatic pressure (Eq. (44)) in the EV. With the equilibrium equations (48) - (50), we now consider the possibilities of equilibrium in the spherical and toroidal model of the EV respectively. For simplicity, we will drop the subscript "0" on the equilibrium quantities in the following equations.

First consider the spherical model of the EV. We can reasonably assume that the fields \mathbf{E} and \mathbf{B} in the equilibrium equations are given by Eqs. (23) and (24), and the term $(\mathbf{u} \cdot \nabla) \mathbf{p}$ (a centrifugal force) in Eq. (49) is negligible compared with electric force $ne\mathbf{E}$. In this case, Eq. (49) becomes

$$n e (\mathbf{E} + \mathbf{u} \times \mathbf{B}) = 0. \quad (51)$$

This equation means that the electric repulsive force in the EV is balanced by the magnetic force which is caused by the perpendicular (to magnetic field \mathbf{B}) motion

$$\mathbf{u}_\perp = (\mathbf{E} \times \mathbf{B}) / B^2 \quad (52)$$

and the parallel motion $\mathbf{u}_\parallel = \mathbf{E} \cdot \mathbf{B} / B^2$ of the electron fluid, corresponding to the currents $\mathbf{j}_\perp = ne\mathbf{u}_\perp$ and $\mathbf{j}_\parallel = ne\mathbf{u}_\parallel$ respectively. Notice that the perpendicular motion \mathbf{u}_\perp of Eq. (52) is just the $\mathbf{E} \times \mathbf{B}$ drift velocity of the electron (Fig 1). This result is reasonable. For the EV electron plasma, we have from Eqs. (12), (13), (23), and (24) that

$$|\rho_e \frac{\partial B}{\partial r}| \sim 3\rho_e \frac{B}{r_0} \sim 10^{-3} B < B \quad \text{and} \quad |\frac{1}{\omega_c} \frac{\partial B}{\partial t}| \sim \dot{v} B / \omega_{ce} v \sim 10^{-9} B < B.$$

This means that the electron motion in the EV may be approximated by electron guiding center motion. The physical mechanism is also clear. We know that the expansion force caused by the thermal pressure of a plasma in a magnetic field \mathbf{B} can be balanced by the magnetic force caused by the diamagnetic drift motion of the plasma fluid element, $\mathbf{u} = -\nabla p \times \mathbf{B} / B^2$ ($p = nkT$), which results from the gyromotion of the plasma particle around the magnetic field, as shown in Fig. 1, and the density and/or temperature gradient. In the EV case, the radial electrostatic repulsive force is balanced by the magnetic force caused by the $\mathbf{E} \times \mathbf{B} / B^2$ drift motion of the electron fluid element.

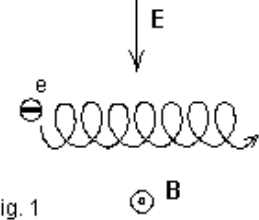


Fig. 1

The electron motion in the crossed electric and magnetic fields. The electron gyrate about the magnetic field lines, accompanied by a drift. The drift velocity is $\mathbf{v} = \mathbf{E} \times \mathbf{B} / B^2$.

We know from Eq. (24) that the magnetic field in the spherical EV is around the axis Z, i.e. around the sphere. The parallel motion of the electron fluid does not change the shape of the EV sphere. However, the perpendicular motion will tend to change the shape of the sphere. Substituting Eqs. (23) and (24) to (52), we have

$$\mathbf{u}_\perp = \frac{c^2}{v \sin \theta} \left[\left(\frac{3v}{c} \sin^2 \theta - \cos \theta \right) \mathbf{e}_r + \mathbf{e}_z \right]. \quad (53)$$

We see that the \mathbf{u}_\perp varies with angle θ , but not along the circle. This process will instantaneously (in about 10^{-16} s) lead to deformation of the spherical cluster to an oblate spheroid and the most likely result will be that the sphere will evolve to a toroidal shape. We will see in the following paragraphs that in the toroidal configuration the electron cluster and electromagnetic field will self-consistently be confined each other and there is no possibility to deform to any other shape which has better equilibrium properties. However, the toroid may disrupt to smaller toroidal groups or become self-destroyed by various instabilities.

Now we consider a toroidal model of the EV. We assume the EV is a toroidal electron plasma loop with minor radius a and major radius R_0 confined by a toroidal magnetic field \mathbf{B}_0 (see Fig. 2). In the EV the toroidal field actually is established by the moving electron cluster itself. We assume that the diameter of the toroidal EV, the $2R$, is the same value as the diameter of the spherical EV, i.e. $2R = 2r_0 = d = 1\mu\text{m}$. In this case, the toroidal magnetic field \mathbf{B}_0 can be roughly approximated by the magnetic field of the spherical EV, Eq. (28), averaging over the surface of the spherical EV, i.e.

$$|\mathbf{B}_0| = \frac{qv}{4\pi\epsilon_0 c^2 r_0^2} \frac{1}{\pi} \int_0^\pi \sin \theta d\theta = \frac{qv}{2\pi^2 \epsilon_0 c^2 r_0^2} = \frac{2n\theta r_0 v}{3\pi\epsilon_0 c^2} = \frac{2n\theta Rv}{3\pi\epsilon_0 c^2} = 4.2 \times 10^5 \text{T} \quad (54)$$

where $R = R_0 + a$.

As an approximation, the toroidal electron loop can be simplified by treating it as an infinitely long ($2\pi R_0 \gg 2\pi a$) cylindrical column of electrons. We further assume that the \mathbf{B}_0 is uniform along the axis of the column. We now select a cylindrical coordinate consistent with the column and assume all of the equilibrium parameters in the steady state ($\partial/\partial t = 0$) are axi-symmetric and uniform in the Z-direction, i.e. $n(\mathbf{r}) = n(r) \mathbf{e}_r$, $\mathbf{u}(\mathbf{r}) = u_\theta(r) \mathbf{e}_\theta + u_z(r) \mathbf{e}_z$ and $\partial n/\partial z = \partial u/\partial z = 0$. The azimuthal current $\mathbf{J}_\theta(r) = neu_\theta(r) \mathbf{e}_\theta$ generally induces an axial self-magnetic field $B_\lambda(r)$ and the axial current $\mathbf{J}_z(r) = neu_z(r) \mathbf{e}_z$ generally induces azimuthal self-magnetic field $B_\theta(r)$. Thus the total magnetic field is $\mathbf{B}(r) = B_\theta(r) \mathbf{e}_\theta + (B_0 + B_\lambda(r)) \mathbf{e}_z$.

The equilibrium equation (49) now becomes a radial force balance equation

$$-\frac{\beta m_e u_\theta^2}{r} = e [E_r + u_z B_\theta + u_\theta (B_0 + B_z)], \quad (55)$$

where $\beta(r) = (1 - u^2(r)/c^2)^{-1/2}$ and the self-generated fields E_r , B_θ , and B_z are determined from the Maxwell equations

$$\frac{1}{r} \frac{\partial}{\partial r} (r E_r(r)) = \frac{e}{\epsilon_0} n(r), \quad (56a)$$

$$\frac{1}{r} \frac{\partial}{\partial r} (r B_\theta(r)) = \mu_0 e n(r) u_z(r), \quad (56b)$$

$$\frac{\partial}{\partial r} B_z(r) = -\mu_0 e n(r) u_\theta(r). \quad (56c)$$

The solutions of the Maxwell Eq. (56) are

$$E(r) = \frac{e}{\epsilon_0 r} \int_0^r n(r) r dr, \quad (57a)$$

$$B_\theta(r) = \frac{\mu_0 e}{r} \int_0^r n(r) u_z(r) r dr, \quad (57b)$$

$$B_z(r) = -\mu_0 e \int_r^\infty n(r) u_\theta(r) dr. \quad (57c)$$

Substituting Eqs. (57) to (55), we have [13]

$$\beta(r) \omega_{re}^2(r) = \omega_{ce} \omega_{re}(r) \left(1 + \frac{\mu_0 e}{B_0} \int_r^\infty n(r) r \omega_{re}(r) dr \right) + \frac{e^2}{\epsilon_0 m_e r^2} \int_0^r n(r) \left(1 - \frac{u_z^2(r)}{c^2} \right) r dr \quad (58)$$

where $\omega_{re}(r)$ is the equilibrium angular velocity of an electron fluid element

$$\omega_{re}(r) = u_\theta(r) / r \quad (59)$$

and $\omega_{ce} = eB/m_e$ is the non-relativistic cyclotron frequency (Eq. (12)). We see that the rotation of the electron plasma is a fundamental characteristics for self-confinement of the EV.

The physical meaning of the force balance equation (55) is obvious. The term on the left side of the Eq. (55), $\beta m_e u_\theta^2/r$, is a centrifugal force. Thus, Eq. (55) means that the ombined electrostatic and centrifugal forces on an electron fluid element are balanced by the inward magnetic force. The magnetic force is caused by the diamagnetic drift motion of the electron fluid element, $\mathbf{E} \times \mathbf{B}/B^2$ drift and $m_e u_\theta^2/r \mathbf{e}_r \times \mathbf{B}/B^2$ drift, i.e. the rotation of the electron fluid around the symmetric axis. Therefore, for a moving toroidal electron cluster, a self-consistent equilibrium is possible, thus, the toroidal EV can exist.

Ken Shoulders [14] has for several years been aware of the probable toroidal nature of high-density electron clusters and has explicitly dealt with the likely nature of their formation.

We consider a simplified case: a non-relativistic electron plasma column with uniform density profile and $u^2/c^2 \ll 1$, $u_z B_0 \ll E_r$ and $B_z \ll B_0$. In this situation the radial force balance equation (58) reduces to

$$\omega_{re}^2 - \omega_{ce} \omega_{re} + \frac{1}{2} \omega_{pe}^2 = 0. \quad (60)$$

Solving the Eq. (60) for ω_{re} gives two equilibrium rotational velocities of the electron column

$$\omega_{re} = \omega_{re}^{\pm} \equiv \frac{1}{2} \omega_{ce} \left[1 \pm \left(1 - \frac{2 \omega_{pe}^2}{\omega_{ce}^2} \right)^{1/2} \right] \quad (61)$$

where ω_{re}^+ (ω_{re}^-) corresponds to a fast (slow) rotation of the electron fluid. In the uniform density profile the rotational velocity ω_{re}^+ or ω_{re}^- are constant, i.e. the electron fluid will make a rigid rotation around the symmetric axis. Using Eq. (54) we have $\omega_{ce} = eB_0/m_e = 7.4 \times 10^{16}$ rad/sec. Substituting the ω_{ce} and Eq. (4) for ω_{pe} to the Eq. (61) gives $2\omega_{pe}^2/\omega_{ce}^2 = 0.77$, $\omega_{re}^+ = 0.74 \omega_{ce} = 5.5 \times 10^{16}$ rad/sec and $\omega_{re}^- = 0.26 \omega_{ce} = 1.9 \times 10^{16}$ rad/sec. (With relativistic treatment, we will have $\omega_{re}^{\pm} \sim 10^{13}$ rad/sec.) These are super high speed rotations.

We note especially from Eq. (61) that when $2\omega_{pe}^2/\omega_{ce}^2 > 1$, the rotation velocity ω_{re} becomes imaginary, that is the radial equilibrium does not exist. This means a necessary condition for existence of equilibrium EV is

$$2\omega_{pe}^2/\omega_{ce}^2 = 2 n m_e / \epsilon_0 B_0^2 \leq 1 \quad (62a)$$

or

$$B_0 \geq (2 n m_e / \epsilon_0)^{1/2} \quad (62b)$$

Substituting Eq. (54) for B_0 to the Eq. (62b) will give **radial equilibrium criteria** or **EV criteria**:

$$\begin{aligned} nd^2 v^2 &\geq 18 \pi^2 c^2 m_e / \mu_0 e^2 \\ &\geq 4.5 \times 10^{32} \text{ meter/sec}^2 \end{aligned} \quad (63a)$$

or

$$\begin{aligned} nWd^2 &\geq 9 \pi^2 c^2 m_e^2 / \mu_0 e^2 \\ &\geq 2.1 \times 10^{21} \text{ meter/sec}^2, \end{aligned} \quad (63b)$$

where $d = 2R$ is the dimension of the EV, v is directional velocity and W is the corresponding kinetic energy (in units of eV) of the EV electron.

This criteria tells us that the electron density n , directional velocity v (or kinetic energy W) and the size of the EV, the d , are related to each other in comprising a equilibrium EV. Or in other words, the EV could exist at various combinations of n , v (or W) and d in accordance with this criteria.

As a test for the criteria, let's examine K. Shoulders' EV data [2]. With $n = 6.6 \times 10^{29} \text{ m}^{-3}$ and $v = 0.1 c = 3 \times 10^7 \text{ m/sec}$, the criteria (63) gives $d \geq 0.87 \mu\text{m}$. This is close to the size range that Shoulders measured. Therefore, agreement between this theory and experimental data is excellent.

According to the criteria, let's estimate the EV size at low directional energy, $W = (10 \text{ to } 100) \text{ eV}$ situation. If we assume the electron density is still $n = 6.6 \times 10^{29} \text{ m}^{-3}$, then the criteria (63) gives $d \geq (13 \text{ to } 4) \mu\text{m}$,

corresponding to electron number (5.9×10^{13} to 5.6×10^{12}) in the EV. That is, equilibrium in larger dimension EVs is possible, as long as the EV is formed and launched. However, some of the EVs could be broken up into smaller ones through instabilities. In the double layer, near surface and crack regions of a hydrated metal cathode, a number of large EVs could be produced and may have an important role in nuclear transmutation. A large EV may contain or transport a larger number of positive nuclear ions and thereby the nuclear reactions rate may be increased.

At low electron density, for example $n \sim 3 \times 10^{25} \text{ m}^{-3}$ (\sim air density), and the directional energy on the order of room temperature energy, $W \sim 0.025 \text{ eV}$, the criteria gives $d \geq 5 \text{ cm}$. This is the size range of ball-lightning. The ball-lightning may be a huge EV.

Now we consider a more general case where density $n(r)$ is not uniform. In this case the Eq. (54) reduces to

$$\omega_{re}^2 - \omega_{ce} \omega_{re} + \frac{e^2}{\epsilon_0 m_e r^2} \int_0^r n(r) r dr = 0. \quad (64)$$

The solution of the Eq. (64) is

$$\omega_{re} = \omega_{re}^\pm(r) \equiv \frac{1}{2} \omega_{ce} \left[1 - \left(1 - \frac{4e^2}{\epsilon_0 m_e \omega_{ce}^2 r^2} \int_0^r n(r) r dr \right)^{1/2} \right]. \quad (65)$$

We see that, in general, the equilibrium angular velocity of the electron fluid is not constant, but varies with radius of the column, i.e. there exists a shear in the angular velocity profile.

The angular velocity shear has an important effect on the instability of electron plasma. The *diocotron* instability [13, 15] is one of the most ubiquitous instabilities in low density electron plasmas with shear in flow velocity. In the relatively low density region with $\omega_{pe}^2 / \omega_{ce} \ll 1$ in the EV, such instability could be developed. This instability is likely one of the reasons that a large EV may be broken up into several smaller EV's.

In the above, we considered a simplified case, i.e. $u^2 / c^2 \ll 1$, $u_z B_\theta \ll E_r$, and $B_z \ll B_\theta$. In a more general case, these restrictions should be removed and the toroidal effect must be included. This general case is beyond the scope of this paper.

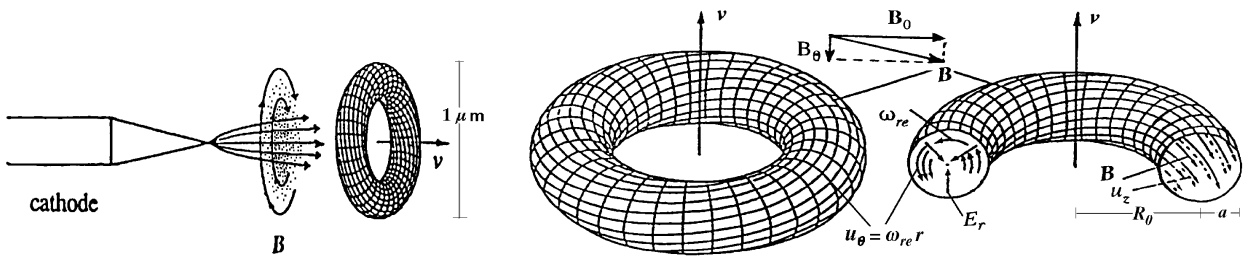


Fig. 2 A Toroidal model of the EV. The combined radial electrostatic force $-neE(r)\mathbf{e}_r$ and the centrifugal force $nm_e u_\theta^2 / r \mathbf{e}_r$ on the electron fluid element are balanced by the inward magnetic force $neu_\theta (B_0 + B_z) \mathbf{e}_r$ and $neu_z B_\theta \mathbf{e}_r$, through the high speed angular rotation of the element.

According to the above discussion, we imagine a toroidal EV as shown in Fig. 2. The electron plasma is mainly confined by the toroidal magnetic field \mathbf{B}_θ which is established by the directional motion of the electrons in the applied potential difference. The radial electrostatic force neE_r and centrifugale force $m_e u_\theta^2 / r$ on the electron fluid element is balanced by inward magnetic force which is caused by $\mathbf{E} \times \mathbf{B} / B^2$ drift

and $\frac{m_e u_0^2}{r} \mathbf{e}_r \times \mathbf{B}/B^2$ drift motion of the electron fluid element. Meanwhile, directional acceleration motion of the electron cluster, nonuniform electron density profile, and diamagnetic pressure gradient drift, $-\nabla p \times \mathbf{B}/B^2$ etc., may cause the toroidal component of the plasma flow velocity u_z , or current J_z , and poloidal magnetic field B_θ . The inside current J_z could contribute to confine outside electrons, and the outside magnetic field B_θ contribute to confine the inside current. Thus, electron plasma, electric and magnetic fields and currents etc., may self-consistently be formed as a self-sustained, closed-equilibrium system.

G. RADIATION

Electromagnetic radiation from the EV can be expressed approximately by using the accelerated point charge when the observation distance is far larger than the EV size. The energy transported by electromagnetic field is determined by the Poynting vector $\mathbf{S} = (\mathbf{E} \times \mathbf{B})/\mu_0$. The electromagnetic field far from the moving EV, can be expressed by the Eqs. (16) and (17). Thus, the Poynting vector can be calculated as

$$\mathbf{S} = \frac{q^2 |\mathbf{e}_r \times \dot{\mathbf{v}}|^2}{16 \pi^2 \epsilon_0 c^3 r^2} \mathbf{e}_r = \frac{q^2 \dot{v}^2 \sin^2 \theta}{16 \pi^2 \epsilon_0 c^3 r^2} \mathbf{e}_r, \quad (66)$$

where θ is the angle between the direction of the acceleration and the direction to the observation point. And the power transported across a small surface $\Delta s = r^2 d\Omega \mathbf{e}_r$ is $dP = \mathbf{S} \cdot d\mathbf{s}$ or

$$\frac{dP}{d\Omega} = \frac{q^2 \dot{v}^2 \sin^2 \theta}{16 \pi^2 \epsilon_0 c^3}, \quad (67)$$

where $d\Omega$ is the solid angle subtended by the surface ΔS . The total power emitted into all directions is given by

$$P = \int_0^{2\pi} \int_0^\pi \frac{dP}{d\Omega} \sin \theta d\theta d\phi = \frac{q^2 \dot{v}^2}{6 \pi \epsilon_0 c^3}, \quad (68)$$

which is known as *Larmor's formula*.

Let's estimate the power of radiation of the EV. Substituting the Eq. (22) for $\dot{\mathbf{v}}$ and the Eq. (2) for q to Eq. (68), we have electromagnetic radiation power $P = 0.13$ watt.

It is well known that an electron gyrating in a magnetic field $B_0 \mathbf{e}_z$ emits cyclotron radiation. How is this spontaneous emission affected by the electron motion in the crossed electric and magnetic fields, like $E_r(r) \mathbf{e}_r$ and $B_\theta \mathbf{e}_\theta$ in the EV? Davidson et al. [16] have shown that in the crossed $E_r(r) \mathbf{e}_r$ and $B_\theta \mathbf{e}_\theta$ fields the orbit of the electron perpendicular to \mathbf{e}_z in the laboratory frame will become *biharmonic*, with two rotational frequencies ω_{re}^+ and ω_{re}^- defined in Eq. (61). The energy radiated per unit frequency interval per unit solid angle is given by [16]

$$\eta(\omega) \equiv \frac{1}{T} \frac{d^2 I}{d\omega d\Omega} = \frac{e^2 \omega^2 T}{8 \pi^2 c^3} \left\{ \frac{\sin^2(\Omega^+ T/2)}{(\Omega^+ T/2)^2} \frac{\omega_{re}^2}{(\omega_{re}^+ - \omega_{re}^-)^2} (v_\perp^2 + \omega_{re}^{-2} r^2) \right.$$

$$\begin{aligned}
& + \frac{\sin^2(\Omega^- T/2)}{(\Omega^- T/2)^2} \frac{\omega_{re}^{-2}}{(\omega_{re}^+ - \omega_{re}^-)^2} (v_{\perp}^2 + \omega_{re}^{+2} r^2) \\
& - \frac{2 \omega_{re}^+ \omega_{re}^-}{(\omega_{re}^+ - \omega_{re}^-)^2} \frac{\sin(\Omega^+ T/2) \sin(\Omega^- T/2)}{(\Omega^+ T/2)(\Omega^- T/2)} \\
& \times \left[(v_{\perp}^2 + \omega_{re}^+ \omega_{re}^- r^2) \cos\left(\frac{(\Omega^+ - \Omega^-) T}{2}\right) \right] \Bigg\}, \tag{69}
\end{aligned}$$

where $T = L/v_z$ is the length of time that the electron is in the interaction region; k_z is the wave number and Ω^{\pm} is defined by

$$\Omega^{\pm} \equiv \omega - k_z v_z - \omega_{re}^{\pm}. \tag{70}$$

We see that the electron cyclotron emission spectrum $\eta(\omega)$ has two maxima located at $\Omega^+ = 0$ and $\Omega^- = 0$, or equivalently

$$\omega - k_z v_z - \omega_{re}^{\pm} = \frac{1}{2} \omega_{ce} \left[1 \pm \left(1 - \frac{2 \omega_{pe}^2}{\omega_{ce}^2}\right)^{1/2} \right]. \tag{71}$$

For $2 \omega_{pe}^2 / \omega_{ce}^2 \rightarrow 0$, the Eq. (71) gives $\omega_{re}^+ \rightarrow \omega_{ce}$ and $\omega_{re}^- \rightarrow 0$. As the $2 \omega_{pe}^2 / \omega_{ce}^2$ increase, ω_{re}^+ shifts downward and ω_{re}^- shifts upward. Therefore, from measuring the cyclotron emission from the EV, we may determine the parameter $2 \omega_{pe}^2 / \omega_{ce}^2$ or n/B_o^2 . If we know n (or B_o), then we can determine the value of B_o (or n) for the EV.

H. CONCLUSIONS

In this paper, we have analyzed the macroscopic equilibrium properties for a moving electron cluster (EV) based on the electron plasma fluid description. We have shown that the self-consistent equilibrium is possible only in the toroidal system, that is the *EV is a toroidal electron vortex*.

We further deduced a necessary condition or criteria in which an EV could exist. The criteria indicate that the EV could exist at various combinations of the electron density, the directional velocity (or energy), and the size of the EV.

From the theory and results shown in this paper, we could imagine the EV process as follows: A large number of electrons are locally emitted in a very short time, $< 1/\omega_{pe}$. In the same time scale, a directional motion of a cluster of electrons are produced by a directional electric field. At the formation, the shape of the electron cluster may be spherical, ellipsoidal or spheroidal but will almost instantaneously be adjusted to a toroidal shape by the force balance requirement (Eq. (55)). A toroidal EV satisfying the criteria (Eq. (63)) will be formed. During the subsequent motion of the EV, along with the increase of the directional velocity, the electron density and the size of the EV will be changed or a large EV could be broken up into two or more smaller EV's in accordance with the equilibrium criteria, or destroyed by instabilities.

As a non-neutral electron plasma, it is expected that the various electrostatic and electromagnetic instabilities will occur in the EV. Therefore, an EV is not expected to exist in a field-free region. The presence of some

dielectric interface, low density plasma, or wave-guide support etc. will greatly enhance the stability of the EV. These important problems are the subject for a future paper.

REFERENCES

1. K.R. Shoulders, EV - A Tale of Discovery, Austin, TX (c1987). A historical sketch of early EV work having: 246 pages, 153 photos and drawings, 13 references.
2. See U.S. Patents by K.R. Shoulders, 5,018,180 (1991) - 5,054,046 (1991) - 5,054,047 (1991) - 5,123,039 (1992) and 5,148,461 (1992).
3. Kenneth and Steven Shoulders, "Observations on the Role of Charge Clusters in Nuclear Cluster Reactions," *Journal of New Energy*, vol 1, no 3, Fall 1996, 22 figs, 7 refs.
4. G.A. Mesyats, "Ecton Processes at the Cathode in a Vacuum Discharge," Proceedings of the XVIIth International Symposium on Discharges and Electrical Insulation in Vacuum, Berkeley, CA, pp 721-731, July 21-26, 1996.
5. Richard W. Ziolkowski and Michael K. Tippet, "Collective Effect in an Electron Plasma System Catalyzed by a Localized Electromagnetic Wave," *Physical Review A*, vol 43, no 6, pp 3066-3072, 15 March 1991.
6. Petr Beckmann, "Electron Clusters," *Galilean Electrodynamics*, Sept./Oct., vol 1, no 5, pp 55-58, 1990.
7. David L. Book, NRL Plasma Formulary, Naval Research Lab. (revised 1987).
8. J.D. Jackson, Classical Electrodynamics, John Wiley & Sons, Inc., New York (c1962).
9. H. Fox, R.W. Bass, and S.X. Jin, "Plasma Injected Transmutation," *Journal of New Energy*, vol 1, no 3, Fall 1996, 4 figs, 23 refs.
10. G.H. Miley and J.A. Patterson, "Nuclear Transmutations in Thin-Film Nickel Coatings Undergoing Electrolysis," *Journal of New Energy*, vol 1, no 3, Fall 1996.
11. T. Mizuno, T. Ohmori, and M. Enyo, "Isotopic Changes of the Reaction Products Induced by Cathodic Electrolysis in Pd," *Journal of New Energy*, vol 1, no 3, Fall 1996.
12. R. Kopecek and J. Dash, "Excess Heat and Unexpected Elements from Electrolysis of Acidified Heavy Water with Titanium Cathodes," *Journal of New Energy*, vol 1, no 3, Fall 1996.
13. R.C. Davidson, Theory of Non-Neutral Plasmas, Addison-Wesley, Reading, Massachusetts (c1989).
14. Kenneth R. Shoulders, Private communications (1992-1996)
15. O. Bunemann, R.H. Levy and L.M. Linson, "Stability of Crossed Field Electron Beam," *J. Applied Phys.*, vol 37, p 3203 (1966).
16. R.C. Davidson and W.A. McMullin, "Influence of Intense Equilibrium Self Fields on the Spontaneous Emission from a Test Electron in a Relativistic Non-Neutral Electron Beam," *Phys. Fluids* vol 27, p 1268 (1984).

NUCLEAR TRANSMUTATION IN COLD FUSION EXPERIMENTS

Hideo Kozima, Masahiro Nomura, Katsuhiko Hiroe and Masayuki Ohta¹

ABSTRACT

Nuclear transmutation in chemical and biological systems are investigated with use of Trapped Neutron Catalyzed Fusion Model (TNCF model). In the TNCF model, it is possible to analyze experimental data consistently and quantitatively. We present the investigation of experimental results in cold fusion systems with various materials and various methods in this paper.

1. INTRODUCTION

There are many experimental results in cold fusion research showing the existence of nuclear transmutation, i.e. generation of new isotopic species or new elements in the experimental system. The nuclear transmutation has been difficult to understand by conventional physics, but if we make an assumption that trapped thermal neutrons exist in the sample (TNCF model [1,6]), it is possible to analyze consistently and quantitatively with an accuracy of one or two orders of magnitude. In this paper we give results of the analyses of various experimental results of nuclear transmutation.

2. THEORETICAL BASIS OF THE ANALYSIS

If we make an assumption that the thermal neutron exists in the sample, the following reactions would be expected:

$$n + {}^A_Z M = {}^{A+1}_Z M, \quad (1)$$

$${}^{A+1}_Z M = {}^{A+1}_{Z+1} M' + e^- + \bar{\nu}_e, \quad (2)$$

$$n + {}^{A+1}_Z M = {}^{A+2}_Z M, \quad (3)$$

$${}^{A+2}_Z M = {}^{A+2}_{Z+1} M' + e^- + \bar{\nu}_e \quad (4)$$

$$n + {}^{A+1}_{Z+1} M' = {}^{A+2}_{Z+1} M' \quad (5)$$

$${}^{A+2}_{Z+1} M' = {}^{A+2}_{Z+2} M'' + e^- + \bar{\nu}_e \quad (6)$$

These reaction formulas begin with a thermal neutron and a nucleus ${}^A_Z M$, where ${}^A_Z M$ is a nucleus of the sample materials or a minor element with mass number A and atomic number Z.

The number $d v_i(t)$ of the reaction (1) occurring in a short time duration dt at time t is expressed as follows:

¹ Dept. of Physics, Faculty of Science, Shizuoka University, Japan
from Proc. ICCF6, Oct. 14 - 17, 1996, Hokkaido, Japan

$$d v_1(t) = 0.35 n_n u_n \rho_0(t) \sigma_1 dt . \quad (7)$$

Where $\rho_0(t)$ is the density of ${}^A_Z M$, n_n and u_n are the density and the thermal velocity of the tapped thermal neutron and σ_1 is the absorption cross section of the thermal neutron by the nucleus ${}^A_Z M$. And there is a following relation between $v_1(t)$ and $\rho_0(t)$;

$$\rho_0(t) = \rho_0 - v_1(t) , \quad (8)$$

where ρ_0 is the density of ${}^A_Z M$ at $t = 0$. From the equation (8) and an integration of the equation (7) with time t , we obtain a relation,

$$\rho_0(t) = \rho_0 e^{-0.35 n_n u_n \sigma_1 t} , \quad (9)$$

So the density $\rho_1(t)$ of the nucleus ${}^{A+1}_Z M$ is expressed as follows:

$$\rho_1(t) = \rho_0 (1 - e^{-0.35 n_n u_n \sigma_1 t}) . \quad (10)$$

Next, in the reaction (3), the number $d v_3$ of the reaction (3) in a short time duration dt is given as

$$d v_3 = d \rho_3(t) = C \rho_1(t) \sigma_3 dt , \quad (11)$$

where $\rho_3(t)$ is a density of ${}^{A+2}_Z M$. In this reaction, the density $\rho_1(t)$ of the nucleus ${}^{A+1}_Z M$ changes as follows by the reaction (3):

$$\rho_1(t) = \rho_0 (1 - e^{-C \sigma_1 t}) - \rho_3(t) . \quad (12)$$

In these equations C is $0.35 n_n u_n$ and σ_3 is the absorption cross section of the thermal neutron by the nucleus ${}^{A+1}_Z M$.

Similarly, we obtain the density $\rho_3(t)$ of the nucleus ${}^{A+2}_Z M$:

$$\rho_3(t) = \rho_0 \left[(1 - e^{-C \sigma_3 t}) - \frac{\sigma_3}{\sigma_3 - \sigma_1} \times (e^{-C \sigma_1 t} - e^{-C \sigma_3 t}) \right] . \quad (13)$$

When the half life times of ${}^{A+1}_Z M$, ${}^{A+2}_Z M$ and ${}^{A+2}_{Z+1} M'$ in the reactions (2), (4) and (6) are very short, the number of β decays to yield ${}^{A+1}_{Z+1} M'$, ${}^{A+2}_{Z+1} M'$, and ${}^{A+2}_{Z+2} M''$ are equal to v_1 , v_3 and v_3 respectively, and densities of the reactant nuclei are $\rho_1(t)$, $\rho_3(t)$ and $\rho_3(t)$.

3. EXPERIMENTAL RESULTS AND ANALYSIS OF THE DATA

Here we take up some experimental results and investigate them using the method explained above.

1) I.B. Savvatimova et al.[2].

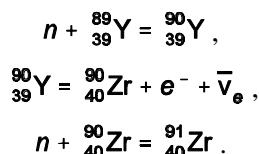
In the glow discharge experiments with D_2 gas (and other gases) and Pd cathode (and other transition metal cathodes), they measured the excess heat and nuclear transmutation of various isotopes and elements using a multi-layer cathode. After the discharge time of 4 hours, the sample was submitted for mass spectrometry (SIMS) and the results showed its isotope composition there about 3 ~ 6 [ppm]. Here we examine two elements:

1 - a) Decrease of ^{32}S

The authors detected a decrease of ^{32}S from 7 to 2 ~ 3 ppm through the glow discharge with D_2 gas using Pd cathode. We can assume that the density of ^{32}S was changed by the reaction (1) only, because ^{31}S does not exist (half life is 2.61s), and that ^{31}P did not exist in the Pd cathode. From the equation (9), we get a density of the trapped thermal neutrons n_n , as $2.2 \times 10^{12} \text{ cm}^{-3}$ using the values of the average speed of the thermal neutron $v = 2.2 \times 10^5 \text{ cm/s}$, the absorption cross section $\sigma_1 = 0.53$ barn of n for ^{32}S and a duration of experiment $t = 10^7 \text{ s}$ (≈ 4 months).

1 - b) Change of Isotopic Composition of Zr

Before the experiment, few ^{90}Zr and ^{91}Zr existed in Pd cathode, but after experiment they increased with a ratio of $^{90}\text{Zr} : ^{91}\text{Zr} = 57 : 34$ (in contrast with 51: 11 by natural abundance). From the nuclear data, ^{89}Zr is unstable and natural abundance of ^{89}Y is 100%, i.e. all other Y are unstable. So, we can assume there were a few ^{89}Y in the Pd cathode and the following reactions would occur:



The absorption cross sections of neutron for ^{89}Y and ^{90}Zr are 1.0×10^{-3} and 5.0×10^{-2} barns, respectively. From the equations (12) and (13) and a relation $\rho_1(t) : \rho_3(t) = 57 : 34$, a density of the trapped thermal neutron was calculated as $2.6 \times 10^{13} \text{ cm}^{-3}$.

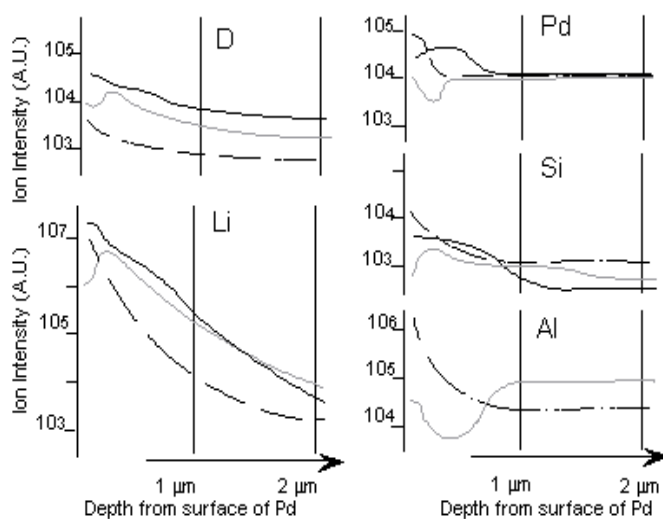


Fig. 1 Examples of Depth Profiles for Each Element

— Neutron & excess heat
 - - - Neutron
 . . . No event

2) V.A. Romodanov et al. [3].

Romodanov et al. measured a lot of tritium with cylindrical Mo cathode in a glow discharge with D_2 gas. The pressure of the gas was 1 atm in the cylinder and 0.2 atm outside. With a cylindrical cathode of $2.5 \text{ cm}\phi \times 10 \text{ cm}$ with thickness of 5 mm, they measured tritium production of 10^7 s^{-1} . In this case, the temperature of the cathode was very high (up to 3000°C) and we may assume that following reaction would occurred in the whole volume of cathode material:



The fusion cross section of d for n is $\sim 5.5 \times 10^{-4}$ barns and a rate of tritium

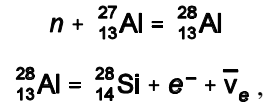
generation is $10^6 \text{ cm}^{-3} \text{ s}^{-1}$. The number of the reaction can be expressed by equation (9). Putting into the formula values obtained or determined in the experiment, we obtain a relation between n_n and n_d ;

$$n_n n_d \sim 3 \times 10^{27} \text{ cm}^{-6},$$

where n_d is the density of deuteron. If we assume two values for the average density of deuterium in the sample $n_n = 10^{20} \text{ cm}^{-3}$ (10^{18}), then we have the density of the trapped thermal neutron $n_n \sim 3 \times 10^7 \text{ cm}^{-3}$ (3×10^9).

3) M. Okamoto et al. [4].

In an experiment in the series of works on Pd/D+ LiOD system conducted hitherto, they determined distributions of Pd, D, Li, Al, and Si atoms in the Pd cathode. As we can see in Fig. 1, densities of those elements changed drastically at near surface of a width $\sim 1 \mu\text{m}$. Especially, Al decreased to $\sim 20\%$ of the original value and Si increased. We assume following reactions would occurred:

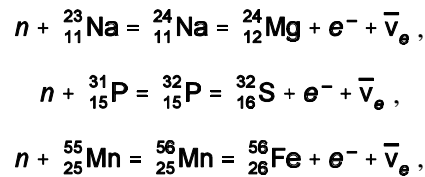


because natural abundance of ${}^{27}_{13}\text{Al}$ is 100 % and ${}^{28}_{13}\text{Al}$ is unstable for β decay (half-life time is 2.27 m). From the equation (9), we obtain a density of the trapped thermal neutron n_n , as $4.9 \times 10^{13} \text{ cm}^{-3}$ with the values of the absorption cross section $\sigma_1 = 0.23$ barn of n for ${}^{27}_{13}\text{Al}$ and a duration of experiment $t = 1.87 \times 10^6$ s.

4) Biotransmutation [5]

Finally we take up the Biotransmutation. From page 25 of Kushi's book [5], the elemental transmutation in a biological system is considered as "most likely taking place at the cellular level" and "it was concluded that granted the existence of transmutation." We investigate three transmutations observed in the biological system Na to Mg, P to S and Mn to Fe.

If we make the same assumption as above, that the thermal neutron exists in a living body, we can assume that there occurs the following reactions:



where natural abundance of ${}^{23}_{11}\text{Na}$, ${}^{31}_{15}\text{P}$ and ${}^{55}_{25}\text{Mn}$ are all 100% and all intermediate nuclei produced from them (${}^{24}_{11}\text{Na}$, ${}^{32}_{15}\text{P}$ and ${}^{56}_{25}\text{Mn}$) are unstable for β decay. Furthermore, we know the absorption cross sections of ${}^{23}_{11}\text{Na}$, ${}^{31}_{15}\text{P}$ and ${}^{55}_{25}\text{Mn}$ for thermal neutron are 0.534, 2.2 and 13.3 barn, respectively from data of nuclides. Compared with the values of the absorption cross section used in the other analyses in this paper, we recognize that these values are fairly large. Therefore, if such elements as Na, P and Mn are in a living body with a lot of trapped neutrons, it is possible to expect the occurrence of nuclear transmutations to Ca, S and Fe.

4. CONCLUSION

We made simple assumptions to investigate the experimental results that there were trapped thermal neutrons with the constant density n_n , in the sample and that they react with hydrogen isotopes in the sample or minor elements, then we can determine the density n_n . The estimated values from other analyses [6] were in a range of $n_n = 10^3 \sim 10^{12} \text{ cm}^{-3}$. The results suggest that the TNCF model is one of the most realistic theories [to explain cold fusion experimental data]. The other three papers [6, 7, 8] given in this conference will help to understand the physics of the cold fusion.

REFERENCES

1. H. Kozima, "Trapped Neutron Catalyzed Fusion of Deuterons and Protons in Inhomogeneous Solids," *Fusion Technol.*, vol 26, p 508 (1994).
2. I.B. Savvatimova, Ya.R. Kucherov, A.B. Karabut, "Cathode Material Change after Deuterium Glow Discharge Experiments," *Fusion Technol.*, vol 26, p 389 (1994).
3. V.A. Romodanov, V.I. Savin and Ya.B. Shuratnik, "The Demands to System Plasma Target for Obtaining a Balance Energy from Nuclear Reactions in Condensed Media," *Proc. RCCFNT2* (Sept. 1994, Sochi, Russia), p 99 (1995).
4. M. Okamoto, H. Ogawa, Y. Yoshinaga, T. Kusunoki O. Odawara, "Behavior of Key Elements in Pd for the Solid State Nuclear Phenomena Occurred in Heavy Water Electrolysis," *Proc. ICCF-4*, vol 3, p 14 (1995).
5. U.S. Army Material Technology Laboratory, "Energy Development from Elemental Transmutations in Biological System," (1978).
6. H. Kozima, "On the Existence of the Trapped Thermal Neutron in Cold Fusion Materials," *Proc. ICCF-6* (to be published).
7. H. Kozima, K. Hiroe, M. Nomura, M. Ohta, "Analysis of the Electrolytic Cold Fusion Experiments on TNCF Model," *Proc. ICCF-6* (to be published).
8. H. Kozima, M. Ohta, M. Nomura, K. Hiroe, "Analyses of the Nickel-Hydrogen Isotope System on TNCF Model," *Proc. ICCF-6* (to be published).

HYDROGEN REDISTRIBUTION BY CATASTROPHIC DESORPTION IN SELECT TRANSITION METALS

Mitchell R. Swartz ¹

ABSTRACT

The Catastrophic Active Medium (CAM) hypothesis treats loaded select Group VIII transition metals (such as palladium in heavy water) as active media capable of catastrophic *in situ* desaturation with secondary redistribution of the relatively low weight hydrogen isotope. The moving interstitials within the palladium are augmented by recruitment and coupling with the generated phonons. The surface energy required to rupture the palladium temporarily prevents the escape of the reactants during their accumulation secondary to the catastrophic reactions, and thereby maintains close contact for the desired reactions.

Positive feedback accrues from the saturation-temperature relationship and also from phonon-softened diffusion.

Unfortunately, when the internal pressures are able to exceed the energy needed to create fresh new surfaces in the loaded palladium, then destructive changes are wrought. Leakage now occurs and the sample becomes, at best, loco-regionally inactive.

INTRODUCTION

Despite its appeal, conventional deuteron-deuteron fusion remains elusive because of the electrostatic repulsion between the deuterons [1,2,3,4], which makes the reaction probability negligible until a separation distance of only a few fermis [1] is achieved. Hydrogen isotope tunneling could be facilitated by screening electrons [3,5,6], changes in the effective mass of both the electrons [7,8] and deuterons [9], deuteron energy fluctuations [10,11], and coherent screening [12]. However, within the crystalline metal the average internuclear deuteron separation distance in Pd is larger at low to moderate loadings than diatomic D₂ [13], and therefore very high loadings >~0.85 are a *sine qua non* for the desired reactions of cold fusion. Yet cold fusion does work. Explanations for both the interdeuteron separation requirement and the lack of many normal reaction products (no to negligible neutrons and gamma-rays, and (⁴He) helium at only a third of the expected ash given the generated excess heat [14]) are required for any complete explanation of the cold fusion phenomenon [15,16] with its distinctly non-plasma-type pathway(s).

The Catastrophic Active Medium (CAM) model [17] answers the former and focuses upon the deuteron solubility in, and the solubility-temperature relationship of, select transition (usually Group VIII) metals such as nickel, palladium, and some of its alloys. Unlike most metals [18] characterized by low solubility (~one deuteron per 10,000 metal atoms), the deuteron solubility in palladium is quite large. Perhaps more importantly, the solubility decreases with temperature. The CAM hypothesis begins with treating the metal as an active medium capable of rapid *in situ* desorption of the lower nuclear weight hydrogen (deuterons) with potential for recruitment of even more deuterons [17]. Full, or near-full, loading of palladium with isotopic fuel appears to be the requisite – but insufficient by itself – of the cold fusion phenomena and the CAM model. The catastrophic nature does not refer to acoustic propagation speed but rather to the feedback effects resulting in additional deuteron recruitment. The model includes two possible positive feedback loops which

¹ © JET Energy Technology, Inc., P.O. Box 81135, Wellesley Hills, MA 02181

may account for both the temporal bursts of anomalous behavior noted in these systems and some of the plethora of termination sequelae which declare themselves as destructive material changes.

THREE COMPARTMENTS WITHIN THE ACTIVE MEDIUM

As discussed previously [17], following adequate loading [19,20,21], the CAM model microscopically considers all types of sites in which the intra-electrode deuterons can reside, including potentially deeper traps supplementing the octahedral and tetrahedral sites (Fig. 1). Macroscopically, the model separates the palladium electrode into three compartments based upon the metallurgical properties of the hydrided material (Fig. 2). The first compartment is the deuteron-laden periodic (crystalline) palladium. The second compartment is the location in which the desired reactions occur, and is hypothesized to be small in volume relative to the other compartments, and physically consists of the "gamma" γ -sites. The third compartment includes grain boundary dislocations and larger defects. Compartment 1 is distinguished from 3 in that it is **not** patently connected to the ambient and can enable lattice-related coherence effects. With subsequent cracking, fissuring, or other dislocations, there results communication from the central portion of the electrode to the ambient, and the proportion of compartment 3 grows over time at the expense of compartment 1. The amount of each compartment (mainly compartments 1 and 2) is related through the fractional defect parameter, χ_{Pd} , which is the fractional volume of non-crystalline (non-periodic) lattice. Within the crystalline lattice a fixed number of active binding sites enables the definition of the occupancy factor, or fractional saturation $\Gamma_{D,Pd}$. $\Gamma_{D,Pd}$ is 0 when the metal is void of deuterons and approaches 1 only as the crystalline metal becomes fully loaded with all α , β and γ sites filled. The deuteron saturation curve $[\Gamma_{D,Pd}(T)]$ falls rapidly in palladium [17,37] with a 7-fold decrease in content from 5 to 50° Centigrade [38] at equilibrium (Fig. 3).

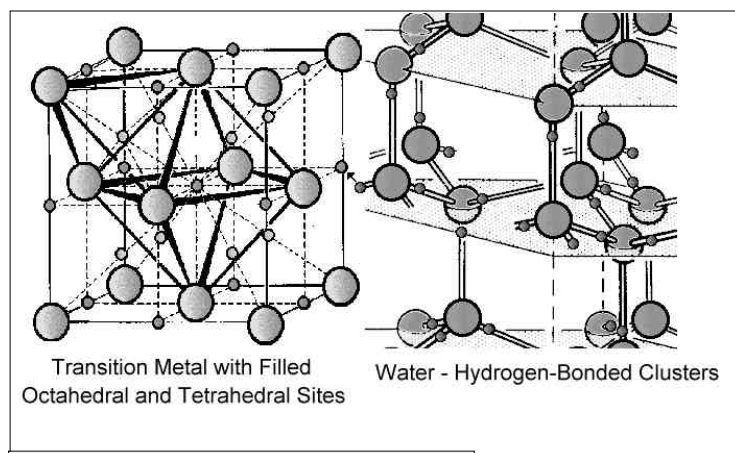


Fig. 1 - Loaded Palladium and D_2O

Palladium must be fully filled with deuterons to generate the reactions. The face-centered cubic fully loaded metallic structure is shown on the left, totally filled with deuterons obtained from the heavy water on the right hand side. The heavy water contains "hydrogen"-bonded D_2O in a near heavy ice- I_h -like structure. The deuterons are represented as small spheres. As a result of both electric polarization and a molecular vibration, there is intermolecular deuteron transfer into the electrode. The important net result (small arrow) is the filling up of one octahedral site within the palladium. The figure on the right side was adapted from J. Mara [27].

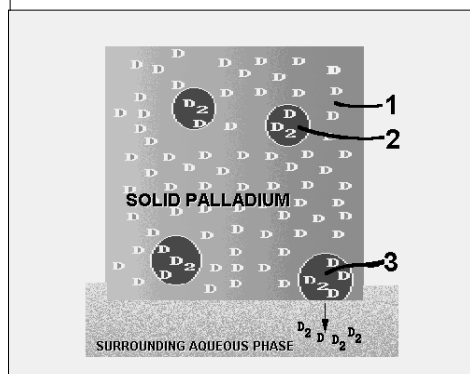


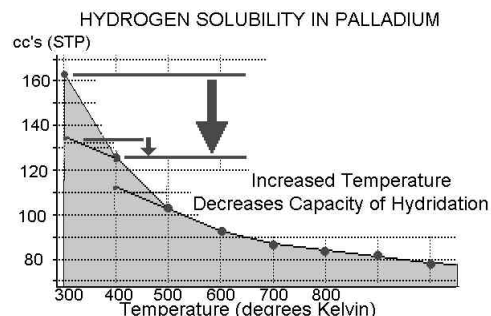
Fig. 2 - Compartment Model of Fully Loaded

Palladium Cathode

Schematic continuum model of the electrode as the CAM model assumes it to be, that the palladium is fully loaded, as from electrochemical loading using heavy water. The bulk metal crystalline lattice is represented by a simple square, and is compartment 1, and neither its full periodicity nor its heterogeneous nature is stressed in this schematic figure. Also shown are reaction sites greatly enlarged – not open to the ambient – which may be filled with deuterons and homonuclear diatomic deuterium, and which comprise compartment 2. With subsequent crack, fissure, or other dislocation formation, only one of which is shown on the lower right of the palladium, compartment 3 is formed.

Fig. 3 - Deuteron Loaded Palladium

The quantity of hydrogen in fully loaded palladium is markedly temperature dependent. The saturation curve shows the quantity (cubic centimeters {STP}) which can be contained in 100 grams of palladium.



INTRA-ELECTRODE HYDROGEN ISOTOPE DIFFUSION

Moderate loading alone, however, appears to be insufficient to overcome the Coulomb barrier. However, the solid state offers other opportunities not found in hot fusion. The CAM hypothesis involves not only the fractional saturation, but also phonons and moving interstitials within the palladium. There are two separate phonon spectra which result from the small mass of the deuteron in the transition metal [22]. The deuteron vibrational modes are far above the lattice modes [17,22-24,30,31]. The phonon energies (~32-48 millieV) have significant zero point motions [25,26] and therefore initially the phonons are optical. The phonons, and the periodic lattice enabling coherent effects, permit the non-ionizing radiation pathway to satisfy the momentum requirements. Eventually the acoustic phonons may contribute to the observed excess enthalpy, directly and indirectly through migration in the palladium. As discussed elsewhere [19,27] defects, grain boundary dislocations, "zeolite"-like diffusion [28], differences in phases [29], and fissures may all influence deuteron diffusion in the palladium. Deuteron migration is aided by phonons at lower temperatures [30,31], and may offer a pathway for phonon-assisted tunneling [32]. The intramaterial deuteron flux, propelled by sudden desaturation, is a reasonable assumption because of the natural characteristics of palladium and its deuteron diffusivity. The latter increases with temperature [33] and with characteristic increasing grain-boundary formation [28,34] which would form during such catastrophic changes.

A computed model [17] relating the normalized deuteron fugacity, temperature, and the fractional saturation has been discussed (Fig. 4). As Fig. 4 shows, with early loading there is a steady increase in deuterium content within the cathode, consistent with some models [19] and experimental observations [29]. Although the deuteron fugacity [$\Theta_{D,Pd}$] rises slightly, in closed systems conservation of mass results in the external partial pressure ($P_{D2,EXT}$) falling as the loading begins; thereby demonstrating the non-identity of $\Theta_{D,Pd}$ and $P_{D2,EXT}$. Prior to destruction of the lattice (see below), this desaturation creates a rapid increase in the local intrinsic hydrogen isotope (and gas) pressure which yields the intra-electrode deuteron flux.

Because of the fractional saturation-temperature effect, dynamic inversion of $\Gamma_{D,Pd}(t)$ occurs as $\Theta_{D,Pd}(t)$ and temperatures reach crescendo levels. As a result, after sufficient decompression time, compartment 2 is suddenly and catastrophically "fed deuterons" from the large vicinal volumes of the crystalline-loaded palladium lattice [compartment 1], further increasing the likelihood of additional temperature-incrementing reactions. On the gripping hand, however, the surface energy required to rupture the palladium prevents the escape, for a while, of the reactants while they continue to accumulate in compartment 2 by the catastrophic reactions and thereby maintain close contact for the desired reactions.

In the active material model, the positive feedback comes from the catastrophic behavior secondary both to the saturation-temperature relationship and also to the phonon-softened coupling to diffusion. The thermodynamics of fully deuterated β -phase suggests that deuteron desaturation from $\Gamma_{D,Pd} = 1$ to 0.8 is

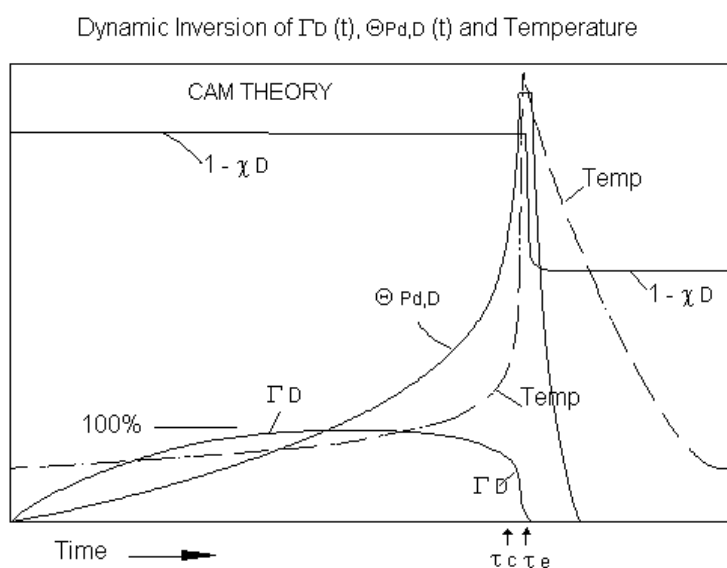


Fig. 4 - CAM Model of Burst and Metallurgical Catastrophic Behavior

This figure shows several curves representing a hypothetical successful cold fusion burst. The loading is shown to first rise continuously, based upon the fractional saturation of the deuterium sites (Γ_D). At some time just after τ_c , the catastrophic reaction occurs and the fugacity ($\Theta_{Pd,D}$) rises with the temperature lagging but then going critical. This continues until there are catastrophic changes in the material (χ_D approaches 1) and there is outgassing, loss of saturation, and ultimate fall off of temperature. The second catastrophic change to the system (formation of compartment 3) begins at τ_e .

causes locoregional inversion of the fractional saturation. The observed temperature rise occurs when the acoustical and optical phonons become unable to carry off all the momentum and excess energy of the reactions. The temperature further rises. The model emphasizes that the result is an *in situ* "depressurization" with redistribution of the low-nuclear weight isotopic fuel into compartment 2. Because of the ratio of the volumes, the catastrophic transfer of deuterons to compartment 2 must greatly increase the pressure *in situ* at that location [17] to produce a dynamic instability. This is what generates the astronomic fugacities [15,36,39]. Only by such catastrophic redistributions are produced the positive feedback loops which produces unusually close deuterons consistent with these fugacities. The tunneling probability, previously vanishingly small, grows as the D-D internuclear separation distance decreases to less than ~ 0.7 Angstroms [5] secondary to the catastrophic reactions.

ENERGETIC CONTRIBUTIONS TO THE DESIRED REACTIONS

The reactions occur at select sites of the deuterium-loaded lattice driven by sudden local catastrophic fractional desaturation and the secondary redistribution of deuterons. The CAM theory relates the crescendo fugacity increase to a concomitant intra-electrode deuterium flux, in concert with other reactions to generate the observed excess enthalpy. In the catastrophic active media model, it is the movement of deuterons to compartment 2 that begins the cold fusion process augmented by feedback, phonon-flux coupling, and confinement. Moreover, the lattice directly further enhances the fusion because the diffusion flux of deuterons within the palladium appears to be proportional to the tunneling matrix element [5]. There are many factors that may contribute to increase the likelihood of possible fusion: electrical charging of the

exothermic [33] and is the model's first positive feedback point. From $\Gamma_{D,Pd} = 0.6$ to $.75$, the desaturation is endothermic, which is also consistent with why the excess enthalpic reactions require even higher loadings.

The second positive feedback is that the isotopic fuel, driven in space by catastrophic fractional desaturation of deuterons, is focused towards the reaction site (compartment 2). The intrapalladium deuterium flux is postulated to migrate in directions of phonon mode softening as it does occur for some vacancies in some transition metals [17,34]. This focused low molecular weight interstitial diffusion pattern is consistent with corrosion theory [36] because hydrogen diffusion there is known to be both intermittent and characterized by flow towards imperfections.

CATASTROPHIC *IN SITU* DEPRESSURIZATION

As the loading drops below $\Gamma_{D,Pd} = 0.8$, the lattice will reabsorb some of the energy produced also limiting the temperature rise. After a certain point, a critical catastrophic event – a local temperature fluctuation rise –

cathode to a high negative voltage, the deuteron band structure [26], Bloch-symmetric Bose-Bloch condensates [40], plasmon exchange [41], electron screening [42], the increased effective mass of the deuterons due to polarons [23], and cooperative phonon (phuson) effects [43]. With the increased screening from the additional electrons secondary to the electrical circuit, further enhancement leading to the increased possibility for fusion would result. Other additional sources of energy able to contribute to the activation energy required for potential fusion reactions, including intrinsic anharmonic motion driven by the Jahn-Teller displacement [44]. Other sources of heat include lattice deformation and fracture, diatomic deuterium formation, and any potential fusion reactions. For example, within defect sites there may occur gas formation by way of deuterons to D_2 gas able to contribute energy towards the activation energy required for fusion [45]. Although the energy release per deuterium recombination is only ~ 7 eV or less, the CAM hypothesis is based upon the volume and catastrophic desaturation surrounding a small compartment. A radius of only several hundred lattice lengths gives the requisite energies consistent with fusion activation.

If fusion could be achieved, one further immediately helpful factor for further fusion is the magnitude of the generated energy per fusion reaction [4] [Q_T] which will result in further amplification of the catastrophic changes. Based upon data [14] concerning the first excited state of the helium nuclear, Q_T may be as much as 20– ~ 22.4 MeV. Production of ^4He occurs with collapse of the system through the strong force as the linear momentum is conserved by internal conversion (phonon coupling to the lattice) generating even more phonons and interstitial transport. Such a reaction would generate significant local heat causing release of even more deuterons.

The CAM model suggests that internal conversion, by way of phonons and possibly plasmons coupled to the "long-range" coherent lattice, may produce the observed branching ratios by enabling deexcitations to couple with phonons. The phonon deexcitation modes are relatively slow and would therefore produce significantly longer transitional times. However, coupled with movement of those phonons during that transitional time, there would be more than adequate recruitment of lattice sites to account for significant energy transfer to the lattice. Further coupling of such optical phonon modes [17,22,30] to the lattice occurs through polaron [43], and possibly Mössbauer coupling.

BOTH COMPLETE DESATURATION AND ULTIMATE DEGRADATION MAY LIMIT REACTIONS

The fusion of deuterium is hypothesized to continue until the crystalline palladium (the active medium because of its high fractional saturation and its exothermic desaturation tendency) is spent of its deuterons or until, by a second catastrophic process, the fusion-defect-site is no longer confined. The latter occurs because the material structural strength is ultimately limited, and is impacted by the loading and the desired reactions. In any case, the reactions described cannot continue indefinitely, but are limited by the structural integrity of the material in which they occur. However, because no material can withstand an indefinite buildup, there comes a time when the internal pressures are able to exceed the energy needed [47] to create fresh new surfaces in the palladium. Leakage now occurs and the sample becomes, at best, locoregionally inactive. In contrast with the fractofusion theories [48,49,50] where cracks create cold fusion by the high electric field generated across crystalline fractures, but consistent with theories of adhesion and surface energy requirements [47] for generating new surfaces in a material, the CAM theory hypothesizes that the desired reactions end with the production of the cracks which absorb, rather than create, the activation energy for any fusion reactions. A portion of the intracathodic compartment 3 is similar to the better-known endstage hydrogen embrittlement, which declares itself when the hydrogen explodes into the ambient as the metal fissures or otherwise irrefutably changes shape.

Some of the expected findings of the catastrophic active medium model are also consistent with metallurgical examination of electrodes which have exhibited successful excess heat reactions. Irregular surface cracks, increased intra-granular roughness and other features [51], pitting [52] and other significant morphologic changes occur consistent with compartment 3 formation. Four probe resistance measurements confirm the development of subsurface cracks following deuteron loading. The CAM hypothesis is even consistent with the observation that the increases in the volume for better-performing cold fusion palladium samples are less, corresponding to the suggestion that compartment 3 effectively terminates the favorable reactions.

SUMMARY

Select Group VIII transition metals are active media capable of catastrophic *in situ* depressurization with secondary redistribution of the low-weight hydrogen isotope. These moving interstitials within the palladium are augmented by recruitment and can couple with the generated phonons. The surface energy at compartment 2 (the loci at which the desired reactions occur) required to rupture the palladium does temporarily prevent the escape of the hydrogen isotopic fuel during its accumulation. Positive feedback results from the shape of the saturation-temperature curve and from intra-electrode diffusion which is primarily along phonon-softened directions. When the internal pressures are excessive, destructive changes are wrought leading to leakage and, at best, locoregional inactivity.

ACKNOWLEDGMENTS

The author thanks Profs. Peter Hagelstein, Keith Johnson, Marcus Zahn, and Gayle Verner for their very helpful comments and suggestions which have contributed to the development of this model. Their support is greatly appreciated.

REFERENCES

1. M. Rabinowitz, Y.E. Kim, V.A. Chechin and V.A. Tsarev, "Opposition and Support for Cold Fusion," Proceedings: Fourth International Conference on Cold Fusion, Vol 2 (sponsored by EPRI and the Office of Naval Research, December 1994), pp 15-1 to 15-12.
2. H. Hora et al., "Screening in Cold Fusion Derived from D-D Reactions," *Physics Letters A*, vol 175, pp 138-143 (1993).
3. G. Preparata, "Some Theories on Cold Nuclear Fusion," *Fusion Technology*, vol 20, no 1, p 82 (1991).
4. G.H. Miley, Fusion Energy Conversion, American Nuclear Society, Urbana, Illinois (1975).
5. T. Tajima, H. Iyetomi, S. Ichimaru, "Influence of Attractive Interaction Between Deuterons in Pd on Nuclear Fusion," *J. of Fusion Energy*, vol 9, p 437 (1990).
6. R.H. Parmenter, et al., "Cold Fusion in Palladium: A More Realistic Calculation," *Proc. Nat. Acad. Sci., USA*, vol 87, p 8652 (1989).
7. T. Matsumoto, "Nattoh Model for Cold Fusion," *Fusion Technology*, vol 16, p 532 (1989).
8. C. Walling, J. Simons, "Two Innocent Chemists Look at Cold Fusion," *J. Phys. Chem.*, vol 93, p 4693 (1989).
9. M. Rabinowitz, D.H. Worledge, "An Analysis of Cold and Lukewarm Fusion," *Fusion Technology*, vol 17, p 344 (1990).
10. Y.E. Kim, R.A. Rice, G.S. Chulick, M. Rabinowitz, "Cluster-Impact Fusion with Cluster Beams," *Modern Physics Letters A*, vol 6, p 2259 (1991).
11. R.A. Rice, G.S. Chulick, Y.E. Kim, "Effect of Velocity Distribution and Electron Screening on Cold Fusion," Proc. ACCF-1, Salt Lake City, p 185 (1990).
12. J. Schwinger, "Cold Fusion: A Hypothesis," *Zeitschrift f. Natur. A*, vol 45, p 756 (1990).
13. S.H. Wei, A. Zunger, "Instability of Diatomic Deuterium in FCC Palladium," *J. of Fusion Energy*, vol 9, p 367 (1990).

14. M.H. Miles, R.A. Hollins, B.F. Bush, J.J. Lagowski, R.E. Miles, "Correlation of Excess Power and Helium Production During D₂O and H₂O Electrolysis Using Palladium Cathodes," *J. Electroanal. Chem.*, vol 346, pp 99-117 (1993); M.H. Miles, B.F. BUSH, "Heat and Helium Measurements in Deuterated Palladium," Proceedings: ICCF-4, Vol. 2, pp 6-1 to 6-7 (1994).
15. M. Fleischmann, S. Pons, "Electrochemically Induced Nuclear Fusion of Deuterium," *J. Electroanal. Chem.*, vol 261, p 301 (1989); M. Fleischmann, S. Pons, M.W. Anderson, L.J. Li, M. Hawkins, "Calorimetry of the Palladium-Deuterium-Heavy Water System," *J. Electroanal. Chem.*, vol 287, p 293 (1990).
16. M. Fleischmann, S. Pons, "Calorimetry of the Pd-D₂O System: From Simplicity via Complications to Simplicity," *Physics Letters A*, vol 176, pp 118-129 (1993); M. Fleischmann, S. Pons, "Some Comments on the Caper "Analysis of Experiments on Calorimetry of LiOD/D₂O Electrochemical Cells";" R.H. Wilson et al., *J. Electroanal. Chem.*, vol 332, pp 33-53, (1992).
17. M. R. Swartz, "Catastrophic Active Medium Hypothesis of Cold Fusion," Proceedings: ICCF-4, Vol. 4, pp 22-1 to 22-12 (1994) .
18. C. J. Smithell, Metals Reference Book, Butterworths Scientific Press, London (1949).
19. M. R. Swartz, "Quasi-One-Dimensional Model of Electrochemical Loading of Isotopic Fuel into a Metal," *Fusion Technology*, vol 22, p 296-300 (1992).
20. M. R. Swartz, "Isotopic Fuel Loading Coupled to Reactions at an Electrode" Proceedings: ICCF-4, Vol.2, pp 33-1 to 33-7 (1994).
21. M. R. Swartz, "Generalized Isotopic Fuel Loading Equations," Cold Fusion Source Book, International Symposium on Cold Fusion and Advanced Energy systems, ed. Hal Fox, Minsk, Belarus (1994).
22. P. L. Hagelstein, "Coherent Fusion Theory," *J. of Fusion Energy*, vol 9, p 451 (1990); P. Hagelstein, S. Kaushik, "Neutron Transfer Reactions," and P. Hagelstein, "Lattice-Induced Atomic and Nuclear Reactions," Proceedings: ICCF-4, Vol. 1, pp 10-1 to 11-27 (1994).
23. R.W. Bussard, "Virtual-State Internal Nuclear fusion in Metal Lattices," *Fusion Technology*, vol 16, pp 231-236 (1989).
24. C.R.A. Catlow, "Atomic Transport in Heavily Defective Solids," *Phil. Magazine A*, vol 64, pp 1011-1024, 5, (1991).
25. B. M. Klein, R. E. Cohen, "Anharmonicity and the Inverse Isotope Effect in the Palladium-Hydrogen System," *Phys. Rev. B*, vol 45, p 21, 405 (1992).
26. D. A. Papaconstantopoulos, B.M. Klein, et al., "Band Structure and Superconductivity of PdD_x and PdH_x," *Physical Review*, vol 17, no 1, pp 141-150 (1977).
27. A. Von Hippel, D.B. Knoll, W.B. Westphal, "Transfer of Protons Through 'Pure' Ice I_h Single Crystals," *J. Chem. Phys.*, vol 54, p 134 (also 145) (1971).
28. S. Szpak, C.J. Gabriel, J.J. Smith, R.J. Nowak, "Electrochemical Charging of Pd Rods," *J. Electroanal. Chem.*, vol 309, pp 273-292 (1991); S. Szpak, P.A. Mosier-Boss, J.J. Smith, "On the Behavior of Pd Deposited in the Presence of Evolving Deuterium," *J. Electroanal. Chem.*, vol 302, p 255 (1991).
29. H. Zuchner and T. Rauf, "Electrochemical Measurements of Hydrogen Diffusion in Intermetallic Compound LaNi₅," *J. Less-Common Metals*, vol 172-174, pp 611-617 (1991).
30. H. Teichler, "Theory of Hydrogen Hopping Dynamics Including Hydrogen-Lattice Correlations," *J. Less-Common Metals*, vol 172-174, pp 548-556 (1991).
31. H.R. Schober, A.M. Stoneham, "Diffusion of Hydrogen in Transition Metals," *J. of the Less-Common Metals*, vol 172-174, pp 538-547 (1991).
32. A. Pusch, W. Fenzl, J. Peisll, "Hydrogen in Niobium Under Pressure," *J. Less-Common Metals*, vol 172-174, pp 709-717 (1991).
33. C. A. Hampel, Rare Metals Handbook, Reinhold Publishing Corp, New York (1954).
34. R.V. Bucur, "Interaction of Hydrogen with the Microstructure in Pd and Pd₇₇Ag₂₃," ICCF-2, Como, Italy (1991) [not in Proceedings, but reviewed in *Fusion Facts*, vol 3, no 1, July 1991, p 21]; G.L. Powell, J.R. Kirkpatrick, J.W. Conant, "Surface Effects in the Reaction of H and D with Pd-Macroscopic Manifestations," *J. Less-Common Metals*, vol 172-174, pp 867-872 (1991).
35. E. Wicke, H. Brodowsky, "Hydrogen in Palladium and Palladium Alloys," Hydrogen in Metals II, G. Alefield, J. Volkl, eds., Springer, Berlin (1978).

36. H. H. Uhlig, Corrosion and Corrosion Control, Wiley (1971).
37. P. A. Rock, W. H. Fink, et al., "Energy Balance in the Electrolysis of Water with a Palladium Cathode," *J. Electroanal. Chem.*, vol 293, p 261 (1990).
38. M.C.H. McKubre, R. C. Rocha-Filho, J. Chao, et al., "Calorimetry and Electrochemistry in the D/Pd System," Procc. ACCF-1, p 20 (1990).
39. J. O'M Bockris, A.K.N. Reddy, Modern Electrochemistry, Plenum Press (c1970); H. H. Uhlig, Corrosion and Corrosion Control, John Wiley & Sons, Inc. (1971).
40. T.A. Chubb, S.R. Chubb, "Bloch-Symmetric Fusion in PdDx," *Fusion Technology*, vol 17, p 710 (1990).
41. M. Baldo, R. Pucci, P.F. Bortignon, "Relaxation Toward Equilibrium in Plasmon-Enhanced Fusion," *Fusion Technology*, vol 18, p 347 (1990).
42. H. Ezaki, M. Morinaga, S. Watanabe, "Hydrogen Overpotential for Transition Metals and Alloys, and its Interpretation Using an Electronic Model," *Electrochimica Acta*, vol 38, pp 557-564 (1993).
43. M.R. Swartz, "Phusons in Nuclear Reactions in the Solid State," *Fusion Tech.*, for Mar. 1997, vol 31, pp 228-236 (1996).
44. K. H. Johnson, "Jahn-Teller Symmetry Breaking and Hydrogen Energy in g-P.d. "Cold Fusion" as Storage of the Latent Heat of Water," Cold Fusion Source Book, *ibid.*, p 75 (1994).
45. R. Seitz, "Fusion in from the Cold?" *Nature*, vol 339, p 185 (1989).
46. P. Vargas, L. Miranda, L. Rodriguez, M. Lagos, J. Rogan, "Quantum Diffusion in Transition Metals," *J. Less-Common Metals*, vol 172-174, p 557-571 (1991).
47. E. Orowan, "Surface Energy and Surface Tension in Solids and Liquids," *Proc. Roy. Soc. Lond. A*, vol 316, pp 173-191 (1970).
48. F.J. Mayer, J.S. King, J. R. Reitz, "Nuclear Fusion from Crack-Generated Particle Acceleration," *Journal of Fusion Energy*, vol 9, pp 269-271 (1990); F.J. Mayer, J. R. Reitz, "Nuclear Energy Release in Metals," *Fusion Technology*, vol 19, pp 552 (1991).
49. V. A. Klyuev, A. G. Lipson, et al., "High Energy Processes Accompanying the Fracture of Solids," *Sov. Tech. Phys. Lett.*, vol 12(11), p 551 (1986).
50. J.T. Dickinson, L. C. Jensen, et al., "Fracto-Emission from Deuterated Titanium: Supporting Evidence for a Fracto-Fusion Mechanism," *J. Mater. Res.*, vol 5, p 109 (1990).
51. D.R. Rolison, P. P. Trzaskoma, "Morphological Differences between Hydrogen-Loaded and Deuterium-loaded Palladium as Observed by SEM," *J. Electroanal. Chem.*, vol 287, p 375 (1990).
52. T. Matsumoto and K. Kurokawa, *Fusion Technology*, vol 20, pp 323-329 (1991).

“EXCESS HEAT” MEASUREMENT IN GAS-LOADING D/PD SYSTEM

Xing Zhong Li, Wei Zhong Yue, Gui Song Huang
Hang Shi, Lan Gao, Meng Lin Liu¹, Feng Shan Bu*

ABSTRACT

A gas-loading D/Pd system has been designed to measure "excess heat." The preliminary result has shown that the calorimetric feature of the D/Pd system is distinct from that of its twin H/Pd system. The difference between these twin systems can be attributed to "excess heat" on the order of watts per cubic centimeter of palladium.

INTRODUCTION

The "heat after death" phenomenon [1] has revealed a fact that electrolysis is not necessary for "excess heat" phenomena. Provided that enough deuterons are absorbed in the palladium crystal lattice, we may expect to see the "excess heat" in a gas-loading system as well. We are particularly interested in the gas-loading system, because we have been engaged with the gas-loading system for several years [2-7]. Early in 1993, Manduchi et al. [8] showed that the palladium samples might be soldered together during the gas-loading process with the deuterium gas. It was explained as an evidence of "excess heat" in this gas loading system. Manduchi's experiments worked out with both the Russian palladium and the British palladium samples. It seems that the only important pretreatment in his experiment is the annealing at the high temperature (900° C) in vacuum. This result is consistent with the early basic research on the gas loading experiments. Oats and Flanagan [9] did the gas loading experiments early in 1971. They showed that the only pretreatment was just the flame heating before use. The loading ratio was as high as 0.94 in their experiments as a matter of routine. The surprising point was that the gas-loading was done at low hydrogen pressure (1.5 Torr, 25° C). The key element was a heated tungsten wire which dissociated the hydrogen molecules into hydrogen atoms. These features of operating under the low pressure and heating by a tungsten wire facilitate the combination of a calorimetric system with a gas-loading system.

EXPERIMENTAL APPARATUS

The low pressure feature makes the thin wall stainless steel Dewar system applicable for a closed gas loading system (Fig. 1). Palladium wire of ϕ 0.34mm is wound on a quartz frame. A pair of such quartz frames with palladium wire winding are made for D₂-loading and H₂-loading, respectively. They are put into an electrical oven to be heated to 900° C in vacuum (10⁻³ Pa). Then they are cooled gradually with the oven. Before they are put into the stainless steel Dewar, a piece of tungsten filament (ϕ 0.1mm) is mounted at the center of the quartz frame. The resistance of the palladium wire is measured by the four-lead method in order to determine the loading ratio (D/Pd and H/Pd) *in situ*. The leads for palladium wire and for tungsten filament can be used for both

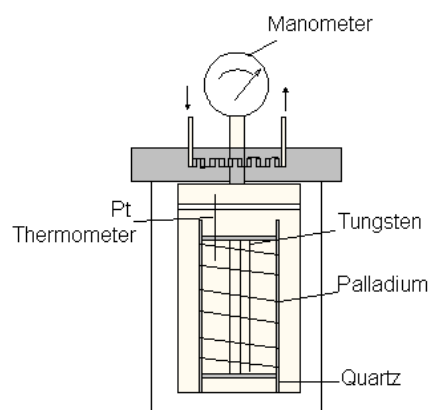


Fig. 1 A Combination of a Calorimeter with a Gas-Loading System

¹ Department of Physics, Tsinghua University, Beijing, China

*Beijing General Research Institute for Non-Ferrous Metals, Beijing, China

heating the Dewar vessel and measuring their resistance. A platinum thermometer is put into the gap between the tungsten filament and the palladium wire in order to measure the temperature change during the process of gas-loading and the calorimetric heating. A manometer is monitoring the gas pressure to evaluate the loading ratio, and a diffusion pump is used to pump out the air to 7×10^{-4} Pa.

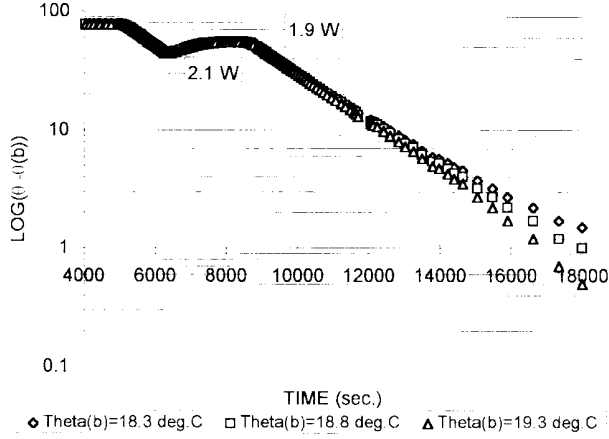


Fig. 2
Calorimetric Feature of the Stainless Steel Dewar System

when the heat source, S , is a constant source; the temperature in the platinum thermometer, θ approaches a constant value θ_f .

$$\theta_f = \theta_b + \frac{S}{k} \quad (2)$$

Here, k is the heat conduction coefficient in the Newton's Law of heat transfer. θ_b is the room temperature. The relaxation time of this system is determined by the reduced heat conduction coefficient:

$$\hat{k} = \frac{k}{MC_p} \quad (3)$$

MC_p is the equivalent heat capacity of the calorimetric system. The equation can be written as

$$\frac{d\theta}{dt} = -\hat{k} \left[\theta - \left(\theta_b + \frac{S}{k} \right) \right] \quad (4)$$

When S is a constant

$$\theta = \left(\theta_b + \frac{S}{k} \right) + \left[\theta_0 - \left(\theta_b + \frac{S}{k} \right) \right] e^{-\hat{k}(t-t_0)} \quad (5)$$

or

$$\log \left[\theta - \left(\theta_b + \frac{S}{k} \right) \right] = -\hat{k}(t-t_0) + \log \left[\theta_0 - \left(\theta_b + \frac{S}{k} \right) \right] \quad (6)$$

Here, θ_0 is the initial temperature of the Dewar system at time t_0 . This is the straight line section shown in Fig. 2. The slope of the straight line gives the value of the reduced heat conduction coefficient, \hat{k} ; the constant $\left(\theta_b + \frac{S}{k} \right)$ may include the information for both the applied heat source, P and the internal heat

CALORIMETRIC FEATURE

This stainless Dewar vessel is different from the glass or quartz Dewar electrolytic cell in Fleischmann and Pons' experiments. Instead of radiation, the heat conduction plays the dominant role in the heat transfer. Fig. 2 shows the temperature, θ , in the Dewar as a function of time. It can be described by the following equation

$$MC_p \frac{d\theta}{dt} = -k(\theta - \theta_b) + S \quad (1)$$

sources, Q. The applied heat source, P, is the heating power given by the experimentalist; however, the internal heat sources, Q, may include the "excess heat" which is what we are searching for.

There are two ways to determine $(\theta_b + \frac{S}{k})$:

(1) Heating method: Given a constant heating power (e.g. a constant current through the tungsten wire), the temperature, θ , approaches a constant value, θ_f .

$$\theta_f = \theta_b + \frac{S}{k} \quad (7)$$

(2) Cooling method: When we plot the Fig. 2 using the experimental data, we have to have a correct value for $\theta_b + \frac{S}{k}$ in order to make a straight line for cooling part. Fig. 2 shows that the least squares fit is able to find the value of $\theta_b + \frac{S}{k}$ with a precision better than 3%. 0.5°C change in $\theta_b + \frac{S}{k}$ may make the straight line visibly distorted (i.e., bent upward or downward, if the $\theta_b + \frac{S}{k}$ is not a correct number.)

Fig. 2 shows also the sensitivity of our calorimetric system. When a small power of 2.73 W is applied onto the calorimetric system through a current in the tungsten wire, the temperature goes up to a constant value of 96.0°C. Then the current is shut off, and we see a straight line of cooling curve with no heat source (see equation (6)). Later, we turn on the current in the tungsten wire again with a power of 2.55 W, a clear inflection point appears to stop the straight line, and levels to a new constant value. Particularly, the curve goes up continuously at a power of 2.1 W and turns horizontal at a power of 1.9 W. Thus, we are confident that this system is able to detect the "excess heat" at the level of 1 W per cc palladium while we put 0.234 cc palladium wire into this calorimetric system.

TEMPERATURE DIFFERENCE BETWEEN TWIN SYSTEMS

A calibration is necessary to quantify the "excess heat;" however, if we are able to show that there are sharp differences in the calorimetric features between the H/Pd and D/Pd twin systems, then we may qualitatively show the evidence of the "excess heat."

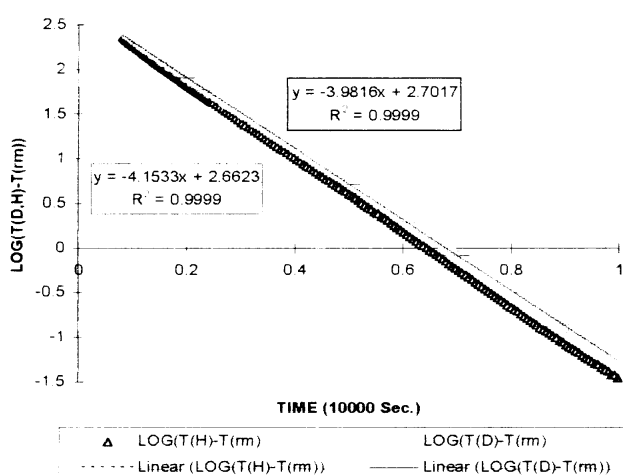


Fig. 3(a) Cooling Feature for D/Pd and H/Pd Systems
(43---32 Deg. C for D; 41---31 Deg. C for H)

To load the hydrogen or deuterium gas into the palladium, an electrolytic cell was supposed to be necessary to provide enough "chemical potential;" otherwise, high pressure and low temperature was supposed to be necessary. R.F. power, a piece of incandescent tungsten wire (2000°C), or D.C. discharge were found to be able to provide the hydrogen or deuterium atoms in stead of the electrolytic current. However, we found that even if the tungsten wire was turned off, as long as the correct pre-treatment of the palladium wire was done, the loading ratio (H/Pd or D/Pd by atomic number) might achieve 0.74 at a pressure much less than 1 atm. This is discussed in two associated papers [10] and [11]. Here, we just discuss the calorimetric feature of the gas-loading system.

In order to detect the possible "excess heat" in a D/Pd system, we intentionally built a pair of twin systems. No. 1 bottle is for deuterium loading, and No. 2 bottle is

for hydrogen loading. These two systems have same Dewar structure, and similar quartz frames. The palladium wires in both bottles are cut from same batch (ϕ 0.34mm); and have been pre-treated with same procedures. The weight of palladium wires in two bottles are 2.846g. and 2.844g., respectively. The tungsten wires are cut from same batch (ϕ 0.1 mm). The resistances of tungsten wire are 4.1 Ω (in D bottle), and 4.3 Ω (in H bottle), respectively. After being pumped to 10^{-3} Pa, the No. 1 bottle was filled with deuterium gas up to 660 mm Hg; and the No. 2 bottle was filled with hydrogen gas up to 660 mm Hg also. Fig. 3 shows the cooling curves for bottles No. 1 and No. 2. A straight line is drawn to fit the experimental data using the least squares fit. From this straight line, the reduced heat conduction coefficient, \hat{k}_D and \hat{k}_H , is

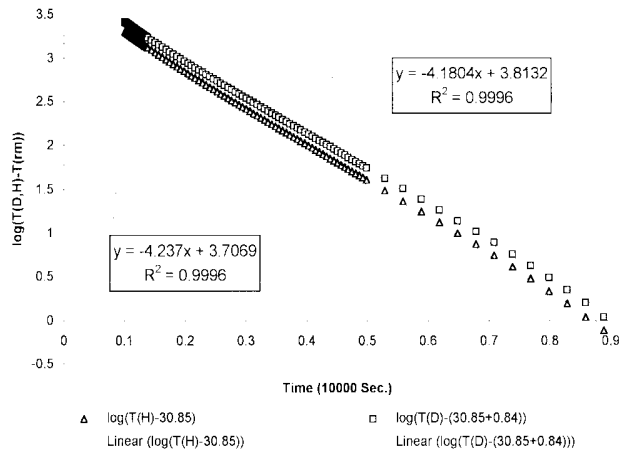


Fig. 3(b) Cooling Feature of D/Pd and H/Pd Systems (62---32 Deg. C for D; 58---32 Deg. C for H)

calculated. To maximize the correlation coefficient R^2 , we may determine the value of $(\theta_b + \frac{S}{k})$ for that straight line. Table 1 gives the corresponding values for the reduced heat conduction coefficients \hat{k}_D and \hat{k}_H ; the constants $(\theta_b + \frac{S}{k})_D$ and $(\theta_b + \frac{S}{k})_H$; and the correlation coefficients R_D^2 and R_H^2 .

Table 1 Calorimetric Feature for Cooling Curve of D/Pd and H/Pd Systems

| Temperature °C | | Reduced Heat Conduction Coefficient \hat{k} sec ⁻¹ | $\theta_b + \frac{S}{k}$ °C | R^2 |
|-------------------|---|--|--------------------------------|--------|
| 41.456 → 31.173 | H | $(4.15 \pm 0.02) \times 10^{-4}$ | 30.94 | 0.9999 |
| 42.785 → 31.803 | D | $(3.98 \pm 0.02) \times 10^{-4}$ | $30.94 + 0.579$ | 0.9999 |
| 58.047 → 31.741 | H | $(4.24 \pm 0.04) \times 10^{-4}$ | 30.85 | 0.9996 |
| 62.161 → 32/728 | D | $(4.18 \pm 0.03) \times 10^{-4}$ | $30.85 + 0.84$ | 0.9996 |

It is clearly shown that the reduced heat conduction coefficients are same for both bottles with the precision better than 5%. However, the constants, $\theta_b + \frac{S}{k}$, are different for D/Pd and H/Pd systems. The difference between them increases, when the temperature range expands. Since the information of "excess heat" is included in this constant, $\theta_b + \frac{S}{k}$, we investigated further by another method: i.e. we heat the systems using the electrical current in the tungsten wire. Through the constant current at 0, 0.1965A, 0.359A, 0.464A, 0.601A, 0.753A and 0.801A; the D/Pd and H/Pd systems are heated to different temperatures. From these

temperatures, we may have another estimate of the constant, $(\theta_b + \frac{S}{k})$. Table 2 lists the results of these heating experiments. The difference of $\theta_r - \theta_b = \left[\left(\theta_b + \frac{S}{k} \right) - \theta_b \right]$ gives the $\frac{S}{k} \equiv \frac{P+Q}{k}$.

In the experiments, the tungsten wires in the D/Pd and H/Pd are connected in series such that the electrical current, I_w , is same in both tungsten wires. This heating power enhances the temperature, θ , in both bottles, and eventually makes a steady state value, θ_r . We can measure the temperature difference at the steady state between the inside and the outside of the Dewar, $\theta_r - \theta_b$, which should be equal to the constant $\frac{S}{k} \equiv \frac{P+Q}{k}$.

In this case, P is the heating power in tungsten wire, Q is the possible "excess power," k is the heat conduction coefficient. It is interesting to notice that when the heating power increases, the temperature difference, $\theta_r - \theta_b$, in D/Pd system increases much faster than that in H/Pd system. This could be attributed to the possible "excess power" in the D/Pd system. In order to estimate this "excess power," we need the value for heat conduction coefficient, k_D . Since the reduced heat conduction coefficients, \hat{k}_D and \hat{k}_H for D/Pd and H/Pd are almost same (see Table 1). It is reasonable to assume that the heat conduction coefficients, k_D and k'_H , are same also. Based on this assumption, the "excess power" in the D/Pd system is calculated. It may achieve up to 0.639 W (see the last column in Table 2) while the heating power is about 3.5 W. An additional evidence of this "excess power" in D/Pd system is the change of the resistance of the tungsten wire. Initially, the resistance of the tungsten wire in H/Pd system (4.46 Ω) is a little higher than that of D/Pd system (4.15 Ω). When the heating power is increased to ~3.5 W, the resistance of the tungsten wire in H/Pd system (5.38 Ω) becomes smaller than that of D/Pd system (5.47 Ω). Using the resistance temperature coefficient $\alpha_w = 4.8 \times 10^{-3} K^{-1}$ for tungsten wire, we have the temperature for the tungsten wires in the H/Pd and D/Pd system, 73.5°C and 96.9°C, respectively. The temperature in D/Pd system is much higher than that of H/Pd system. This is consistent with the former calculation of the "excess power" inside the D/Pd system.

Table 2 Calorimetric Features for Heating Curve of D/Pd and H/Pd System

| I_w | D | | H | | $Q_{ex}^D = \left[\frac{P_w + Q_{ex}}{k} \right]_D P_w^H - P_w^D$ (W) |
|-------|----------------|--|----------------|--|---|
| | P_w^D (W) | $\theta_r - \theta_b$ $= \left[\frac{P_w + Q_{ex}}{k} \right]_D$ (°C) | P_w^H (W) | $\theta_r - \theta_b$ $= \left[\frac{P_w + Q_{ex}}{k} \right]_H$ (°C) | |
| (A) | (W) | (°C) | (W) | (°C) | (W) |
| 0.197 | 0.161 | 2.44 | 0.173 | 2.48 | 0.009 |
| 0.359 | 0.551 | 8.34 | 0.569 | 7.70 | 0.065 |
| 0.464 | 0.960 | 14.2 | 0.977 | 12.9 | 0.115 |
| 0.601 | 1.73 | 24.6 | 1.71 | 21.5 | 0.227 |
| 0.753 | 2.99 | 39.8 | 2.93 | 33.9 | 0.450 |
| 0.801 | 3.51 | 46.3 | 3.45 | 38.5 | 0.639 |

CONCLUDING REMARKS

While a pair of twin calorimetric systems are heated by the same amount of electrical power, the systems approach different temperatures at steady state. The D/Pd system is hotter than the H/Pd system. The temperature difference may achieve the value of 7.8°C measured by the platinum thermometer. Since the cooling curves have shown the reduced heat conduction coefficients for both systems are same, this temperature difference means that there must be an "excess heat" source in the D/Pd system.

We are using platinum resistance thermometers and the Keithley digital multi-meter to measure the temperature. The precision of the measurement is better than 0.1°C. Hence, we are confident about the existence of this temperature difference. This is a qualitative proof of the "excess heat" in D/Pd system.

To quantify this excess heat, we need two assumptions: First the heat conduction coefficient is assumed to be same for the twin systems; second, the excess heat in the H/Pd system is assumed to be zero. The first assumption is supported by the equality of $\hat{k}_D = \hat{k}_H$ and the second assumption just makes a conservative estimate on "excess heat." If there is any "excess heat" in the H/Pd system also, then the "excess heat" in D/Pd system should be greater than this estimate. It is, at least at a level of 1 W per cc palladium. We have observed this excess heat for more than 5 months, (from April 20 to September 29, in 1996) in a D/Pd system with 2.846g. of palladium. It is about 10^3 eV for each palladium atom, which is very difficult to be attributed to any chemical resource. This gas-loading system has the advantage of being operated at a higher temperature which is essential to enhance the heat energy efficiency as an energy source.

ACKNOWLEDGMENTS

This work is supported by the State Commission of Science and Technology, the Natural Science Foundation of China, the Basic Research Fund of Tsinghua University. Many thanks to Mr. Karl Chang, the co-founder of VeriFone Inc., for his generous support.

REFERENCES

1. S. Pons and M. Fleischmann, "Heat after Death," *Fusion Technology*, vol 26, no 4T, p 87, (1994).
2. X.Z. Li et al., "The Analysis of the Neutron Emission from the Glow Discharge in Deuterium Gas Tube and the Gas Loading in Palladium," *Fusion Tech.*, vol 26, no 3, p 84 (1994).
3. X.Z. Li et al., "Anomalous Nuclear Phenomena and Solid State Nuclear Track Detector," *Nucl. Tracks Radiat. Meas.*, vol 22, p 599 (1993).
4. X.Z. Li et al., "The Precursor of 'Cold Fusion' Phenomenon in Deuterium/Solid System," AIP Conf. Proc., 228, Anomalous Nuclear Effects in D/Pd System, Provo, Utah, Oct 22-25, 1990, edited by S.E. Jones et al. (New York, 1991), p 419.
5. D.W. Mo, X.Z. Li et al., "Search for Precursor and Charged Particles in 'Cold Fusion,'" Italian Physical Society Conf. Proc., vol 33, the Science of Cold Fusion, Proc. II Annual Conf. on Cold Fusion, edited by T. Bressani et al., Como, 29 June - 4 July 1991 (Bologna, Italy, 1991), p 123.
6. D.W. Mo, X.Z. Li et al., "Real Time Measurements of the Energetic Charged Particles and Loading Ratio (D/Pd)," Frontiers of Cold Fusion - Proc. Third Intern'l. Conf. on Cold Fusion, Oct. 21-25, 1992, Nagoya, Japan. edited by H. Ikegami (Universal Academy Press, Inc. Tokyo, Japan, 1993), p 535.
7. G.S. Huang, X.Z. Li et al., "The Measurements and the Control of the Loading Ratio of Deuterium in Palladium," Proc. Fourth Intern'l. Conf. on Cold Fusion, Vol. 1, Lahaina, Hawaii, USA, Dec. 6-9, 1993, p 20-21.
8. C. Manduchi et al., "Anomalous Effects During the Interaction of Subatmospheric D₂(H₂) with Pd from 900° C to Room Temperature," *Nuovo Cimento*, vol 107A, no 2 (1994), p 171.
9. W.A. Oates and Ted B. Flanagan, "Formation of Nearly Stoichiometric Palladium-Hydrogen Systems," *Nature Physical Science*, vol 231, p 19 (1971).
10. F.S. Bu and X.Z. Li, "Loading Ratio Study in a Gas-Loading System," (see Proc. of ICCF-6, 1996).
11. G.S. Huang and X.Z. Li, "A Possible Phase Transition in a Gas-Loading D/Pd System," (see Proc. of ICCF-6, 1996).

NUCLEAR REACTION CAUSED BY ELECTROLYSIS IN LIGHT AND HEAVY WATER SOLUTIONS

Reiko Notoya, Toshiyuki Ohnishi and Yohichi Noya ¹

ABSTRACT

A series of analyses of the products of some nuclear reactions caused by electrolysis was performed by a gamma-ray or liquid scintillation spectroscopy. The electrolysis was carried out by use of the so-called thermally open cell which was equipped with the cathode made of porous nickel or platinized platinum, in 0.1 ~ 0.5 mole/liter Li_2CO_3 , Na_2CO_3 , K_2CO_3 , Rb_2SO_4 and Cs_2SO_4 light and heavy water solutions. The result obtained by the analysis and that of our previous works indicated that;

1. gamma peaks due to ^{22}Na and ^{24}Na , ^{40}K , ^{89}Rb and ^{92}Sr , or ^{134}Cs and ^{135}Xe occur during each electrolysis of Na^+ , K^+ , Rb^+ or Cs^+ solution, respectively,
2. gamma peaks due to ^{56}Co , ^{64}Cu and ^{65}Zn were shown in the cases of all electrolytes including even Li^+ solutions,
3. a gamma peak due to the positron annihilation was also observed in every solution, at 511 keV,
4. liquid scintillation spectra showed the increment of tritium produced by electrolysis in all light and heavy solutions except for Rb^+ , and
5. some nuclear reactions were caused by electrolysis and occurred as the branching reactions of the hydrogen evolution reaction.

INTRODUCTION

The cold fusion occurring in the deuterium-palladium system becomes gradually not-so curious owing to many scientists' efforts in the world, since Fleischmann and Pons proposed it on the basis of finding anomalous large heat evolution during electrolysis in a heavy water solution of Li^+ [1]. On the other hand, by use of the so-called low over-voltage metals for hydrogen electrode reaction, large heat evolution and some amount of tritium production were observed during electrolysis, even in light water solutions of various alkali-metallic ions M^+ [2]. Furthermore, a few methods of chemical analysis of the electrolytes used for electrolysis provides some evidence of nuclear reactions, for example, Ca in K^+ [2]² or 132-140X in Cs^+ solution [3], and so forth. For the last a few years, evidence of the nuclear reactions caused by electrolysis has rapidly increased owing to accumulation of works, experimental and theoretical. In particular, the simultaneous measurements of the excess heat and the radioactivity in an electrolytic cell are notable during electrolysis. In these systems, the reaction mechanism was determined as follows on the basis of the result of our studies using the galvanostatic transient method [4]:



where M(I) , H(a) , \Rightarrow and \rightarrow mean the inter-metallic compound between M and the electrode material, an adsorbed hydrogen, the rate non-determining and the rate determining steps, respectively.

¹ Catalysis Research Center, Hokkaido University, Sapporo 060, JAPAN

² First done by J.O'M. Bockris. -Ed.

The aim of this work is to find the evidence for the nuclear reactions of M(I), which must be occurring even in light water solutions. The data concerning the positron annihilation is reported in another place [5]. Therefore, it will be mentioned summarily in this paper.

2. Experimental Part

The electrolytic cell and electrodes were the same as described in the previous papers [2,3]. Namely, we used porous nickel or platinized platinum as a cathode (1.0 x 0.5 cm in size, ≤ 0.1 cm in thickness). The same cathode was usually used a few times for electrolysis in the same kind of electrolyte. Twenty or thirty milliliters of 0.5 mole/l LiOH, Na₂CO₃, K₂CO₃, or 0.3 mole/l Rb₂SO₄, or 0.1 mole/l Cs₂SO₄ solution with light or heavy, or mixed water, was used as the electrolyte. Some series of observations of excess heat and γ -ray spectra were performed simultaneously during electrolysis of 6~100 hours in a dark chamber made of lead walls 10 cm in thickness. After electrolysis, the electrolytes were analyzed by use of a liquid scintillation spectrometer. The procedure was the same as described in a previous paper [6].

3. Results and Discussion

3.1. γ -ray Spectra

Fig. 1 shows the typical spectrum observed in K⁺ solution by a γ -ray spectrometer equipped with a pure germanium detector (made by Nippon Atomic Industry Group Co. LTD).

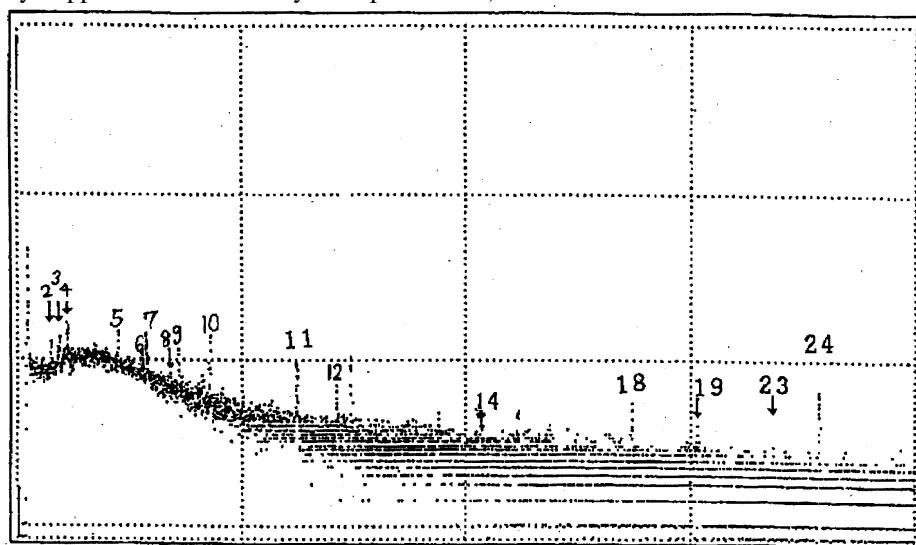


Fig. 1. γ -ray spectrum observed in K⁺ solution on Ni: energy region, 0~1.6 MeV, duration and input power of electrolysis, 50 hour, 0.65 w. Peaks are numbered the same way in Table 1.

Table 1. Identified Nuclear Species and Their Amounts.

| Nuclear Species | Energy (keV) | Amount (Bq) | Limit of Detected Value (Bq) | Peak No. |
|-----------------|--------------|-----------------------|------------------------------|----------|
| Th-234 | 63.33 | $2.11E-1 \pm 1.21E-1$ | $< 3.65E-1$ | 2 |
| Hg-197 | 77.11 | $1.22E-2 \pm 6.51E-3$ | $< 1.96E-2$ | 3 |
| Th-234 | 92.48 | $2.34E-1 \pm 6.04E-2$ | $1.81E-1$ | 4 |
| U-235 | 185.79 | $7.41E-3 \pm 2.54E-3$ | $< 7.64E-3$ | 5 |
| Ra-225 | 185.79 | $1.03E-1 \pm 3.52E-2$ | $< 1.06E-1$ | 5 |
| Pb-212 | 238.65 | $9.11E-3 \pm 3.51E-3$ | $< 1.05E-2$ | 6 |

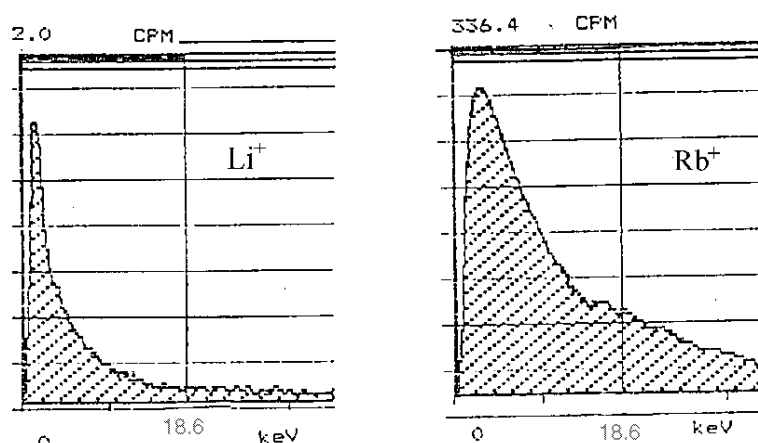
| | | | | |
|--------|---------|-----------------------|-------------------|----|
| Pb-214 | 241.94 | $3.04E-2 \pm 1.19E-2$ | $\langle 3.60E-2$ | 7 |
| Tl-208 | 277.48 | $1.05E-2 \pm 1.01E-2$ | $\langle 3.08E-2$ | 8 |
| Pb-214 | 295.31 | $1.51E-2 \pm 6.43E-3$ | $\langle 1.93E-2$ | 9 |
| Pb-214 | 351.98 | $1.51E-2 \pm 2.54E-3$ | 7.59E-3 | 10 |
| Cu- 64 | 511.26 | $2.53E-2 \pm 6.70E-3$ | 2.00E-2 | 11 |
| Zn- 65 | 511.26 | $1.04E-1 \pm 2.75E-2$ | 8.23E-2 | 11 |
| Co- 56 | 511.26 | $6.76E-3 \pm 1.78E-3$ | 5.35E-3 | 11 |
| N - 13 | 511.26 | $3.35E-1 \pm 8.86E-2$ | 2.65E-1 | 11 |
| Tl-208 | 582.96 | $1.46E-3 \pm 8.14E-4$ | $\langle 2.45E-3$ | 12 |
| Co- 56 | 846.53 | $4.93E-4 \pm 4.82E-4$ | $\langle 1.46E-3$ | 14 |
| Zn- 65 | 1119.84 | $1.95E-3 \pm 1.92E-3$ | $\langle 5.80E-3$ | 18 |
| Co- 56 | 1238.00 | $8.87E-4 \pm 3.90E-4$ | $\langle 1.19E-3$ | 19 |
| Na- 24 | 1368.63 | $1.35E-3 \pm 1.28E-3$ | $\langle 3.91E-3$ | 23 |
| K- 40 | 1458.72 | $1.89E-2 \pm 3.73E-3$ | 1.11E-2 | 24 |

The amount of each nuclear species estimated from the peak value shown in Fig. 1 was listed in Table 1, respectively.

These quantities estimated from the observation of γ -ray spectra are found in the region of 0.001 ~ 0.1 Bq. In Li^+ solution, merely the peaks due to the positron annihilation, ^{64}Cu and ^{65}Zn were increased by electrolysis. In the case of Na^+ , ^{22}Na (1,276 keV) was often detected together with ^{24}Na (1,366 keV).

In K^+ solution, ^{40}K (1,461 keV) is increased always twice from 0.02 Bq to 0.04 Bq in 24 hours electrolysis with 0.5 ~ 0.6 w.

In the case of Rb^+ solution, ^{89}Rb (1,032 and 1,250 keV) was produced by electrolysis and sometimes ^{92}Sr . In the case of Cs^+ , a small amount of ^{134}Cs (609 and 794 keV) and ^{135}Xe (251 keV) were detected. But in Cs^+ solution, the peak due to positron annihilation showed the highest. The reason is not clear at this time.



Figs. 2a and 2b Liquid scintillation spectra observed by use of Li^+ and Rb^+ samples.

3.2. Liquid Scintillation Spectra

A liquid scintillation spectro-analyzer (Packard CA 2550) was used for determination of tritium concentration in electrolyte after electrolysis. Two types of a liquid scintillation spectra were exemplified in Fig. 2a and

Fig. 2b, observed by use of the samples of Li^+ and Rb^+ solutions. The maximum position shown in Fig. 2, and those of the spectra in the samples of Na^+ , K^+ and Cs^+ solutions, agree with that of the authentic sample of tritium. But, the maximum point of spectrum shown in Fig. 2b moved towards higher energy, that was strongly affected by the presence of ^{87}Rb (the natural abundance: 27.835%). The rates of generation of tritium by electrolysis were determined in all kinds of electrolytes of light and heavy water except for Rb^+ , which were listed in Table 2.

Table 2. Generation Rate of Tritium in Various Electrolytes on Porous Nickel.

| Electrolyte | | $W_{\text{input}}^{\text{a}}$ | Excess Heat | $^3\text{T}^{\text{b}}$ |
|------------------|---|-------------------------------|-------------|-------------------------|
| Ion | Water | w | % | Bq/20ml · 24 hr. |
| 1. Li^+ | H_2O | 0.75 | 53 | 0.25 |
| 2. " | " | 0.73 | 52 | 0.032 |
| 3. Na^+ | H_2O | 0.61 | 134 | 1.92 |
| 4. " | " | 0.77 | 59 | 0.222 |
| 5. " | $\text{H}_2\text{O} + \text{D}_2\text{O}$ | --- | --- | 2.006 |
| 6. K^+ | H_2O | 0.47 | 97 | 0.89 |
| 7. " | $\text{H}_2\text{O} + \text{D}_2\text{O}$ | --- | --- | 3.42 |
| 8. " | D_2O | 0.65 | 110 | 393.0 |
| 9. Cs^+ | H_2O | 0.71 | 62 | 32.0 |
| 10. " | " | 0.72 | 61 | 72.0 |
| 11. " | " | 0.41 | --- | 7.0 |

a: Input power

b: Bq denotes tritium amount generated in 20 ml electrolyte during 24 hrs. electrolysis.

3.3. Nuclear Reactions Caused by Electrolysis

A clear peak was found at 511 keV, which must be due to the positron annihilation. In particular, it was remarkable that the peak appeared on all spectra which were observed during the electrolysis of all electrolytes used for this work. The increase of the peaks characterized by ^{64}Cu , ^{65}Zn and ^{56}Co with the increase of duration of electrolysis were common to all solutions. Besides, the increase of the products of some nuclear reactions described above can be estimated on the basis of γ -ray spectral data. These radioactive species are well known to be produced easily in a nuclear furnace, for example. $^{23}\text{Na}(\text{n},\gamma)^{24}\text{Na}$, $^{23}\text{Na}(\gamma,\text{n})^{22}\text{Na}$, $^{39}\text{K}(\text{n},\gamma)^{40}\text{K}$, $^{56}\text{Fe}(\text{p},\text{n})^{56}\text{Co}$, $^{63}\text{Cu}(\text{n},\gamma)^{64}\text{Cu}$, $^{64}\text{Zn}(\text{n},\gamma)^{65}\text{Zn}$, and $^{133}\text{Cs}(\text{n},\gamma)^{134}\text{Cs}$. ^{89}Rb , ^{92}Sr and ^{135}Xe may be produced through a series of some elementary reactions. Ca and the elements of the mass number from 132 to 140 were produced in the same way, which had been detected in the electrolysis of K^+ and Cs^+ ions.

REFERENCES

1. M. Fleischmann and S. Pons, *J. Electroanal. Chem.*, vol 261, p 301 (1989).
2. R. Notoya, "Cold Fusion by Electrolysis in a Light Water-Potassium Carbonate Solution with a Nickel Electrode," *Fusion Technol.*, vol 24, p 202 (1993).
3. R. Notoya, Y. Noya and T. Ohnishi, "Tritium Generation and Large Excess Heat Evolution by Electrolysis in Light and Heavy Water-Potassium Carbonate Solutions with Nickel Electrodes," *Fusion Technol.*, vol 26, p 179 (1994).
4. A. Matsuda and R. Notoya, *Denkikagaku*, vol 34, p 169 (1966).
5. R. Notoya et al., in preparation.
6. R. Notoya, *Enviro. Res.Forum*, V 1-2 (1996), pp 127-140, Transtec Pub.

A NEW APPROACH TOWARDS FUSION ENERGY WITH NO STRONG NUCLEAR RADIATION

Xing Zhong Li ³

ABSTRACT

An energy releasing state in the D/Pd systems has been identified with a life-time of 10^4 seconds. It is shown that this life-time is the characteristics of the resonance tunneling of the Coulomb barrier via lattice confined deuterons. It opens a new approach towards fusion energy with no strong nuclear radiation.

INTRODUCTION

After the careful calorimetric analysis of the D/Pd systems, it has been shown that the D/Pd system may continue to release the "excess heat" even if the electrolysis current has been shut off. [1-2] During this energy releasing period the rate of excess enthalpy generation is of the order of 200 W per cm^3 palladium. This energy releasing process continues in a period of the order of 10^4 seconds. This characteristic time period appears ubiquitously in the open electrolytic cell [1], in the closed electrolytic cell [2]. This time period ($\sim 10^4$ seconds) has been observed in different size of electrodes ($\Phi 1$ mm - $\Phi 4$ mm), and at different temperature of electrolyte (51.524°C - 99.605°C). However, this phenomenon appears only in the Pd and Pd-alloy electrodes cathodically polarized in D_2O solutions. It does not appear in the Pd based cathodes in H_2O based electrolytes, or in the Pt cathodes in H_2O or D_2O based electrolytes. It suggests that there is an energy releasing state in the D/Pd system and the life-time of this energy releasing state is of the order of 10^4 seconds.

In order to search for the origin of this characteristic time period, the theory of the penetration of the Coulomb barrier is reexamined. In terms of resonance tunneling via lattice confined ions, this characteristic time period is related to the Coulomb barrier between two lattice confined deuterons.

1. Penetration of the Coulomb barrier.

In the traditional analysis of the barrier penetration, the nuclear fusion reaction rate, Λ , is always assumed to be

$$\Lambda = \lambda |\Psi(0)|^2 \quad (1)$$

Here $\Psi(r)$ is the normalized wave function describing the relative motion of two reactants; λ is a reaction constant which is related to the low-energy behavior of the corresponding nuclear cross-section. [3]

$$\lambda = \left[\frac{E\sigma(E)}{\mu C^2} \frac{C}{\pi \alpha} \exp(2\pi \eta) \right]_{E \rightarrow 0}; \quad (2)$$

$$\eta = \frac{e^2}{(2E \hbar^2 / \mu)^{1/2}} \quad (3)$$

³ Department of Physics, Tsinghua University, Beijing 100084, China

For example, for deuteron-deuteron reaction,

$$\lambda_{dd} = 1.5 \times 10^{-16} \text{ cm}^3 \text{ sec}^{-1} \quad (4)$$

from the low energy beam-target fusion cross-section. [3]

In the most of the analysis, λ is fixed as an experimental parameter, and $\Psi(0)$ is obtained by numerical solution of Schrodinger equation. [3,4] In these calculations, the numerical solution starts from the outside of the Coulomb barrier. The wave function, $\Psi(r)$, is exponentially depressed when the wave passes through the barrier region. Various models for the potential function in the barrier and outside the barrier region have been assumed, but the potential inside the Coulomb barrier has not been included in these calculations. It was tacitly accepted that once the wave tunnels through the barrier, it will react immediately. The wave function, $\Psi(r)$, is considered as being independent of the reaction constant λ .

Physically, this is not true. Since the amplitude of the wave function should depend on not only the source term, but also on the sink term. The source term is due to the tunneling from the outside of the barrier. The sink term is just the reaction in the nuclear interaction region, i.e. the reaction described by λ . Hence, the value of the wave function in the nuclear interaction region should be dependent on the reaction constant λ . This dependence may be shown in the following model.

2. Modeling the deuteron-palladium systems.

The d-d reaction in the D/Pd systems is very different from the beam target d-d reaction. Here the projectile is no longer described by plane wave, instead, the projectile is a trapped deuteron in the palladium crystal lattice. The main differences between a deuteron in a lattice well and a deuteron in a beam are their energy spectrum (discrete or continuum); and their boundary condition (vanish or finite at infinity). In Fig. 1, the region III represents the lattice potential well, and a deuteron is supposed to be confined in this region on an energy level, E_L , and to be described by a wave function connected to an exponentially decaying function at the boundary, $r = c$. In the region I, a deep potential well is assigned to represent the nuclear force interaction inside the Coulomb barrier II. Although the shape of the nuclear well is uncertain yet, the energy level in it, E_N ,

is essential to describe the resonance tunneling effect. Usually, we expect that when the energy level, $E_L = E_N$ an important resonance effect will greatly enhance the tunneling of the Coulomb barrier. However, $E_L = E_N$ is only the necessary condition for a resonance tunneling. There is another important condition: i.e. the weak damping condition. When $E_L = E_N$, the tunneling wave will reverberate in the nuclear well, and build-up due to the constructive interference between the tunneling wave and the reverberating wave. Since the Coulomb barrier reduces the tunneling wave function by an exponentially large factor, θ , it is necessary to reverberate θ times to build-up the reduced wave function in order to enhance the wave function $\Psi(0)$ in equation (1) to a detectable value. On the other hand, once the tunneling wave enters the nuclear well region, the nuclear reaction will damp the wave function also. In fact, the greater the reaction constant, λ , is the stronger the damping effect in the nuclear well. In other words, the λ will affect the amplitude of the wave function $\Psi(0)$. λ and $\Psi(0)$ are not independent. An imaginary part of the potential, U_1^i , is introduced to describe this damping effect on the wave function in the nuclear well. Now the situation is quite different from that in the conventional quantum mechanics scattering problems, where the incident wave function is a plane wave with a real energy E , and the absorption in the nuclear well will be balanced by the incident current density. Now in the lattice, there is no plane wave function in the lattice potential well. We have to assign another source term in the lattice

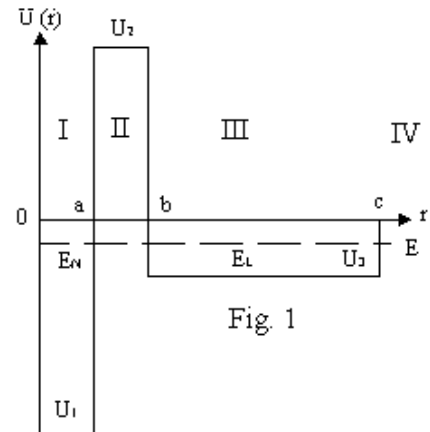


Fig. 1

well region III: i.e. an imaginary potential in the region III, U_3^i . In order to keep the energy, E , real; the U_1^i ; and U_3^i have to satisfy a balance equation as follows.

The Schrödinger equation is:

$$i\hbar \frac{\partial \Psi}{\partial t} = \left(-\frac{\hbar^2}{2\mu} \nabla^2 + U \right) \Psi \quad (5)$$

When U is a complex number, the conservation of the probability current is written as:

$$\frac{\partial |\Psi|^2}{\partial t} = -\nabla \cdot \vec{j} + \frac{2U^i}{\hbar} |\Psi|^2 \quad (6)$$

$$\vec{j} = -\frac{i\hbar}{2\mu} (\Psi^* \nabla \Psi - \Psi \nabla \Psi^*) \quad (7)$$

Here U^i is the imaginary part of the potential. When E is kept real, the left hand side of the equation (6) equals zero. Integrating equation (6) over the whole region from $r=0$ to $r=c$ (Fig. 1), we have zero for the first term in the right hand side of equation (6), because there is no current in and out at the origin ($r=0$) or at the boundary ($r=c$). What we have is

$$\int_0^c U^i |\Psi|^2 d^3r = 0 \quad (8)$$

or

$$\int_0^a U_1^i |\Psi|^2 d^3r = -\int_b^c U_3^i |\Psi|^2 d^3r \quad (9)$$

Physically, equation (9) assures the conservation of the probability current, i.e. the source term in the lattice region balances the sink term in the nuclear region; therefore, it keeps the energy, E , real (i.e. a steady state).

We are interested in the life-time of d-d reaction state in the nuclear well. The life-time is defined as

$$\tau_{xh} \equiv \frac{\int_0^a |\Psi(r)|^2 d^3r}{\left| \int_0^a \nabla \cdot \vec{j} d^3r \right|} \quad (10)$$

Using equation (6) we have

$$\tau_{xh} \equiv \frac{\hbar}{2 |U_1^i|} \quad (11)$$

The imaginary part of the potential, U_1^i , can be expressed by the real and the imaginary pairs of the wave number, k_1^r and k_1^i through the identity

$$U_1^i = -\frac{\hbar^2}{\mu} k_1^r k_1^i \quad (12)$$

Here wave number, k_1 , is defined as

$$k_1^2 = \frac{2\mu}{\hbar^2} (E - U_1) \quad (13)$$

Hence

$$\tau_{xh} = \frac{\mu}{2\hbar} \cdot \frac{1}{k_1^r} \cdot \frac{1}{k_1^i} \quad (14)$$

Since there is supposed to be an energy level in the nuclear well, k_1^i is of the order of a^{-1} . Consequently,

$$\tau_{xh} = \frac{\mu}{2\hbar} \cdot a^2 \cdot \frac{1}{(k_1^i a)} \quad (15)$$

This equation evaluates the life-time of d-d reaction state in the nuclear well, when the order of magnitude of $(k_1^i a)$ is given by the following calculation.

3. Evaluation of $(k_1^i a)$

Square well model in Fig. 1 is used to evaluate the order of magnitude of $(k_1^i a)$. It is straight forward to extend this result to realistic potential configuration. Using the new matrix formalism [5,6], we have the eigen equation for the energy E (see Appendix (A.28))

$$\frac{\cos(k_1 a + \alpha_a)}{\cos(k_1 a - \alpha_a)} = \theta^2 \frac{\sin[k_3(c-b) - (\alpha_c + \alpha_b)]}{\sin[k_3(c-b) - (\alpha_c - \alpha_b)]} \quad (16)$$

Here

$$k_j^2 = \frac{2\mu}{\hbar^2} (E - U_j); \quad (j = 1, 3) \quad (17)$$

$$\beta_j^2 = \frac{2\mu}{\hbar^2} (U_j - E); \quad (j = 2, 4) \quad (18)$$

$$\alpha_a = \text{arc cot} \frac{k_1}{\beta_2} \quad (19)$$

$$\alpha_b = \text{arc cot} \frac{k_3}{\beta_2} \quad (20)$$

$$\alpha_c = \text{arc cot} \frac{k_3}{\beta_4} \quad (21)$$

When U_1 , and U_3 are complex numbers, k_1 and k_3 , are complex also, and so do the α_a , α_b , and α_c . However, the imaginary parts of these α 's turn out to be very small, and may be neglected in the latter calculations. θ is an exponentially large number

$$\theta \equiv \exp[\beta_2(b-a)] \quad (22)$$

which is related to the famous Gamow barrier penetration factor

$$T_{GW} \propto \theta^2 \quad (23)$$

For the deuteron-deuteron interaction, θ is of the order of 10^{27} . [3,7] When k_1 and k_3 are both complex numbers, there are four unknowns in this complex eigen equation (16). However, the resonance condition provides two more equations: i.e.

$$\sin [k_3^r(c-b) - (\alpha_c^r + \alpha_b^r)] = 0 \quad (24)$$

$$\cos (k_1^r a - \alpha_a^r) = 0 \quad (25)$$

Here, superscript r, denotes the real part of k_j . Solving the equations (16), (24), and (25) we have, (see Appendix B, (B.15) and (B.16))

$$(k_1^r a) = O\left(\frac{1}{\theta}\right) \quad (26)$$

$$k_3^r (c-b) = O\left(\frac{1}{\theta}\right) \quad (27)$$

The apparent feature is that both $(k_1^r a)$ and $(k_3^r (c-b))$ are of order of θ^{-1} . Substituting $(k_1^r a)$ into the expression for τ_{xh} , equation (15), we have

$$\tau_{xh} \approx \frac{\mu}{2\hbar} a^2 \theta \quad (28)$$

Using the conventional evaluation of θ (Koonin [3] and Zel'dovich [7]) for the deuteron-deuteron pair, we have

$$\tau_{xh} \approx 10^4 \text{ sec} \quad (29)$$

This is just the experimental value for the life-time of the d-d energy releasing state in the D/Pd systems.

4. Formation of the energy releasing state.

The physics involved in the calculation in the previous section is that we keep the dependence of the wave function, $\Psi(0)$, on the damping factor $(k_1^r a)$. When the damping factor $(k_1^r a)$ is so small that

$$(k_1^r a) \propto \theta^{-1}; \quad (30)$$

then, the deuteron wave function will not disappear immediately after tunneling Coulomb barrier. The wave will reverberate in the nuclear well. When the energy $E_L = E_N$, the phase of the reverberating wave just interferes with the tunneling wave in a constructive way. The damping factor $(k_1^r a)$, will damp the reverberating wave only after θ times reverberations. So the wave function will build-up by a factor of θ , i.e.

$$\Psi(0) \rightarrow \theta \Psi_{GM}(0) \quad (31)$$

$\Psi_{GM}(0)$ is the wave function with no resonance (Gamow case). At the same time the reaction constant λ is reduced by a factor of θ since the reaction constant is proportional to $(k_1^r a)$ (see equations (6) and (12)). Therefore, the nuclear reaction rate

$$\Lambda \propto \lambda |\Psi(0)|^2 \propto \theta^{-1} \lambda_{GM} \cdot |\theta \Psi_{GM}(0)|^2 \propto \theta \Lambda_{GM} \quad (32)$$

On the other hand, the conventional nuclear reaction rate, Λ_{GM} , is calculated in terms of an experimental value λ_{dd} and exponentially depressed wave function $\Psi_{GM}(0) \propto \theta^{-1}$. Thus,

$$\lambda_{GM} \propto \lambda_{dd} |\Psi_{GM}(0)|^2 \propto \theta^{-2} \quad (33)$$

θ^{-2} is the famous Gamow tunneling factor.

Hence, in the resonance tunneling case, the reaction rate Λ is greater than the conventional value by a factor of θ . This results in the observable "excess heat" effect.

5. Selective tuning for the long life-time energy releasing state.

It is interesting to check what is the life-time corresponding to the reaction constant in the low energy beam-target experiment ($\lambda_{dd} = 1.5 \times 10^{-16} \text{ cm}^3/\text{sec}^{-1}$). Since the deuteron-deuteron nuclear reaction range is of the order of 10^{-13} cm . [8] the volume of the nuclear well, V , is about $4 \times 10^{-39} \text{ cm}^3$. The reaction rate in equation (1) could be written in terms of life-time τ :

$$\Lambda = \int_0^a \frac{|\Psi(r)|^2}{\tau} d^3r \approx \frac{V}{\tau} |\Psi(0)|^2 \quad (34)$$

So the life-time of the d-d state in the beam-target experiment, τ_b , is:

$$\tau_b \approx \frac{V}{\lambda_{dd}} \approx 3 \times 10^{-23} \text{ sec.} \quad (35)$$

The reverberation time of the deuteron wave in the nuclear well is on the order of

$$\tau_r \approx \frac{a}{\frac{\hbar k_1^r}{\mu}} \approx \frac{\mu a^2}{\hbar} \approx 10^{-23} \text{ sec.} \quad (36)$$

Therefore, the d-d state formed in the low-energy beam-target experiment has a very short life-time. The deuteron wave will disappear after less than 10 reverberations.

In terms of imaginary potential U_1^i , and using equations (11) and (12) we may calculate

$$(k_1^i a) \approx \frac{U_1^i}{\frac{\hbar^2}{\mu} k_1^r} a \approx \frac{U_1^i}{\hbar} \cdot \frac{a}{\frac{\hbar}{\mu} k_1^r} \approx \frac{1}{2\tau_1} \cdot \tau_r \quad (37)$$

Hence, if the life-time, $\tau_1 = \tau_b$, is of the same order of flying time, τ_r ; them the corresponding $(k_1^i) \gg \theta^{-1}$. This is not the solution of the eigen equation in the resonance case (eq.(26)). In reality, the lattice confined deuteron always satisfies the equation (24), i.e. $E = E_L$ but it does not always satisfy the resonance condition (equation (25)), that is $E_L \neq E_N$. Then, we have the solution (see Appendix B, (B.17) and (B.18))

$$\begin{aligned} (k_1^i a) &\approx O(1) \\ k_3^i (c - b) &\approx O(\theta^{-2}) \end{aligned} \quad (38)$$

We may notice that the $k_3^i (c - b)$ is reduced by a factor of θ^{-1} in comparison with the resonance case (equation (27)). This will greatly reduce the tunneling current density, j , because

$$j = \frac{1}{4\pi b^2} \frac{\hbar}{2\mu} |A_b|^2 \sin 2\alpha_b^r \left[k_3^i \left(1 - \left| \frac{B_b}{A_b} \right|^2 \right) - 2k_3^r \text{Im} \left(\frac{B_b}{A_b} \right) \right] \propto k_3^i \quad (39)$$

When the lattice parameters are changing in the various processes, the energy level of the lattice confined ions may shift up and down, and may pass through the energy level in the nuclear well. When $E_L = E_N$, and the E_N corresponding to a long life-time nuclear state, the resonance happens. The tunneling current would be enhanced to a value much greater than the conventional Gamow tunneling current by a factor of θ . When

the energy level of the lattice confined ions, E_L , is not in resonance with the nuclear energy level (i.e. $E_L \neq E_N$) then, the tunneling current would decrease to the conventional Gamow tunneling current (i.e. $j \propto \theta^{-2}$).

One might ask the question that if the energy level of the lattice confined ions is equal to an energy level of the nuclear well (i.e. $E_L = E_N$), but this nuclear energy level is a short life-time energy level, what would happen? In fact, this situation can not be realistic. When $E_L = E_N$, but $(k_1^i) \gg \theta^{-1}$, equation (8) can not be satisfied; therefore, we have no longer a steady state for such a combination of parameters. Consequently, the lattice confined ions become a selective fine tuning system (just like a radio-receiver). When the lattice confined energy level is not coincident with the nuclear energy level, $E_L \neq E_N$, the tunneling is negligible. When $E_L = E_N$, only the long life-time nuclear state can be in resonance with the lattice confined ions; then, the tunneling current is enhanced by a factor of θ , and a long life-time d-d state is formed in the nuclear well. The short life-time nuclear state has no chance to be in resonance with any lattice confined ions. Just like the radio receiver, if the signal is very weak, and the quality factor (Q value) of the radio receiver is low, then, there will be no signal received, even if the receiver has been tuned to that frequency. Only if the quality factor for that frequency is greatly enhanced (or the damping is greatly reduced), we may have a chance to pick out that weak signal in terms of resonance.

6. Concluding remarks.

The "heat after death" experimental data suggested the existence of a long life-time energy-releasing state. This state can be in resonance with the lattice confined ions. The life-time of 10^4 seconds just fit with the Coulomb barrier between deuteron-deuteron ($\theta \approx 10^{27}$). It also consists with the "incubation time" established in various experiments [1,2,9]. While 10^4 seconds is necessary to absorb a pair of deuteron wave in the nuclear well, it needs at least 10^4 seconds to generate this state in the nuclear well also. The shortest "incubation time" reported was that in the ultrasonic cavity induced reaction [9] where the ultrasonic vibration may provide more chance for resonance tunneling during the excursion of the size of lattice well. They observed the "excess heat" effect only 3 hours after the start-up of their ultrasonic cavity system.

This resonance tunneling via the lattice confined deuteron also solves the puzzle of excess heat without strong nuclear radiation. The neutron emission or triton production are all the products of the strong nuclear interaction. Their reaction constant is too large to be in resonance with the lattice confined deuterons. Although Gamma emission process ($d+d \rightarrow {}^4\text{He} + \gamma + 23.8 \text{ MeV}$) is much slower than neutron emission [10], it is still too fast to be in resonance with the lattice confined deuterons ($\lambda_\gamma \approx 10^{-7} \lambda_b$; hence, $(k_\gamma^i a) \approx 10^{-8} \gg \theta^{-1}$).

Although the life-time of this nuclear energy level with no nuclear radiation is quite long, it is still a valuable energy source. It has been feasible already to load the palladium with deuterium to the density of $6.8 \times 10^{22} \text{ cm}^{-3}$. Even if only a part of them are in the resonance state, even if the reaction energy E_r is only 100 keV per reaction, the power density will be

$$P \approx \frac{n}{T} E_r \approx 10 \text{ kW/cm}^3$$

In the Fleischmann and Pons experiments, a power density of 3.7 kW/cm^3 of excess heat has been observed. This is greater than the power density in the fuel rod of the fast-fission-breeder already.

Appendix A. Eigen Equation for Square-Well Case.

In order to have some estimations for the actual situation, the numerical calculations are necessary for the actual potential configuration. However, there is no precise data for the nuclear potential well or the lattice potential well. We would rather set up a square-well

model (Fig. 1) to obtain some idea about the order of magnitude.

Using the new matrix formalism developed in Ref. [5,6], we choose the two exponentially decaying and growing solutions in the barrier region II as the base functions.

$$\begin{aligned}\phi_{ad}(r) &= \exp[-\beta_2(r-a)] \\ \phi_{ag}(r) &= \exp[\beta_2(r-a)]\end{aligned}\quad (\text{A.1})$$

Here, $\Psi(r) = \phi(r) / (\sqrt{4\pi} r)$, and

$$\beta_2^2 = \frac{2\mu}{\hbar^2} (U_2 - E) \quad (\text{A.2})$$

The solutions connected to ϕ_{ad} and ϕ_{ag} in region I are ϕ_{a1} and ϕ_{a2} , respectively.

$$\begin{aligned}\phi_{a1}(r) &= \cos [k_1(a-r) - \alpha_a] \\ \phi_{a2}(r) &= \cos [k_1(a-r) + \alpha_a]\end{aligned}\quad (\text{A.3})$$

Here,

$$k_1^2 = 2\frac{\mu}{\hbar^2} (E_2 - U) \quad (\text{A.4})$$

$$\alpha_a = \text{arc cot} (k_1 / \beta_2) \quad (\text{A.5})$$

α_a is defined in such a way that the logarithmic derivative, (ϕ'_{a1} / ϕ_{a1}) , equals (ϕ'_{ad} / ϕ_{ad}) at point a; and the (ϕ'_{a2} / ϕ_{a2}) equals (ϕ'_{ag} / ϕ_{ag}) .

The exponentially decaying and growing solutions at point b are

$$\begin{aligned}\phi_{bd}(r) &= \exp[-\beta_2(b-r)] \\ \phi_{bg}(r) &= \exp[\beta_2(b-r)]\end{aligned}\quad (\text{A.6})$$

This choice just makes the logarithmic derivative, (ϕ'_{bg} / ϕ_{bg}) , equals (ϕ'_{ad} / ϕ_{ad}) ; and the (ϕ'_{bd} / ϕ_{bd}) equals (ϕ'_{ag} / ϕ_{ag}) .

This set of solutions in region II at point b will be connected to a set of solutions in well region III, ϕ_{b1} and ϕ_{b2}

$$\begin{aligned}\phi_{b1}(r) &= \cos [k_3(r-b) - \alpha_b] \\ \phi_{b2}(r) &= \cos [k_3(r-b) + \alpha_b]\end{aligned}\quad (\text{A.7})$$

$$k_3^2 = \frac{2\mu}{\hbar^2} (E - U_3) \quad (\text{A.8})$$

$$\alpha_b = \text{arc cot} (k_3 / \beta_2) \quad (\text{A.9})$$

and we have the logarithmic derivative, (ϕ'_{b1} / ϕ_{b1}) , equals (ϕ'_{bd} / ϕ_{bd}) at point b, and the (ϕ'_{b2} / ϕ_{b2}) equals (ϕ'_{bg} / ϕ_{bg}) .

In the barrier region IV, we choose a set of exponentially decaying and growing solutions, ϕ_{cd} and ϕ_{cg} as the base functions,

$$\begin{aligned}\phi_{cd}(r) &= \exp[-\beta_4(r-c)] \\ \phi_{cg}(r) &\equiv \exp[\beta_4(r-c)]\end{aligned}\quad (\text{A.10})$$

$$\beta_4^2 = \frac{2\mu}{\hbar^2} (U_4 - E) \quad (\text{A.11})$$

This set of solutions is connected to a set of oscillating solutions at point c, i.e. ϕ_{c1} and ϕ_{c2} ,

$$\begin{aligned}\phi_{c1}(r) &= \cos [k_3(c-r) - \alpha_c] \\ \phi_{c2}(r) &= \cos [k_3(c-r) + \alpha_c]\end{aligned}\quad (\text{A.12})$$

$$\alpha_c = \text{arc cot} (k_3 / \beta_4) \quad (\text{A.13})$$

and we have that the logarithmic derivative, (ϕ'_{c1} / ϕ_{c1}) , equals (ϕ'_{cd} / ϕ_{cd}) at point a, and the (ϕ'_{c2} / ϕ_{c2}) equals (ϕ'_{cg} / ϕ_{cg}) . When U_1 and U_3 are complex numbers, k_1 and k_3 are complex also, and so are the α_a , α_b , and α_c . However, the imaginary parts of these α s are very small, and will be neglected in the calculations.

Now we can write down the expansions for the wave function in 4 regions as

$$\phi_{Ia}(r) = A_a \cos [k_1(a-r) - \alpha_a] + B_a \cos [k_1(a-r) + \alpha_a] \quad (\text{A.14})$$

$$\phi_{IIa}(r) = C_a \exp[-\beta_2(r-a)] + D_a \exp[\beta_2(r-a)] \quad (\text{A.15})$$

$$\phi_{IIb}(r) = C_b \exp[-\beta_2(b-r)] + D_b \exp[\beta_2(b-r)] \quad (\text{A.16})$$

$$\phi_{IIIb}(r) = A_b \cos [k_3(r-b) - \alpha_b] + B_b \cos [k_3(r-b) + \alpha_b] \quad (\text{A.17})$$

$$\phi_{IIIc}(r) = A_c \cos [k_3(c-r) - \alpha_c] + B_c \cos [k_3(c-r) + \alpha_c] \quad (\text{A.18})$$

$$\phi_{IVc}(r) = C_c \exp[-\beta_4(r-c)] + D_c \exp[\beta_4(r-c)] \quad (\text{A.19})$$

and we have the forms for all the matrices which connect these coefficients in the expansions:

$$\begin{bmatrix} A_a \\ B_a \end{bmatrix} = C_{WB}^a \begin{bmatrix} C_a \\ D_a \end{bmatrix} \quad C_{WB}^a \equiv \frac{1}{\cos \alpha_a} \begin{bmatrix} 1 & 0 \\ 0 & 1 \end{bmatrix} \quad (\text{A.20})$$

$$\begin{bmatrix} C_a \\ D_a \end{bmatrix} = B_{ab} \begin{bmatrix} C_b \\ D_b \end{bmatrix} \quad B_{ab} \equiv \begin{bmatrix} 0 & \theta \\ \theta^{-1} & 0 \end{bmatrix} \quad (A.21)$$

$$\begin{bmatrix} C_b \\ D_b \end{bmatrix} = C_{BW}^b \begin{bmatrix} A_b \\ B_b \end{bmatrix} \quad C_{BW}^b \equiv \cos \alpha_b \begin{bmatrix} 1 & 0 \\ 0 & 1 \end{bmatrix} \quad (A.22)$$

$$\begin{bmatrix} A_b \\ B_b \end{bmatrix} = W_{bc} \begin{bmatrix} A_c \\ B_c \end{bmatrix} \quad W_{bc} \equiv \frac{1}{\sin 2\alpha_b} \begin{bmatrix} \sin[k_3(c-b) - (\alpha_c - \alpha_b)] & \sin[k_3(c-b) + (\alpha_c + \alpha_b)] \\ -\sin[k_3(c-b) - (\alpha_c + \alpha_b)] & -\sin[k_3(c-b) + (\alpha_c - \alpha_b)] \end{bmatrix} \quad (A.23)$$

$$\begin{bmatrix} A_c \\ B_c \end{bmatrix} = C_{WB}^c \begin{bmatrix} C_c \\ D_c \end{bmatrix} \quad C_{WB}^c \equiv \frac{1}{\cos \alpha_c} \begin{bmatrix} 1 & 0 \\ 0 & 1 \end{bmatrix} \quad (A.24)$$

Hence,

$$\begin{bmatrix} A_a \\ B_a \end{bmatrix} = C_{WB}^a B_{ab} C_{BW}^b W_{bc} C_{WB}^c \begin{bmatrix} C_c \\ D_c \end{bmatrix} = \frac{\cos \alpha_b}{\cos \alpha_a \sin 2\alpha_b \cos \alpha_c} \begin{bmatrix} -\theta \sin[k_3(c-b) - (\alpha_c + \alpha_b)] & -\theta \sin[k_3(c-b) + (\alpha_c - \alpha_b)] \\ \theta^{-1} \sin[k_3(c-b) - (\alpha_c - \alpha_b)] & \theta^{-1} \sin[k_3(c-b) + (\alpha_c + \alpha_b)] \end{bmatrix} \begin{bmatrix} C_c \\ D_c \end{bmatrix} \quad (A.25)$$

The boundary condition at $r = c$ makes $D_c = 0$; thus

$$\frac{A_a}{B_a} = -\theta^2 \frac{\sin[k_3(c-b) - (\alpha_c + \alpha_b)]}{\sin[k_3(c-b) - (\alpha_c - \alpha_b)]} \quad (A.26)$$

On the other hand, the boundary condition at $r = 0$, $\phi_{1a}(0) = 0$, gives

$$\frac{A_a}{B_a} = -\frac{\cos(k_1 a + \alpha_a)}{\cos(k_1 a - \alpha_a)} \quad (A.27)$$

As a result, we have the energy eigen equation

$$\frac{\cos(k_1 a + \alpha_a)}{\cos(k_1 a - \alpha_a)} = -\theta^2 \frac{\sin[k_3(c-b) - (\alpha_c + \alpha_b)]}{\sin[k_3(c-b) - (\alpha_c - \alpha_b)]}, \quad (A.28)$$

Appendix B. The Solution of Eigen Equation

The general solution for eigen equation (A.28) is quite difficult; however, the analytical solution is still possible for the case of interests. Later, we will know that we are only interested in the case where $(k_1^i a) \ll 1$, and $k_3^i(c-b) \ll 1$. In this case

$$\cos(k_1 a + \alpha_a) = x_1 + iy_1 (k_1^i a) \quad (B.1)$$

$$\cos(k_1 a - \alpha_a) = x_2 + iy_2 (k_1^i a) \quad (B.2)$$

$$\sin[k_3(c-b) - (\alpha_c + \alpha_b)] = x_3 + iy_3 [k_3^i(c-b)] \quad (B.3)$$

$$\sin[k_3(c-b) - (\alpha_c - \alpha_b)] = x_4 + iy_4 [k_3^i(c-b)] \quad (B.4)$$

Here,

$$x_1 = \cos(k_1^i a + \alpha_a^i), \quad y_1 = \frac{\partial \cos[k_1 a + \alpha_a]}{\partial (k_1 a)} \Big|_{(k_1^i a) = 0} \quad (B.5)$$

$$x_2 = \cos(k_1^i a - \alpha_a^i), \quad y_2 = \frac{\partial \cos[k_1 a - \alpha_a]}{\partial (k_1 a)} \Big|_{(k_1^i a) = 0} \quad (B.6)$$

$$x_3 = \sin[k_3^i(c-b) - (\alpha_c^i + \alpha_b^i)],$$

$$y_3 = \frac{\partial \sin[k_3(c-b) - (\alpha_c + \alpha_b)]}{\partial [k_3(c-b)]} \Big|_{k_3^i(c-b) = 0} \quad (B.7)$$

$$x_4 = \sin[k_3^i(c-b) - (\alpha_c^i - \alpha_b^i)],$$

$$y_4 = \frac{\partial \sin[k_3(c-b) - (\alpha_c - \alpha_b)]}{\partial [k_3(c-b)]} \Big|_{k_3^i(c-b) = 0} \quad (B.8)$$

Substituting equations (B.1), (B.2), (B.3) and (B.4) into eigen equation (A.28), we have two equations:

$$(k_1^i a) [k_3^i(c-b)] = \frac{\theta^2 x_2 x_3 - x_1 x_4}{\theta^2 y_2 y_3 - y_1 y_4} \quad (B.9)$$

$$\frac{k_1^i a}{k_3^i(c-b)} = \frac{\theta^2 x_2 y_3 - x_1 y_4}{\theta^2 x_3 y_2 - x_4 y_1} \quad (B.10)$$

Hence,

$$(k_1^i a)^2 = \frac{\theta^2 x_2 x_3 - x_1 x_4}{\theta^2 y_2 y_3 - y_1 y_4} \cdot \frac{\theta^2 x_2 y_3 - x_1 y_4}{\theta^2 x_3 y_2 - x_4 y_1} \quad (\text{B.11})$$

$$[k_3^i (c - b)]^2 = \frac{\theta^2 x_2 x_3 - x_1 x_4}{\theta^2 y_2 y_3 - y_1 y_4} \cdot \frac{\theta^2 x_3 y_2 - x_4 y_1}{\theta^2 x_2 y_3 - x_1 y_4} \quad (\text{B.12})$$

Now we apply the resonance condition. When $E = E_L$,

$$x_3 = \sin [k_3^r (c - b) - (\alpha_c^r + \alpha_b^r)] = 0 \quad (\text{B.13})$$

When $E = E_N$,

$$x_2 = \cos [k_1^r a - \alpha_a^r] = 0 \quad (\text{B.14})$$

Then,

$$(k_1^i a) \propto O\left(\frac{1}{\theta}\right) \quad (\text{B.15})$$

$$k_3^i (c - b) \propto O\left(\frac{1}{\theta}\right) \quad (\text{B.16})$$

When $E = E_L \neq E_N$ (non-resonance case), we have only $x_3 = 0$; then

$$(k_1^i a) \propto O(1) \quad (\text{B.17})$$

$$k_3^i (c - b) \propto O\left(\frac{1}{\theta^2}\right) \quad (\text{B.18})$$

In order to see the reasoning for (B.13), we have to go back to a configuration with an extremely high barrier region II. In this case, the absorption in region I has no effect on the lattice well region III, i.e. there is no tunneling current through the barrier region II. Hence, $U_3^i = 0$ and an exponentially decaying solution in region IV ($D_c = 0$) will be connected to a pure exponentially decaying solution in region II ($D_b = 0$). From the connecting matrices C_{WB}^c and C_{BW}^b (see eq. (A.24) and (A.22)), we have $B_c = 0$ and $B_b = 0$. Consequently, we have $\sin [k_3^r (c - b) - (\alpha_c^r + \alpha_b^r)] = 0$ using eq. (A.23). The equation (B.14) is for an energy level in the nuclear well region I, when there is no absorption at all. The infinitely high barrier region II requires an exponentially decaying solution in region II only, i.e. $D_a = 0$. Using connecting matrix (C_{WB}^a , (see eq. (A.20))), we have $B_a = 0$. Then the boundary condition at $r = 0$ requires $\cos [k_1^r a - \alpha_a^r] = 0$. That is equation (B.14).

Glossary of Symbols Used

a = range of nuclear force, cm
 C = velocity of light, cm/sec
 c = range of lattice potential, cm
 E = energy of incident projectile, erg.
 E_L = energy level in the lattice potential well, erg.
 E_N = energy level in the nuclear potential well, erg.
 e = electrical charge of electron, CGSEq
 V = volume included in the nuclear force range for a pair of deuterons, cm^3
 \hbar = Planck constant divided by 2π , erg·sec
 α = fine structure constant (1/137)
 k = wave number, cm^{-1}
 U = potential, erg.
 λ = nuclear reaction constant, $\text{cm}^3 \cdot \text{sec}^{-1}$
 μ = reduced mass, g.
 τ = life-time, sec
 τ_f = flight time, sec
 Ψ = wave function, $\text{cm}^{-3/2}$
 ϕ = reduced radial wave function, $\text{cm}^{-1/2}$
 θ^2 = Gamow tunneling factor

Acknowledgments.

This work is supported by the State Commission of Science & Technology, the Natural Science Foundation of China, and the fundamental research fund from Tsinghua University. Many thanks to Professors Lee Chang; Neng-Kuan Chen; Li-Ming Yang, for helpful discussion, and to Mr. Karl Chang for his generous support.

REFERENCES.

1. S. Pons & M. Fleischmann, "Heat after death," Proc.: 4th Intn'l Conf. on Cold Fusion (ICCF-4), Dec. 6-9, 1993, Lahaina, Hawaii, USA, vol 2, p 8-1.
2. M.C.H. McKubre et al., "Loading, Calorimetry, and Nuclear Investigation of the D/Pd System," Proc.: ICCF-4, Vol 1, p 5-26.
3. S.E. Koonin, and M. Nauenberg, "Calculated Fusion Rates in Isotopic Hydrogen Molecules," *Nature*, vol 339 (1989), p 690.
4. C.D.V. Siclen and S.E. Jones, "Piezonuclear Fusion in Isotope Hydrogen Molecules," *J. Physics G; Nucl. Physics*, vol 12 (1986), p 213.
5. X.Z. Li, "The 3-Dimensional Resonance Tunneling in Chemically Assisted Nuclear Fission and Fusion Reactions," *Transactions of Fusion Technology*, vol 26 (1994), p 480.
6. X.Z. Li, D.Z. Jin, and L. Chang, "The Combined Resonance Tunneling and Semi-Resonance Level in Low Energy d-d Reaction," in Frontiers of Cold Fusion, Edited by H. Ikegami. Universal Academy Press. Tokyo (1993), p 597.

7. Ya.B. Zel'dovich, S.S. Gershtein "Nuclear Reactions in Cold Hydrogen. 1. Mesonic Catalysis," *Soviet Phys. Usp.* vol 3 (1961), p 593.
8. H. Feshbach, Theoretical Nuclear Physics, Wiley & Sons. Inc., Boston (1992), p 488.
9. R. George, private communication (1995).
10. "Cold Fusion Research," A Report of the Energy Research Advisory Board to the United States Department of Energy, p 15. DOE/S-0073, Nov. 1989.

ICCF-7
Vancouver, B.C., Canada
April 19-24, 1998

With the maturation of the field, ICCF-7 seeks to attract a more diverse audience including additional scientists, research institutes, students, national funding agencies, commercial interests, journalists, and spouses. It is the objective of ICCF-7 to provide a productive international forum for communication and education.

Calendar:

June 1997: Local Organizing Committee call for 1-2 paragraph abstracts for sampling of potential presentations. Selection rules and evaluation criteria will be provided at this time.
September 1997: Official call for full, one-page abstracts. Final peer review process begins.
December 1997: Final notification to all presenters regarding the format of their presentation.
January 1998: Deadline for final abstracts to be published in ICCF-7 Program Manual and Website.
April 1998: Conference. All presenters must hand in their final papers during the conference for timely inclusion in the publication ICCF-7 Proceedings.

A different topic is planned for each day at ICCF-7. An invited presentation with summary review or global implications for the entire field will begin each day's topic, followed by five oral presentations on the topic. Afternoons will be entirely devoted to enhanced poster sessions, which include a 3-5 minute oral preview and summary. A "Top Ten" poster presenters will be selected by the attendees, and each will conduct an expanded 15 minute presentation to the full audience on Thursday afternoon. Three evening workshops will also be held.

Topics include: Heat & Related Products, Nuclear Processes & Products, Materials & Innovative Approaches, and Theory & Nuclear Physics.

For more information or to get on mailing list, contact:

ICCF-7 c/o ENECO
391-B Chipeta Way

Phone (801) 583-2000 Fax (801) 583-6245
jaeger@ENECO-USA.com

CARBON PRODUCTION ON PALLADIUM POINT ELECTRODE WITH NEUTRON BURST UNDER DC GLOW DISCHARGE IN PRESSURIZED DEUTERIUM GAS

H. Yamada, H. Nonaka, A. Dohi, H. Hirahara, T. Fujiwara, X. Li and A. Chiba ¹

ABSTRACT

A point-to-plane electrode configuration in slightly pressurized deuterium gas for highly non-uniform electric field was employed to confirm the cold fusion phenomena under glow discharge conditions. A neutron burst took place in 2 runs out of total 37 runs. Using an optical microscope, black deposit was observed to cover the tip surface of two positive electrodes. To the contrary, the tip surfaces of other 35 electrodes were observed to keep their beginning appearance. X-ray photo-electron spectroscopy have revealed the black deposit to be carbon, mixed with palladium at the surface of the palladium point electrode. The total amount of carbon impurity in the palladium electrode and in environment deuterium gas does not account for the large amount of carbon on the tip surface of electrode.

INTRODUCTION

Wada et al. have reported a spontaneous neutron emission from palladium(Pd) electrode in deuterium(D₂) gas, during and after activation by flashover between electrodes (1). The study shows that the nuclear reaction can take place at a solid in D₂ gas atmosphere (2,3), as well as in heavy water (4). In this study, the nuclear reaction in a D₂ loaded Pd point electrode in 2 atm D₂ gas under glow discharge conditions has been investigated by neutron detection and X-ray photo-electron spectroscopy (XPS).

METHODS

A neutron measurement system, including a ³He thermal neutron detector, is used to detect the excess neutrons from the nuclear reaction in Pd point electrode. A neutron moderating system of polyethylene block, as shown in Fig. 1, has a center cavity with a cylindrical shape of 140 mm in diameter and 100 mm high, and enhances the efficiency of the ³He counter by moderating fast neutrons from a test cell. The test cell and the detector are positioned inside the center cavity. Signals from the detector are fed to the single channel analyzer through a preamplifier and an amplifier. The counts are stored on a floppy disk using a personal computer. The noise related to high-voltage application is avoided by adjusting the preamplifier gain and the window of the single channel analyzer.

The test cells, shown in Fig. 2, have a cylindrical shape with volume capacity of 110 cm³. The point-to-plane electrode system with gap spacing about 10 mm was employed in the closed cell to obtain highly non-uniform electric field. A Pd wire of 0.5 mm in diameter

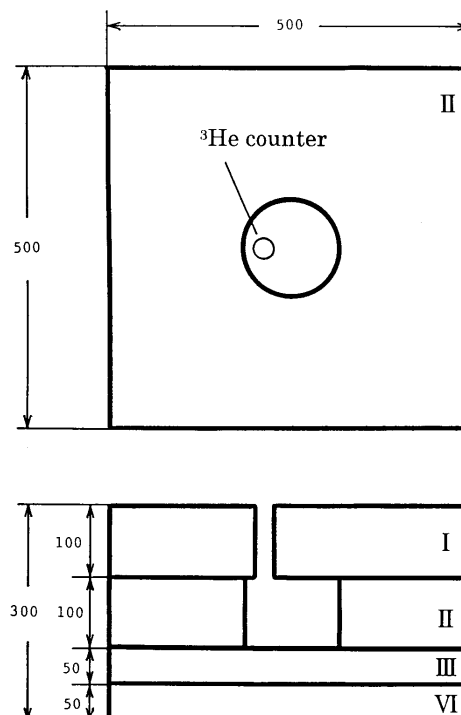


Fig. 1 Neutron Moderating System

¹ Faculty of Engineering, Iwate University, Japan

was cut to about 30 mm in length to be a point electrode. After polishing the surface with sandpaper, the Pd point electrode was vacuum annealed at 400°C for 3 hours under a pressure of about 10^{-4} Torr then cooled down to room temperature, followed by loading of D_2 gas under 2 atm pressure for 24 hours. Next, the Pd point electrode was set into the test cell, followed by filling the test cell with 2 atm D_2 gas. After positioning the cell and the detector inside the center cavity of the moderating system, positive DC 4 or 8 kV was applied to the Pd point electrode. The neutron measurement started just after the voltage application and continued for 24-65 hours. The deuteron to Pd loading ratio was measured to be about 0.6.

The efficiency of the detector was measured to be approximately $\pm 1\%$ using ^{252}Cf source. The average background of neutron flux without the test cell is about 25 counts per hour after the adjusting. The counting characteristics of background neutrons has been stable over total about 3,500 hours of background measurement period for the past 7 years.

RESULTS

The neutron burst was observed in 2 out of 37 runs. The electrodes used in the positive 2 runs are assigned to the names "Electrode-A" and "Electrode-B". The time behavior of the neutron emission rate for Electrode-A is shown in Fig. 3, where the emission started at 6 hours 48 min. after the beginning of the 8 kV application and continued 3 hours 50 min. No excess count was observed for 30 hours after the emission ceased. The highest count rate of 180 counts per 3 min, observed just before the emission ceased, is 140 times larger than that of the background neutron. The number of total neutrons counted was about 900. In the case of Electrode-B, the burst was started just after the voltage application and continued for about 15 min. The next burst started about 5 hours after the first burst and continued for 5 min. The number of neutrons counted during the 2 bursts amounted to 3×10^4 . The highest count rate of 2,700 per 5 sec was 9×10^4 times larger than that of the background neutron.

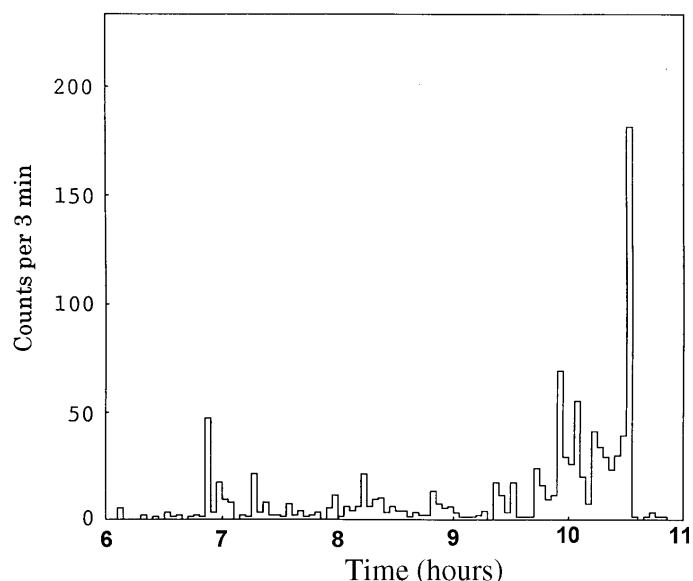


Fig. 3. Time dependence of the neutron counts from deuterium-palladium system. [hours reset to reflect text]

The total number of excess neutrons is estimated to be 35 times larger than that for the Electrode-A, even though the emission period was shorter than that for the Electrode-A. No excess neutrons were observed for 65 hours after the second burst ceased.

The electrodes after the voltage application were viewed by an optical microscope. The tip surface of two positive electrodes was found to be covered with black deposit. **Of particular interest is that several craters of about $10 \mu\text{m}$ in diameter were formed on the tip surface of Electrode-A.** [Emphasis by Ed.] The covered area was measured to be more than 0.32 mm^2 for Electrode-A. To the contrary, the tip surface of negative 35 electrodes was observed to keep its beginning appearance.

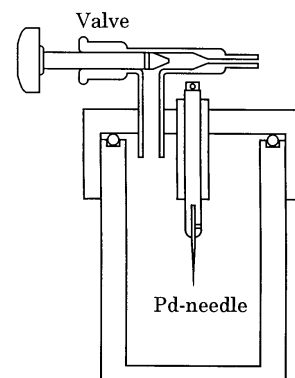


Fig. 2 Test cell

An XPS spectrum for the D_2 loaded Pd point electrode before the voltage application is shown in Fig. 4, where the tip of the electrode was etched in about 0.5 nm depth with argon ion to remove molecules of air

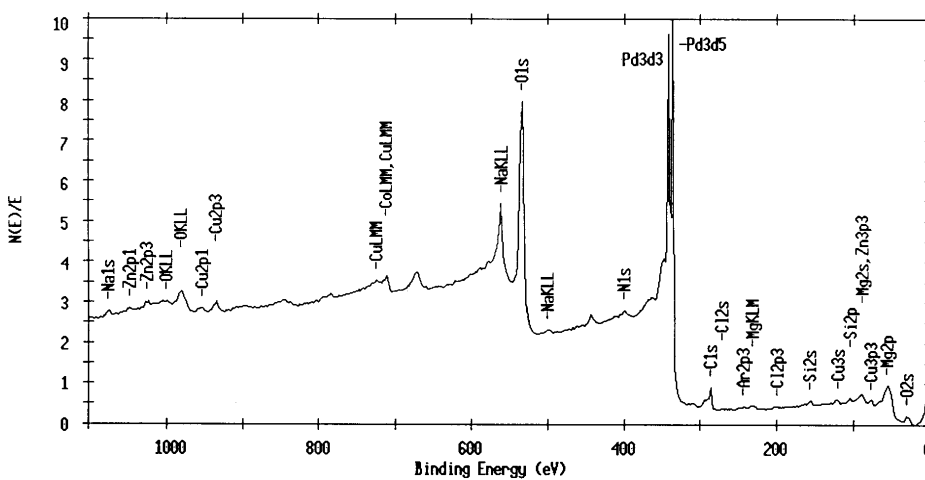


Fig. 4 XPS spectrum of the Pd point electrode before neutron emission

contamination. The figure shows a strong absorption of oxygen on the surface. To the contrary, a large carbon peak is seen in the XPS spectrum of the tip of Electrode-A after the neutron emission, as shown in Fig. 5. It seems that the carbon atoms were mixed with Pd atoms in the bulk region from the electrode surface to the depth in several atomic layers at least.

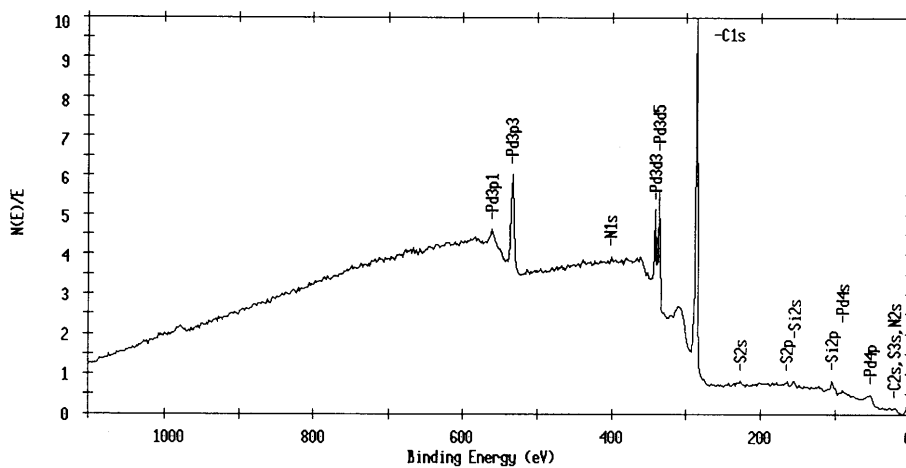


Fig. 5 XPS spectrum of the Pd point electrode after neutron emission

collected should be 17 nm in thickness, based on that the deposit density of 1.5 and carbon impurity of 1 PPM. Whereas, the thickness of the deposit should be more than 340 nm for the deposit to be seen black.

The environmental D_2 gas in the test cell includes 0.4 ppm CO , 0.6 ppm CO_2 and 0.1 ppm CH_4 at most. The total amount of carbon impurity in the gas can form carbon deposit of 250 nm in thickness. Thus, the carbon impurity both in the Pd electrode and in the environment D_2 gas does not account for the large amount of carbon on the surface of Pd point electrode.

The plausible explanation for the neutron burst and the carbon production is that the high current density at the point electrode and its fluctuation by glow discharge would stimulate the accumulation of deuterons to induce a fusion in the bulk near surface of Pd point electrode. The relatively low loading ratio of 0.6 allow us to conceive that high loading ratio is not always necessary but high current density is rather an important factor for the nuclear reaction. An atom such as helium would be produced from deuterons at the first reaction step; carbon would be produced from the atoms next. However, the total excess neutrons estimated was considerably few compared with the estimated number of carbon atoms on the surface of Pd point electrode. This indicates that the first reaction would produce a large number of atoms such as helium but few neutrons.

DISCUSSION

The Pd point electrode may include 1 PPM carbon at most. The point positive condition excludes the possibility that the carbon in the bulk of Pd point electrode was collected and condensed into the surface region by an electro-migration. Even though there exists another unknown mechanism for carbon impurity to migrate to the surface, the carbon

CONCLUSION

The large amount of carbon deposit was observed at the tip of D₂ loaded Pd point electrode after neutron burst under glow discharge condition in 2 atm D₂ gas, even though the phenomena are rare. The phenomena could be explained in terms of a nuclear fusion at the Pd point electrode.

ACKNOWLEDGMENT

This work was supported in part by a Grant-in-Aid for Scientific Research from Ministry of Education, Science and Culture. It was also supported in part by a Grant-in-Aid for Scientific Research from The Thermal and Electric Energy Technology Foundation.

REFERENCE

1. N. Wade and K. Nishizawa, *Jpn. J. Appl. Phys.*, vol 28 (1991), p 380.
2. A. De Ninno et al., *Europhys. Lett*, vol 9 (1989), p 221.
3. T. Mizuno et al., "Anomalous Heat Evolution from a Solid-State Electrolyte under Alternating Current in High-Temperature D₂ Gas," *Fusion Tech.* vol 29 (1996), p 385.
4. A. Takahashi et al., "Windows on Cold Nuclear Fusion & Pulsed Electrolysis Experiments," *Fusion Tech.* vol 19 (1991), p 380.

Editor's Note: The author's are invited to consider the possibility of high-density charge cluster formation. See Shoulders et al., "Observations of the Role of Charge Clusters in Nuclear Cluster Reactions," *JNE*, vol 1, no 3, Fall 1996.

EXPERIMENTAL EVIDENCE FAVORING BRIGHTSEN'S NUCLEON CLUSTER MODEL

Robert W. Bass ¹

ABSTRACT

Brightsen's Nucleon Cluster Model (NCM) predicts that a relatively low-energy photon can stimulate a nuclear transmutation under certain specified conditions. Examination of an experiment by Lin & Bockris demonstrates that the transmutation of mercury-201 to gold-197 induced by a mere exothermic chemical reaction (burning gunpowder) is an actual concrete example of the novel process predicted by the NCM.

INTRODUCTION

Ronald A. Brightsen has already presented considerable evidence [1, 2, 3, 4, 5, 6, 7], both theoretical and experimental, on behalf of the validity of his *Nucleon Cluster Model* (NCM) of the atomic nucleus. Briefly, by painstaking examination of the systematics and periodicities in both (Z,A) plots of the Atomic Number **Z** (i.e. number of protons, **P**), versus the Atomic Mass **A** (i.e. total number of nucleons, including both protons **P** and neutrons **N**, so that $A = P + N$) as well as (Z,N) plots, it is deduced that the nuclei of all beta-stable nuclides are comprised of just 3 basic building blocks: **deuterons**, **tritons**, and **helium-3** nuclei, which for brevity are referred to as **NP**, **NPN**, and **PNP** clusters.

In this author's opinion, the most striking evidence is presented in Figs. 7, 10, and 12-14 of [4], wherein experimental data for thermal neutron fission of U-235, U-233, Pu-239 and Pu-241 is plotted as percentage fission-yield versus Mass **A** (which ranges from $A = 80$ to $A = 160$) in comparison to the 80 predictions from the NCM which are presented. These are complicated double-hill, triple-valley shaped curves, and the *virtually identical agreement* between the NCM predictions and the experimental data (which in most cases is uncertain by up to ten to twenty percent) is truly stunning. In this author's opinion, Nobel Prizes have been awarded for comparable achievements which are not even as conclusively overwhelming, regarding agreement between theory and measurement, as in this case: noting that the experimental data are not perfect, the cited Figures are consistent with the assumption that the NCM *is* perfect and that the measured data *agree perfectly* (within experimental error). Reference [4] is one of the relatively few cases wherein world-class scientific information has been published in the patent literature prior to its appearance in one of the archive journals.

The NCM, in contrast to the more-often considered nuclear shell models based upon Quantum Mechanics (QM) and sub-nucleon models based upon Quantum Chromo-Dynamics (QCD), postulates that aggregates of any or all of the 3 fundamental clusters are present in the nucleus with their own separate quantized properties, such as energy levels, spin, magnetic moment, etc. Accordingly each *isotope* has *many* separate modes of existence, e.g. at different energy levels for *each* of the 3 basic clusters, which it is proposed herein to call the isotope's *isodynes*. In Brightsen's opinion, the observed statistical distributions of the properties of nuclides can be better explained by postulating actually physically distinct existence of each possible isodyne in a multi-isodyne population, as the result of which statistical predictions would be the results of ontologically real *population distributions* rather than being considered, as at present, as merely fictitious probabilistic QM calculations, acausally descriptive but not plausibly explanatory, such as are involved in the well-known Gamow theory of alpha-emission decay (which in the NCM would consist of decay by

¹ Innoventech, Inc., P.O. Box 1238, Pahump, NV 89041-1238, rbrtbass@pahump.com

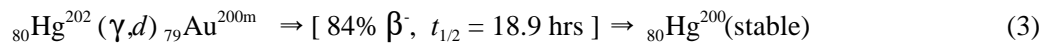
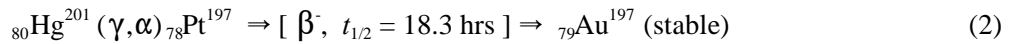
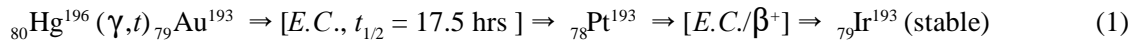
emission of a nucleus of a helium-4 consisting of two NP clusters [each of which could have its own distinct energy level, spin, magnetic moment, etc.]). The present author suggests that this idea is sufficiently meritorious to warrant further investigation.

Among the novel technical processes disclosed in the cited NCM-based patent application [4] is a procedure for artificially inducing fission of dangerous radioactive nuclei in order to produce stable, less hazardous elements. If externally-produced electromagnetic radiation happens to resonate with the magnetic moment of a particular sub-nuclear nucleon cluster, then such a cluster can be excited (independently of other clusters in the target nucleus) to the point where it will jump out of the nucleus, leading to the subsequent transmutation of the nucleus via fission and/or further decay into one or more daughter products of smaller atomic mass and greater natural stability against radioactive decay. The purpose of this note is to call attention to published experimental data which favors the reality of this patent-pending process invented by Brightsen *et al.* [4].

ANALYSIS

In 1992, Lin & Bockris [8] experimented with heating inorganic mixtures to produce anomalous radioactivity and anomalous apparent transmutations, such as mercury into gold, using alleged medieval alchemical methodology, such as boiling mercurous chloride (Hg_2Cl_2) in gunpowder (C, KNO_3 , S). During two such “burns” of gunpowder, anomalous beta radioactivity having half-lives of 17.7 hours and about 20 hours, respectively [average 18.9 hours], was measured.

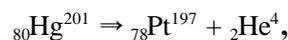
A careful examination of the various **half-lives** $t_{1/2}$ of possible reaction products leads to a limited number of possibilities, all of which proceed from stable isotopes of Hg, involving **triton** $t = {}_1\text{H}^3$, **alpha** $\alpha = {}_2\text{He}^4$, or **deuteron** $d = {}_2\text{H}^1$ emission and either **electron** (β^-) or **positron** (β^+) emission, or **electron capture** (*E.C.*), or **isomeric transition** (*I.T.*) in which the superscript ^m refers to a **meta-stable** nuclide:



All other possible radioactive products are either too short-lived or too long-lived to be consistent with the measured half-lives.

However, both ${}_{80}\text{Hg}^{196}$ and ${}_{80}\text{Hg}^{202}$ would have *zero* spin and *zero* magnetic moment. Since it is specified in the patent-pending process [4] that there must be a resonance between the incident photons (γ) and a sub-nuclear magnetic moment, it is clear that ${}_{79}\text{Au}^{193}$ and ${}_{79}\text{Au}^{200\text{m}}$ can be ruled out. Thus the measured data support the removal of a pair of NP clusters (${}_2\text{He}^4$) from Hg, i.e. artificially stimulated alpha-decay via ordinary thermo-chemical heat containing in its spectrum radiation of the precisely required type.

It is interesting to note that the (NP + NPN) + (PNP) formula shown in the **Atomic and Nuclear Periodic Table of Elements and Isotopes** [7] also balances in this context:



$$(60 + 10) \Rightarrow (58 + 10) + (2 + 0),$$

$$[(9 + 51) + 10] \Rightarrow [(7 + 51) + 10] + [(2 + 0) + 0].$$

CONCLUSION

No other logically consistent possibilities remaining, no possible conclusion seems consistent with well-established microphysical interpretation rules other than to deduce that the cited Lin-Bockris experiment empirically demonstrates a particular, but hitherto unsuspected, example of the patent-pending Brightsen process for artificial low-energy stimulation of specific nuclear transmutations.

REFERENCES

1. R. Brightsen, "Application of the Nucleon Cluster Model to Experimental Results," *J. New Energy*, vol 1, no 1 (1996), pp 68-74, 3 figs, 1 ref.
2. R. Brightsen, "Correspondence of the Nucleon Cluster Model with the Classical Periodic Table of Elements," *J. New Energy*, vol 1, no 1 (1996), pp 75-78, 4 figs, 1 plate.
3. R. Brightsen, *The Nucleon Cluster Model and the Periodic Table of Beta-Stable Nuclides*, available for \$5.00 S&H from Clustron Sciences Corp., 4500 S. Four Mile Run Drive (Ste. 804), Arlington, VA 22204, USA. Also available free on the wide world web at <http://www.gslink.com/~ncmcn/Clustron>.
4. R.A. Brightsen, H. Lowenberg, F. Forscher, D.R. George, E.F. Mallove, inventors, "Methods for Manufacturing and Producing Products," **WO94/03906, PCT/US93/07444**, International Application Published under the PCT, *WIPO*, Geneva, 17 February 1994, 20 figs, 31 claims.
5. Ronald A. Brightsen & Randolph R. Davis, "Application of the Nucleon Cluster Model to Experimental Results," *Infinite Energy*, vol 1, no 3 (July/August 1995), pp 13-15.
6. R.A. Brightsen, "Nucleon Cluster Structures in Beta-Stable Nuclides," *Infinite Energy*, vol 1, no 4 (Sept./Oct. 1995), pp. 55-56.
7. R.A. Brightsen, "Correspondence of the Nucleon Cluster Model with the Periodic Table of Elements," *Infinite Energy*, vol 1, no 5/6 (Nov. 1995/Jan. 1996), pp. 73-74.
8. G.H. Lin & J. O'M. Bockris, "Anomalous Radioactivity and Unexpected Elements as a Result of Heating Inorganic Mixtures," Second Annual Conference on Low-Energy Nuclear Reactions, *J. of New Energy*, vol 1, no 3 (1996), pp 100-105, 1 fig, 1 table, 12 refs.

ELECTRON CHARGE CLUSTER SPARKING IN AQUEOUS SOLUTIONS

By Atul Bhadkamkar and Hal Fox ¹

ABSTRACT

Valve metals (metals whose oxides provide electron emission) can produce luminescence in an aqueous solution. Luminescence increases with the applied electric potential up to a threshold value where sparks are visibly produced. This phenomena is explained by the controlled voltage gradient provided across the oxide layer of the valve metals. Some oxides can support an electric field gradient of one million volts per meter or more. When the gradient exceeds a critical value a **charge cluster** (believed to consist of about one hundred billion electrons) is emitted from the electrode. This charge cluster is believed to be the active mechanism in the **Neal-Gleeson Process** that can be used to fission heavy metal ions and reduce radioactivity.

INTRODUCTION

The discovery (patent pending) of the Neal-Gleeson Process has shown that naturally radioactive thorium and uranium compounds, dissolved in water to make an electrolyte can be stabilized by the use of an appropriate electrochemical reactor [1]. Kenneth Shoulders has shown that high-density charge clusters, under appropriate conditions, can cause nuclear reactions [2]. Sam Faile and Nicholas Reiter have shown that exploding bridge wires under atmospheric pressure and short high-potential electric discharges appear to produce some nuclear reactions [3]. Shoulders has further shown that the fracto-emission of charge clusters is a probable cause of the nuclear events and excess heat in cold fusion [2]. The combination of these experiments have been extended to explain a variety of current and projected experiments [4]. The basic premise proposed was that the creation of high-density charge clusters is much more prevalent than previously considered.

The authors have used the above premise to search the literature for some historic experimental and/or theoretical evidence of charge clusters. This paper reviews some of the literature dating from as early as 1957 (which cites a reference as early as 1906) to 1995. The few papers collected and cited in this article represent an exemplary but not exhaustive review of the historic experimental history of one version of the development of charge clusters.

THE VALVE METALS

In the early days of the growing electron-tube industry, the first electronic tube used as a diode was termed a **Fleming Valve**. The term **valve** for an electron tube was more prevalent in England than in the United States. The early electron emitters were the hot filaments. Later, the cathode was added. To make an effective cathode, a combination of a conducting metal and a substance that was a good emitter of electrons (thermionic emission) was required. It was found that certain metal and metal oxides were suitable. Thus, the term **valve metals**.

¹ Fusion Information Center, P.O. Box 58639, Slat Lake City, UT 84109.

As the solid-state devices (diodes and transistors) became popular, there was also a studied search for material that would provide the basis for controllable displays. Therefore, considerable experimental work was done with luminescence of certain metal oxides. To quote van Geel et al. [5] in their introductory remarks: "It has been known for a long time (cites A. Günthershulze, *Ann. Phys.* vol 21, pp 929-954, c1906) that during the anodic oxidation of several metals, such as Al, Zr, Ta, Zn, W, Mg, a light-effect occurs. In this process the metal is placed as the anode in a suitable electrolyte; during the passage of current oxygen is developed at the anode, an oxide film is formed, whilst at the same time luminescence can be observed." These same oxide films (at least some of them) can serve as electron emitters when suitably heated. The name for this series of metals has been **valve metals**, although it is hard to find literature that defines what precisely is meant by a **valve metal**.

BEYOND LUMINESCENCE

Some of the earliest papers we found [5] reported on experiments with oxide layers on aluminum. Later papers, such as Waring and Benjamini [6], Alwitt and Vijh [7], and Wood and Pearson [8], reported more generally on the development of luminescence and with the magnitude of the breakdown voltage on silicon and valve metals in general.

Some of the interesting observations include the following: van Geel et al., [5] report on the anode and cathode flashes when the aluminum oxide electrodes are powered with 200 cps alternating current at 25 volts. Waring and Benjamini [6] report on the phenomena of **breakdown** with the following comments: "Since the thickness of the oxide is proportional to the voltage ... there seems to be no reason to anticipate a limiting voltage or breakdown. We have, however, noted the increase in bubbling just before breakdown." Further, these authors note that: "Since the field during growth is about 1.6×10^7 v/cm [sic] and therefore near the breakdown limit anyway, this increase is enough to cause the weaker spots in the oxide to give way, thus **showing the sparks**." In their conclusions, the authors state, "**Spark** discharges penetrate into the solution," and, "When **sparking** begins, the general glow decreases; the current and luminescence are concentrated in these limited, intense, breakdown locations."

Alwitt and Vijh report on the breakdown voltage (at which visible sparking was observed) for a variety of valve metals including high-purity aluminum, niobium, tantalum, and zirconium. With the electrolytes used, the breakdown voltages varied from 100 to 350 volts. The authors suggest that the breakdown voltage is related to the thermal and electrical stability of the oxides; that the sparks were associated with a strong field extending into the electrolyte; and that sparking may be the electrical discharge through gas generated at the anode surface.

Wood and Pearson [8] reported that no sparking is observed with their use of molybdenum and vanadium. Tantalum, niobium, zirconium, and hafnium all displayed the spark-producing phenomena. With the electrolytes used, the authors reported no sparking with aluminum, titanium, and tungsten. The breakdown voltages ranged from 118 to 300 volts. Alloying of pure metals appears to reduce the breakdown voltages. A table of values is given for various niobium alloys, showing breakdown voltages ranging from 40 to 270 volts. These experiments were performed on anodes.

S. Ikonopisov provides a ten-page critical review that covers galvanoluminescence, anodic glow, cathode flash, anodic flash, alternating current glow, and continuous cathode glow [9]. Ikonopisov cites the earliest work on galvanoluminescence as being reported in 1887. However, the phenomena of most interest to this review, the breakdown of the oxide layers, are considered "beyond the scope of the present consideration." However, the author does provide a rather complete list of metals that show some degree of galvanoluminescence: Ag, Al, Bi, Cd, Ce, Ga, Hg, In, Mg, Nb, Sb, Si, Sn, Ta, Ti, W, Y, Zn, and Zr with references for each element. Here are a few of the interesting comments: "...even minute traces of halide contamination are known to create punctures or conducting corrosion spots in the anodic film on Al." "The

anode glow brightness increases markedly on simultaneous UV excitation." "...the anode glow-spectrum is continuous while the scintillation spectrum at the sparking voltage consists of lines due to aluminum and oxygen." "The threshold voltage (of anode glow) appeared to be almost independent of the frequency in the range from 16 Hz to 5 kHz but the output decreases at audio frequencies." "UV emission has been observed during anodization of Al, Ta, Si, and Mg...." In aluminum oxide: "The photoluminescent brightness increases with the temperature of previous heating of the films, but heating above 700°C produces an irreversible loss of the photoluminescence." There is evidence that "...the presence of water is indispensable for the anode glow."

S. Tajima [10] reports on luminescence breakdown of anodic oxide films on aluminum. This author states, "Thus the hitherto unsolved problems which had caused confusion in complete understanding of the art are almost solved." This 1977 summary article with 94 references has been followed by about twenty more years and we still have some unresolved mysteries in aluminum luminescence. Tajima does sort out and provide tables of some of the various forms of luminescence which contributes to a better appreciation of the phenomena. The author writes about adding impurities to aluminum to modify the luminescence and reports, "The intensity increases up to 20-30 times by addition of Mn 1.5%." This observation suggests that experimenters may want to try some degree of doping in their investigation of the sparking phenomena. Tajima also observes, "It is well known that in the case of breakdown by electron avalanche, the increase of dielectric film thickness and its temperature rise lower the electric field strength needed for breakdown. ... Therefore, higher formation voltage and thicker barrier layer make easier the breakdown by electron avalanche." Further, the author cites others, "...electrolytic breakdown is apparently controlled at the oxide-electrolyte interface rather than by the bulk oxide." Tajima, in Table 2, lists breakdown voltages for different electrolytes ranging from 20 to 500 volts.

Szklarczyk, Kainthla, and Bockris [11] report on the use of highly pure water and high voltages to explore the breakdown of the water between platinum electrodes. In some cases, the electrodes were coated with wax. Data included voltages as high as 30,000 volts. The following conclusions were reported by the authors: "The breakdown potential is the potential at which the Fermi level of the cathode becomes equal to the energy of the bottom of the conduction band of liquid water. Under such conditions electrons can be readily transferred from the cathode to the anode without interaction with water molecules. At the anode, holes would enter the valency band for water.. The head of the so-called streamers is occupied by electrons moving in the conductivity band of water at a rate too high for chemical interaction to occur."

Xu, Tzeng, and Latham [12] report that substantial emission of diamond-coated molybdenum electrodes can be achieved at potentials as low as 5,000 volts per meter. A most important finding was that points were not necessary. With the diamond coating, it appeared that the emission occurred with graphite impurities embedded in the diamond film. A clever experimental arrangement used a transparent anode so that video camera pictures could be taken of the emissions.

A short paper by Bonifaci, Denai, and Atrazhev [13] reports on experimental findings with various electrolytes on the onset of photoemission as a function of voltage. By using a needle-pointed tungsten electrode, it was found that a field strength of 10,000 volts per centimeter occurred at the tip of the electrode. Schwirzke [14] reports on the emission of electrons from spots on a cathode when the voltage is about 10^7 volts per meter. The author provides important information concerning the formation of a unipolar arc where positive ions are generated on or near the cathode surface and emitted to return to the cathode surface. The author states, "Since the emitting spot cannot deliver j_{CL} [maximum current density] without turning itself off, it must be that $j_{FE} < j_{CL}$." The symbol j_{FE} is the field-emitted current density. The author makes a strong point of the mechanism by which positive ions are produced at the cathode. Experiments were performed. The author indicated that, "The sound velocity of air at room temperature represents a lower limit for the expansion velocity of the desorbed particles." This statement suggests that the experiments were performed at atmospheric pressures. No data is provided to show variations as a function of the pressure of the gases

surrounding the arcing electrodes. However, the description of the formation of the unipolar arc suggests a method by which positive ions could be produced and entrained in a charge cluster and that this plasma sheath could be a part of the mechanism by which short pulses can produce toroid-shaped charge clusters.

Rousar et al. [15], reports on sparking at the cathode in electrochemical machining. The onset of sparking makes for a rougher surface and is to be avoided. Kirkici et al. [16], reports on the erosion of various films due to surface breakdown of the dielectric. It is important to note that the several different dielectrics (diamond on silicon oxide, diamond on silicon, diamond-like carbon on silicon oxide, diamond-like carbon on silicon, and silicon oxide on silicon) all suffer severe degradation after multiple repeated "shots" or breakdowns.

Hurlen and Gulbrandsen [17] show that the growth of the oxide layer is determined by both the growth next to the electrolyte surface and next to the metal surface. They note, "At the metal-oxide interface of a growing anodic film, the whole current is by metal ion transfer and possibly by electron transfer." Later in discussing equations the authors state, "...one should expect the anion transport to gain predominance at low current densities, and the cation transport to do so at high current densities." The authors also define a **passive film**: "...a steady-state passive film is considered to be a compact oxide film which has reached a steady thickness over which metal ions are transmitted from metal to solution at a steady rate, the potential independent steady-state passive current."

Gomer [18], citing 69 references, discusses the essential features and theory of field emission, field ionization, and field desorption. The concept of field emission is considered to be one of the key concepts in the creation of charge clusters. In the section on field emission in liquids, Gomer makes the following observation, "Although not exploited, to my knowledge, field emission can provide a simple method of electron injection into dielectric liquids without the use of either vacuum or high energy accelerators." His 1994 observation was certainly correct. Another observation, "It was also noticed that ion energy distributions were fairly narrow at low fields but broadened on the low energy side as the field increased. **This indicated very clearly that ionization then took place farther and farther in front of the emitter...**" Although these measurements were made in low-pressure gases, they may also be true in liquids, but at smaller dimensions. Gomer also notes a resonance effect that should be carefully studied by any who are working in low-pressure gases. See the potential energy diagram for electrons in an atom near a metal surface, as depicted in Fig. 1 (after figure 10 in Gomer's paper). In his section on field ionization, Gomer notes, "Field emission and field ionization are almost certainly the mechanism of dielectric breakdown in liquids."

One of the models for the onset of field emission is the presence of points, corners, whiskers, or other **projections** on the surface of the material providing the field emission. Jimenez et al. [19], provides evidence for the **projection** model on large-area cathodes. This careful study, using Nb and Au surfaces, supports the concept of **projections** being a useful source for field emission. However, the paper does not cover the high fields necessary for sparking. In contrast, Xu [12] found that with diamond coatings, the spots for field emission were often valleys. This difference was explained by the possible embedded graphite particles in the diamond layer.

Dumin et al. [20], discuss the breakdown of thin oxide layers by high field emission. This paper presents a model of the breakdown of an oxide layer that includes thickness, field, polarity, time, and temperature attributes. However, the article is mainly directed at the semiconductor industry. Metikos-Hukovic discusses the behavior of tin as a **valve**

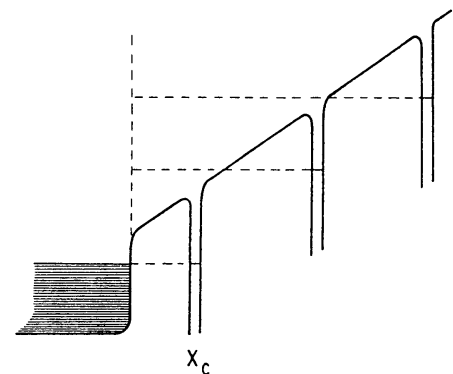


Fig. 1 Potential energy diagram for electrons in an atom near a metal surface in the presence of an applied field, illustrating the resonance effect in field ionization.

metal [21]. Some of the tin oxides are transparent. This feature was used by Xu et al. [12], in a clever method for viewing a cell's operation through a transparent anode window. Plastic deformation of cadmium affects the electroluminescence according to Dragon et al., in their 1995 paper [22].

More recently (1995) Ord and De Stet [23] describe some typical properties of **valve metal oxides** in their study of an ideal transparent anodic oxide film on zirconium. The oxide film grows by a high field conduction mechanism and the potential and film thickness increase linearly with time under constant-current growth. **Valve metal oxides** have a high relative permittivity, are strongly affected by electrostriction, and are optically anisotropic. The oxides exhibit the property of electrochromism, i.e., during cathodic reduction hydrogen is inserted into the oxide forming an optically-absorbing outer layer and the film is returned to its initial transparent state by subsequent anodic oxidation. The film is formed in a carbonate buffered aqueous electrolyte.

Hummel et al. [24], discuss the effect that spark-processing has on later cathode luminescence. The basic effect of spark-processing is to shift the wavelength of the cathode luminescence toward the blue end of the spectrum. Using a stream of compressed air during the spark processing also increases the brightness of the luminescence by as much as an order of magnitude.

A variety of papers have addressed the acceleration that can be provided to electrons by the **breaking of relativistic plasma waves**. Modena et al. [25], report on their efforts to provide improved electron acceleration by making use of the phase velocity of a plasma wave. Up to 44 MeV of accelerated plasma electrons has been achieved by this method. However, in the judgement of the authors of this paper, the creation and acceleration of electron charge clusters which carry positive ions is a more splendid method of creating high impact energies with relatively low input energies.

Jones and Kunhardt (Polytechnic University, Farmingdale, N.Y.) report on the development of pulsed dielectric breakdown in liquids [26]. This paper presents a thoughtful model of the four stages of the breakdown of liquids: 1. Formation of a low-density site near the electrode. 2. Growth and expansion of the local density so that ionization can take place. 3. Electron avalanche and formation of an ionizing front. 4. Propagation of the ionization front. The authors derive mathematical expressions for each of these stages of dielectric breakdown.

The authors would like to suggest a rather novel approach to the formation of bubbles and the **breakdown** phenomena. Julian Schwinger, a Nobel prize winner, suggested that the Casimir energy in filling a dielectric hole is the source of coherent sonoluminescence [27]. The concept is that a bubble of vapor in a dielectric fluid begins to diminish in size as the vapor gradually returns to a liquid state. At some radius of the bubble the Casimir forces become highly predominant and an very strong local blast of energy is produced (such as blue light) as the bubble accelerates to a collapse. The authors of this review paper suggest that the inverse procedure may be the source of some of the observed phenomena associated with the generation of an electron charge cluster.

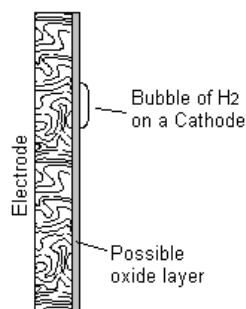


Fig. 2

As shown in Fig. 2, electrical energy is fed into a bubble at some local spot on the surface of an electrode. Because of the Casimir force (which is proportional to the fourth power of the radius), the formation of the bubble requires a considerable amount of local energy to be produced and fed into the bubble formation to overcome the energy of the Casimir force. As the bubble increases in size the expansion forces generated inside and stored in the bubble will overcome the Casimir force and explosively inject the energy into the local region near the electrode. This release of energy may help form the electron charge cluster. As shown by Shoulders [28], an electron charge cluster can ionize the local medium. In fact, it appears that the charge cluster can both provide energy to its

environment, especially by electron emission, and also maintain its own energy. The source of that energy may well be the space energy that produces the Casimir force itself. In this proposed method of breakdown of a dielectric liquid, the electron charge cluster is produced and the charge cluster itself becomes the means for ionizing, at least locally, the dielectric fluid. Apparently, the charge cluster will be expelled from the electrode (especially electrodes having a high-resistance layer where a strong electric field can be generated) into the fluid through the formation of a bubble, often at a surface projection or whisker.

Those who experiment with the creation of electron charge clusters in a dielectric liquid will, hopefully, be guided by reading some of the extensive literature, such as listed in the references to this article. When creating charge clusters to be used for the promotion of nuclear events in an electrolyte, the following protocols should be considered:

1. Sparking at the electrode is necessary but not sufficient for the production of nuclear events. Apparently a charge cluster can produce an observed spark but fails to have sufficient energy to promote a nuclear reaction.

2. It appears necessary to maintain (or periodically renew) the oxide layer on a valve metal to produce nuclear-active charge clusters. It is, of course, the concept that the charge cluster must carry piggy-back positive charges and must achieve a critical energy level to promote nuclear reactions [2].

3. The molarity (and the resulting conductivity of the electrolyte) may be an important operational parameter. The concept is that the charge cluster must be able to persist for some short time period and energetically impact a nucleus in the electrolyte to be able to produce a nuclear reaction. It is believed that the potential gradient between electrodes must be maintained at some critical value for nuclear reactions to be favored. A lower field gradient (higher conductivity) in the electrolyte may lead only to Joule heating and not to the desired level of nuclear reactions.

4. Experimental evidence suggests that the hydrogen and oxygen nuclei are involved in the sometime multiple or sequential nuclear impacts that result in the nuclear reactions.

5. The Coulomb barrier may be much less than the field strength of a charge cluster. The charge cluster must have sufficient electrons so that this field strength can aid in overcoming the Coulomb barrier before nuclear reactions can be expected.

REFERENCES

1. Robert Bass, Rod Neal, Stan Gleeson, & Hal Fox, "Electro-Nuclear Transmutations: Low-Energy Nuclear Reactions in an Electrolytic Cell," *Journal of New Energy*, vol 1, no 3, Fall 1996.
2. Kenneth and Steven Shoulders, "Observations on the Role of Charge Clusters in Nuclear Cluster Reactions," *Journal of New Energy*, vol 1, no 3, Fall 1996.
3. Reiter and Faile, "Spark Gap Experiments," *New Energy News*, Sept 1996, pp 11ff.
4. H. Fox, R.W. Bass & S-X Jin, "Plasma-Injected Transmutation," *Journal of New Energy*, vol 1, no 3, Fall 1996, pp 222-230, 4 figs, 23 refs.
5. W.Ch. van Geel, C.A. Pistorius, & B.C. Bouma, "Luminescence of the Oxide Layer on Aluminum During and after its Formation by Electrolytic Oxidation," *Philips Research Reports*, vol 12, no 6, Dec 1957, pp 465-490, 20 figs, 15 refs.
6. Worden Waring & E.A. Benjamini, "Luminescence during the Anodic Oxidation of Silicon," *J. Electrochem. Soc.*, Nov 1964, vol 111, no 11, 4 figs, 20 refs.
7. R.S. Alwitt & A.K. Vijn, "Sparking Voltages Observed on Anodization of Some Valve Metals," *J. Electrochem. Soc. Solid State Science*, March 1969, vol 116, no 3, pp 388-390, 1 table, 1 fig, 8 refs.
8. G.C. Wood & C. Pearson, "Dielectric Breakdown of Anodic Oxide Films on Valve Metals," *Corrosion Science*, vol 7, 1967, pp 119-125, 3 tables, 12 refs.
9. S. Ikonopisov, "Problems and Contradictions in Galvanoluminescence, A Critical Review," *Electrochimica Acta*, vol 20, 1975, pp 783-793, 158 refs.
10. S. Tajima, "Luminescence, Breakdown and Colouring of Anodic Oxide Films on Aluminum," *Electrochimica Acta*, vol 22, 1977, pp 995-1011, 9 figs, 3 tables, 94 refs.
11. M. Szklarczyk, R.C. Kainthla, & John O'M. Bockris, "On the Dielectric Breakdown of Water: An Electrochemical Approach," *J. Electrochem. Soc.*, vol 136, no 9, pp 2512-21, 21 figs, 32 refs.
12. N.S. Xu, Y. Tzeng, & R.V. Latham, "Similarities in the 'Cold' Electron Emission Characteristics of Diamond Coated Molybdenum Electrodes and Polished Bulk Graphite Surfaces," *J. Physics D: Applied Physics*, vol 26, no 10, Oct 14, 1993, pp 1776-1780, 5 figs, 10 refs.

13. N. Bonifaci, A. Denat, & V.M. Atrazhev, "Work Functions for a High-Voltage Cathode in Non-Polar Liquids," Proc IEEE 1993 - 11th World Conf on Conduction and Breakdown of Dielectric Liquids, 1993, 2 figs, 14 refs.
14. Fred Schwirzke, Michael P. Hallal, Jr., & Xavier K. Maruyama, "Onset of Breakdown and Formation of Cathode Spots," *IEEE Trans. on Plasma Science*, vol 21, no 5, Oct 1993, 9 figs, 8 refs.
15. I. Rousar & T. Riedel, "Sparking at Cathode Tools During Electrochemical Machining in Flow-Through Cells," *J. Applied Electrochemistry*, vol 24, 1994, pp 767-71, 4 figs, 19 refs, 1 table.
16. Hulya Kirkici, M.F. Rose, R. Ramesharm, & R.F. Askew, "Surface Breakdown Characteristics of Polycrystalline Diamond Thin Films in Vacuum," *Annual Report, Conf on Elect Insulation and Dielectric Phenomena 1994, IEEE*, pp 699-704, 4 figs, 6 refs.
17. T. Hurlen & E. Gulbrandsen, "Growth of Anodic Films on Valve Metals," *Electrochimica Acta*, vol 39, no 14, 1994, pp 2169-72, 3 figs, 16 refs.
18. Robert Gomer, "Field Emission, Field Ionization, and Field Desorption," *Surface Science*, vol 299/300, 1994, 12 figs, 69 refs.
19. M. Jimenez, R.J. Noer, G. Jouve, J. Jode, & B. Bonin, "Electron Field Emission from Large-Area Cathodes: Evidence for the Projection Model," *J Appl Phys*, vol 27, 1994, pp 1038-1045, 13 figs, 14 refs.
20. D.J. Dumin, S. Mopuri, S. Vanchinathan, R.S. Scott, R. Subramoniam, & T.G. Lewis, "High Field Emission Related Thin Oxide Wearout and Breakdown," *IEEE/IRPS Annual Proceedings - Reliability Physics 1994*, pp 143-153, 27 figs, 47 refs.
21. M. Metikos-Hukovic, A. Resetic, & V. Gvozdic, "Behaviour of Tin as a Valve Metal," *Electrochimica Acta*, vol 40, no 11, 1995, pp 1777-79, 2 figs, 19 refs.
22. R. Dragon, S. Wacke, & T. Gorecki, "Effect of Plastic Deformation on the Anodic Electroluminescence Accompanying the Early Stage of Electrolytic Oxidation of Cadmium," *J. of Materials Science Letters*, 1995, pp 1019-20, 2 figs, 14 refs.
23. J.L. Ord & D.J. De Stet, "Evidence for an Ideal Transparent Anodic Oxide Film on Zirconium," *J. Electrochem. Soc.*, vol 142, no 3, March 1995, pp 879-882, 7 figs, 14 refs.
24. R.E. Hummel, M.H. Ludwig, & S.S. Chang, "Strong, Blue, Room-Temperature Photoluminescence of Spark-Processed Silicon," *Solid State Commun.*, vol 93, no 3, 1995, pp 237-241, 3 figs, 20 refs.
25. A. Modena, Z. Najmudin, A.E. Dangor, C.E. Clayton, K.A. Marsh, C. Joshi, V. Malka, C.B. Darrow, C. Danson, D. Neely, & F.N. Walsh, "Electron Acceleration from the Breaking of Relativistic Plasma Waves," *Nature*, vol 377, 19 Oct 1995, pg 606.
26. H.M. Jones & E.E. Kunhardt, "Development of Pulsed Dielectric Breakdown in Liquids," *J. Phys. D.*, vol 28, 1995, pp 178-188, 5 figs, 85 refs.
27. Julian Schwinger, "Casimir light: The source," *Proc. Natl. Acad. Sci, USA*, March 1993, pp 2105-6, 6 refs.
28. Kenneth R. Shoulders, "Energy Conversion Using High Charge Density," U.S. Patent 5,018,180, issued May 21, 1991, see also "Circuits Responsible to and Controlling Charged Particles," U.S. Patent 5,054,047, issued Oct. 1, 1991.

SOME FEATURES OF H₂O LOW-PRESSURE DISCHARGE IN PULSE MODE

E.E. Antonov, V.G. Dresvyannikov, V.I. Popovich¹

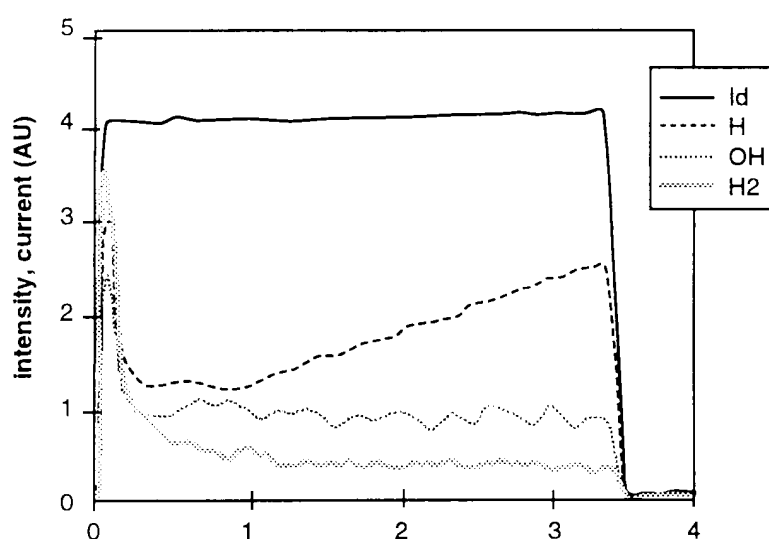
ABSTRACT

Our previous report [1] has been devoted to detailed investigation of plasma-chemical reactions between water molecules and charged particles in stationary low-pressure H₂O discharge plasma. Now we discuss some properties of above plasma in pulse mode. The aim of our research is to investigate the peculiarities of (H, OH, H₂) generation in this regime that is necessary for applied research on water conversion at atmospheric pressure.

DISCUSSION

The details of the experimental set-up are described in our previous report [1]. Low-pressure glow discharge in water vapor was created in cylindrical tubes made from molybdenum glass. A special system was provided for the generation of pulse plasma. The use of a computer diagnostic system allowed us to measure all necessary plasma parameters: density of electrons n_e , electron temperature T_e , temperature of heavy particles T_a and temperature of discharge tube wall T_o , water molecule concentration n_m , electric field strength E_z on the axis of the discharge, and discharge current I_d .

The diffraction monochromator MDR23 with photomultiplier tube FEU100 was provided for spectrum measurements. Optical methods were used for measuring the time dependencies of (H, OH, H₂) density in decaying H₂O plasma and in quasi-stationary regime (during discharge mode) by monitoring the intensity of certain spectral lines.



Plasma was created at total water vapor pressure $P_a = 0.7$ to 2.0 Torr. The pulses of discharge current were rectangular shaped (see Fig. 1, solid curve). The pulses amplitude I_{d0} changed from 20 to 200 mA, their duration $\tau_o = 3.5$ to 6.0 ms, the period of pulses replication $t_p = 6$ to 25 ms.

1. First of all, the flux of gaseous products Q_m from the reaction zone was measured for the discharge mode similar to our experiments [1] in a stationary regime. It was

Fig. 1. Time variation of discharge current I_d and spectral line intensities for discharge mode of water vapor plasma. Gas pressure $P_a = 2.0$ Torr; Amplitude of discharge current $I_{d0} = 200$ mA; Pulse duration $\tau_o = 3.5$ ms.

¹ Scientific-Technical Centre for Coal Energy Technologies, Kiev, 19 Andreevskaya St., 254070, Ukraine

stated that flux Q_m for given t_p depends on τ_o value (see Fig.2). It is important that it is possible to obtain from the curve $Q_m = f(\tau_o)$ the parameter τ_p that characterizes the time of reactions which are reverse to water conversion reactions.

Earlier, [1] we stated that for low-pressures the dissociation of H_2O molecules in discharge mode is provided, basically, by two mechanisms:

(I) by vibrational excitation of water molecules by electron impact with the subsequent conversion of these molecules:



and (ii) by dissociative attachment of electrons to water molecules:



where M is water molecules and/or water conversion products.

For determination of the τ_p value, suppose that the relaxation process for particle density takes place by the following method:

- (a) during the discharge mode the generation of conversion products n_p due to reactions (1) & (2) with the rate ($q n_m$) and their decay in reverse reactions with characteristic time τ_p takes place,
- (b) during the decay mode, the de-generation of conversion products with the rate (n_p/τ_p) occurs.

So, the kinetic equation for relaxation process in discharge mode may be written as:

$$dn_p / dt = q n_m - n_p/\tau_p \quad (3)$$

The solution of this equation may be taken in general form:

$$n_p(t) = q n_m \tau_p + C \exp(-t/\tau_p), \quad (4)$$

where C is the constant which is defined by the initial conditions.

During the discharge mode, the so-called quasi-stationary regime is set up when the quantity of water conversion products n_p generated during the time τ_o is equal to the quantity of products de-generated during the time between pulses ($t_p - \tau_o$). Let n_{p1} be the quasi-stationary concentration of conversion products at the beginning of each discharge pulse and n_{p2} be the same concentration at the pulse end. Then from (4) for $t = 0$ (the moment of the beginning of the discharge pulse under consideration)

$$C = n_{p1}(0) - q \tau_p n_m$$

Let $C_0 = q \tau_p n_m$. Then from (4) for $t = \tau_o$:

$$n_{p2}(\tau_o) = C_0 + (n_{p1}(0) - C_0) \exp(-\tau_o/\tau_p) = n_{p1}(0) \exp(-\tau_o/\tau_p) + C_0 (1 - \exp(-\tau_o/\tau_p))$$

Taking into the account that $n_{p1}(t_p) = n_{p2}(\tau_o) \exp\{-(t_p - \tau_o)/\tau_p\} = n_{p1}(0)$ from above relationships, it is easy to obtain that

$$n_{p2}(\tau_0) = C_1 \{1 - \exp(-\tau_0/\tau_p)\} \quad (5)$$

where $C_1 = C_0 \{1 - \exp(-t_0/\tau_p)\}^{-1}$.

Thus, the dependence $n_{p2} = f(\tau_0)$ represents the characteristic time τ_p of reactions reverse to (1) & (2). For instance, for $t_p = 6.3$ ms and $P_a = 2.3$ Torr (discharge conditions illustrated by Fig. 2), the relaxation time $\tau_p = (1.4 \pm 0.2)$ ms. If one of above reactions dominates, it is possible from τ_p value to obtain the appropriate reaction rate constant.

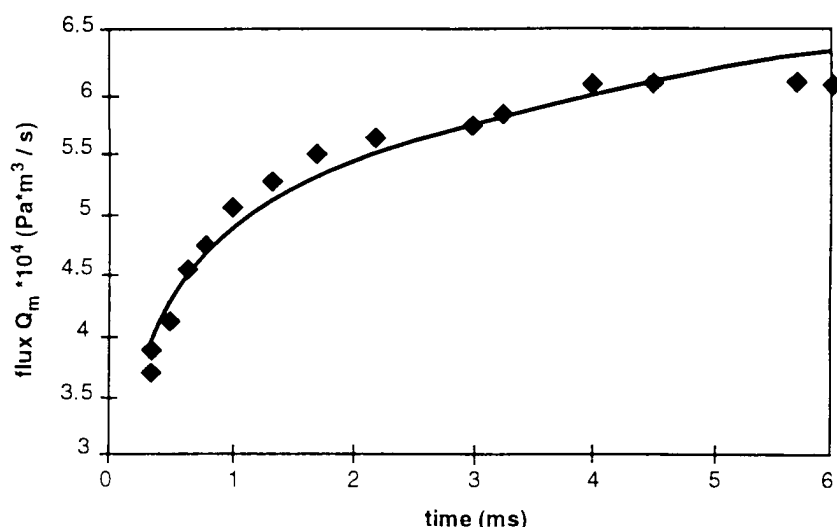


Fig. 2. Flux of gaseous products of water molecule conversion from the reaction zone versus pulse duration τ_0 . Water vapor pressure $P_a = 2.3$ Torr; Amplitude of rectangular discharge current pulse $I_d = 20$ mA; Period of pulses replication $t_p = 6.3$ ms.

2. For the decay mode of water vapor plasma, the intensities of some spectral lines were measured versus the time t_d after the end of discharge pulse. It was stated that for $t_d \sim 1$ mks [microseconds] the intensity of spectral lines of OH(306 nm), H(656 nm) and H₂(630 nm) diminishes to the noise level. It is clear that the time of this phenomenon is ruled by the rate of T_e and n_e relaxation. Due to very short times t_d it was difficult to measure the concentrations of above components during the decay mode by optical methods.

However, for the discharge mode (quasi-stationary regime) optical diagnostics appeared to be very useful. Practically for all investigated discharge regimes the time course of the intensities of OH (306 nm) and H₂ (630 nm) spectral lines (and, accordingly, of above component concentrations) had the similar behavior: at the moment of the discharge gap breakdown ($t_s = 0$) the sharp increase of the density of OH radical and H₂ molecule took place (see Fig. 1 and Fig. 3).

The aperiodical τ ($t_s \sim 20$ mks) oscillating process of concentration stabilization, which is clearly seen in Fig. 3, is connected with some instability of discharge current. For discharge current $I_{d0} = 200$ mA, the oscillating process of discharge current stabilization is limited to $t_s \sim 20$ to 30 mks. The period of the oscillating process for OH and H₂ concentration is seen in Fig. 3. For $t_s = 30$ to 40 mks, the intensity of OH and H₂ molecular bands has the maximum and then diminishes to its stationary value by exponential law. This stationary value of OH and H₂ concentration was stabilized for $t_s = 200$ to 300 mks. The ratio between maximum and stationary

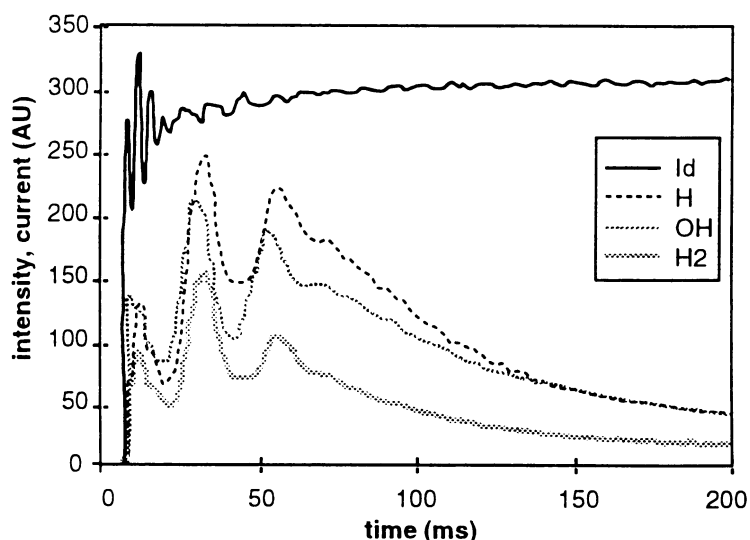


Fig. 3. Time stabilization of spectral line intensities for discharge mode of water vapor plasma. Gas pressure $P_a = 2.0$ Torr; Amplitude of discharge current $I_{d0} = 200$ mA; Pulse duration $\tau_0 = 3.5$ ms.

values of OH and H₂ concentrations depends on the discharge regime (first of all, on the discharge current I_{do} and water vapor pressure P_v) and ranges from 10 to 50.

The time course of H (656 nm) spectral line intensity for t_s = 0 to 200 mks differs very slightly from appropriate curves for OH and H₂ (see Fig. 1). However, the above time course for H differs markedly from the one for OH and H₂ for t_s > 200 mks up to the end of the discharge pulse in all investigated pulse duration ranges. The concentration of atomic hydrogen goes to its minimum for t_s ≈ 250 to 300 mks and then slightly enlarges for its stationary value at t_s ≈ 6 ms (see Fig. 1, dashed curve). Experiments showed that the variation of t_p value in (10 to 25) ms range practically does not influence the relaxation of above component concentration. The pumping of reaction products and the variation of discharge current amplitude I_{do} also has no effect on the time course of OH, H and H₂ concentrations.

3. The increase of H density with the growth of pulse duration for τ_o > 300 to 400 mks is one of the most interesting experimental results for pulsed water plasma. For investigation of this phenomenon let us consider in detail the process of ion-electron dissociation of water vapor.

For the stationary regime, the detailed analysis [1] of plasma-chemical processes was made by the following equation system:

$$JE - n_m / \tau_{vt} \{ \epsilon_v(T_v) - \epsilon_v(T) \} - Q_v(T_v - T_o) / D_o^2 = 0, \quad (6)$$

$$n_m / \tau_{vt} \{ \epsilon_v(T_v) - \epsilon_v(T_g) \} - Q_t(T_g - T_o) / D_o^2 = 0, \quad (7)$$

$$k_1 n_m n_e + k_d n_m n^+ - k_a n_m n_e - k_a^* n_e n_m^* - k_{ei} n_e n^+ = 0, \quad (8)$$

$$k_a n_e n_m + k_a^* n_e n_m^* - k_d n_m n_e - k_{ii} n^+ n^+ = 0, \quad (9)$$

$$n_e + n^+ = n^+, \quad (10)$$

where $\tau_{vt} = k_{10} \cdot n_a \{ 1 - \exp(-\epsilon_{vo}/kT) \}$; k₁₀ is the reaction rate constant for vibrational excitation; n_a is the density of the component at which the relaxation of vibrational excitation of H₂O molecules takes place (in the case of small discharge currents n_a ≈ n_m); ε(T_v) is the average vibrational energy for one water molecule at vibrational temperature T_v; ε_{vo} is characteristic value of vibrational quantum of H₂O molecule; Q_v is the heat-transfer coefficient for vibrationally-excited H₂O molecules; D_o, T_o is the diameter of discharge tube and the temperature of its wall; Q_t is the heat-exchange coefficient; n_m^{*} = n_m exp(-ε/kTv), accordingly.

The numerical solution [1] of above system for stationary regime gives a good agreement between theoretical and experimental data on water conversion. However, this equation system can also be applied for quasi-stationary regime. Really, the density of the power W_z supplied into the quasi-stationary discharge can be written in the form:

$$W_z = J_d(U/d)\tau_o \quad (11)$$

because the main part of the energy is supplied into the discharge during the after-breakdown stage of the discharge. In (11) J_d is the quasi-stationary value of discharge current density; d is the characteristic value of the discharge gap; U is the discharge voltage; τ_o is the discharge pulse duration.

Characteristic time of ionization-recombination kinetics τ_{ic} = 10⁻⁶ to 10⁻⁵ s, time of chemical reactions (including the generation of vibrationally-excited H₂O molecules) τ_{ch} ≈ 10⁻⁴ to 10⁻³ s, time of diffusion processes τ_{dif} ≥ 10⁻³ s. For τ_o > (τ_{ic}, τ_{ch}, τ_{dif}) the discharge can be treated as a quasi-stationary one. The above estimates were obtained for typical parameters of water discharge plasma: P_a ~ 10 to 50 Torr, T_e > T_v > T_g, T_e ~ 0.3 to 1.5 eV, T_v ~ 1000 to 5000 K, T_g ~ 300 to 600 K, n_e/n_a ~ 10⁻⁶, d ~ 1 cm. From the upper side, the

τ_0 value is limited by the characteristic time of plasma instabilities. So, the equation system (6) to (10) can also describe plasma parameters for the stable quasi-stationary molecular plasma.

Reaction rate constant k_{ei} for the process of ion-electron dissociation of water {the term ($k_{ei}n_e n^+$) in Eqs. (6) to (10)} slightly depends on electron temperature ($\sim T_e^{-1/2}$). For the quasi-stationary regime this reaction is the main channel for positive ions de-generation. However, the H_2O^+ ion is not the only positive ion in water vapor plasma. The ion-molecular reactions of primary H_2O^+ ions with neutral H_2O molecules give also the H_3O^+ ions and OH radicals:



Taking into the account that $n_{H_2O} \gg (n_{OH}, n_H, n_{H_2})$ and the fact that reaction (12) is very fast, it can be stated that H_3O^+ ion is one of the main positive ions in the discharge.

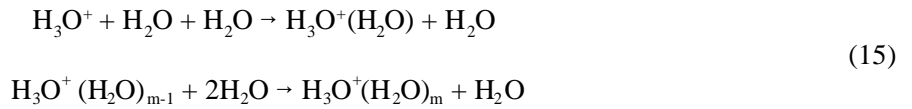
On the one hand, OH radicals formed in (12) produce the atomic hydrogen in the reaction with vibrationally-excited molecules H_2O^* :

$$dn_H/dt \sim k_d n_{H_2O}^* n_{OH} \quad (13)$$

where n_H is the concentration of atomic hydrogen; k_d is the reaction rate constant for the reaction $H_2O^* + OH \rightarrow OH + H_2O_2$. For $T_v = \text{const.}$ the concentration of H atoms in discharge zone is stable due to the counterbalance of all de-generation processes by the process of H generation in reaction (13) and in some other reactions:



On the other hand, the main property of H_3O^+ ion is its ability to form the cluster ions $H_3O^+(H_2O)_m$ ($m=1,2,3,\dots$) [2]. The increase of the difference between T_v and T_g stimulates the increase of cluster ion concentration:



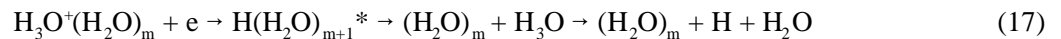
because the reaction rate constant for (15) depends on T_v .

Thus, due to the reactions (12) and (15) the ions H_3O^+ and $H_3O^+(H_2O)_m$ are available in the system. These ions very actively participate in the ion-electron recombination.

The rate of the reactions



slightly decreases with the increase of electron temperature T_e but the rate of the reaction



is independent on T_e [3]. Thus, the total ion-electron recombination rate in quasi-stationary regime is practically constant due to $T_e \cong \text{const.}$

However, for stationary conditions the probability of complex cluster ion formation depends strongly and inversely on gas temperature T_g . Really, for $T_g \sim 600$ K the number $m \sim 2$ to 3, so the binding energy for

cluster particles in not high ($E_c \sim 0.3$ to 0.4 eV) and under the growth of T_g the intensive decomposition of cluster ions $H_3O^+(H_2O)_m$ takes place. Thus, for above conditions the effective coefficient for ion-electron recombination β_{eff} which can be written in the form:

$$\beta_{eff} = (\sum_{(m)} k_{ie}^{(m)} n_{(m)}^+ n_e) / (\sum_{(m)} n_{(m)}^+) = \beta_{eff}(T_g) \quad (18)$$

is also the function of T_g . In (18) $n_{(m)}^+$ is the concentration of cluster ions $H_3O^+(H_2O)_m$, which depends on T_g . So, according to (18) the rate of atomic hydrogen H generation in ion-electron recombination reactions (17) is defined by T_g . In this sense, the situation is similar to the thermal decomposition of water molecules. In that case, under the increase of the power W_z supplied into the discharge, the increase of T_g takes place and, accordingly, the increase of thermally decomposed H_2O molecules occurs.

Earlier [1] our calculations showed that for low W_z value $\{J_d \sim (2$ to $5) 10^{-3} A/cm^3\}$ the temperature T_g is constant and its magnitude is equal to the temperature of discharge tube wall T_o . For pulse discharge under the increase of the power W_z temperature T_g also is increased by more then two times for $t_s \sim 30$ to 100 mks. So, taking into account that neutrals H_3O formed in the reaction (17) are intensively decomposed under the growth of T_g , the time variation of H concentration due to ion-electron cluster recombination (17) can be represented by the following expression:

$$n_H \approx n_H^0 + n_{(H_3O)_m} + n_e k_0^{-4600/T_g(t)} \quad (19)$$

where n_H^0 is the concentration of atomic hydrogen for the discharge mode where $T_g \sim T_o = \text{const}$. The above dependence is shown in Fig. 4. It can see a good agreement with experimental data (Fig. 1, dashed curve). Note, that value $t_s = 30$ to 50 mks defines the characteristic time of pulse duration when the energy W_z supplied into the discharge is consumed for the water conversion process in the most effective way.

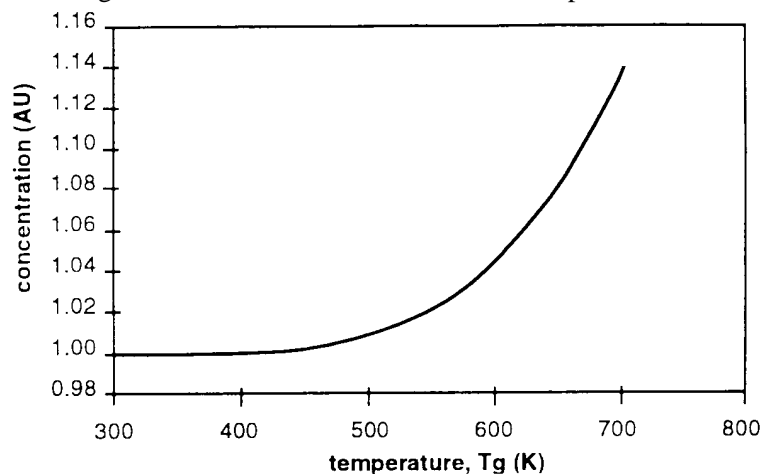


Fig. 4. Concentration of H radicals P_h versus gas temperature T_g for discharge mode of water vapor plasma.

CONCLUSIONS

The pulse discharge at low pressure is a very important step for stimulation plasma-chemical processes of water conversion. To achieve the largest affectivity of such processes, the removal of water conversion products from the discharge reaction zone is necessary. The rate of above removal should be comparable with the rate of reverse reactions. So, one of the possible ways is the use of pulse discharge. Our experimental and theoretical investigations have shown that it is necessary to have pulses not

longer than 50 to 100 mks. For large time durations, the useful product output is being decreased due to the reverse reactions.

The pressure growth in the system and the transition from glow discharge to the other types of high-voltage discharges are necessary to increase the (H_2+O_2) output. This should be accompanied by increasing the pumping rate of initial mixture through the reaction zone. Otherwise, the downturn of the power efficiency of water molecules decomposition processes will take place due to the consumption of supplied energy into the unproductive channels, for example, into the excitation of electronic states of H_2O molecules or into the heating of molecular gas.

The investigation of water vapor discharge in a pulse mode at atmospheric pressure will be the next step in our research. This data is necessary for applied developments in this field and for creation of practical devices for water conversion.

Acknowledgements

The authors deeply thank the German Association of Vacuum Field Energy and DVS President - Dr. Hans A. Nieper for supporting and financing these researches.

REFERENCES

1. E.E. Antonov, V.G. Dresvyannikov, V.I. Popovich, "Dissociation of Water Molecules in Low-Pressure Discharges," *Energy Saving Problems*, 1995, v.4-6, pp.92-109 (Rus.). Deutsche Vereinigung für Schwerkraft-Feld-Energie Brochure, N.34., 1996 (Eng.).
2. E.E. Antonov, V.G. Dresvyannikov, "Generation of Clusterization Centres in H₂O Low-Pressure Discharge," Proc. of XXth Int. Conf. on Phen. in Ionized Gases, Italy, Piza, 1991, v. 1, pp.61-62.
3. V.D. Rusanov, A.A. Fridman, Physics of Chemically Active Plasma, Moscow: Nauka, 1984.- 415 p.

ANTI-GRAVITY IMPLIES INFINITE FREE ENERGY

Robert Bass

ABSTRACT

If the empirical Podkletnov Effect (*Journal of New Energy*, vol 2, no 2, ref 4, p 136) is confirmed to be physically valid as described, then it will be simple to produce unlimited **free energy** from some hitherto untapped renewable source. Indeed, the device described *loc.cit.* [*cf.* also *Business Week*, Sept. 30, 1996, p 42] produces a constant reduction in the measured weight of an arbitrary test mass when run in steady-state at constant power. But this means that the total **energy input** grows **linearly** with time, whereas the total **energy output** stored in a vertically-arrayed flywheel (driven by the torque producible from asymmetric weight-reduction and consequent unbalanced unidirectional torque generated as each successive portion of the flywheel's rim becomes tangent to the Podkletnov beam) grows **quadratically** with time. The announced result follows at once.

INTRODUCTION

The reason for predicting that a rotary engine of the type discussed below will produce more energy than that required to drive it, is the result of the kind of *Gedankenexperiment* (thought experiment) to which Einstein attributed his deepest discoveries and for which he is famous. Start with an acceleration ray [1-3], which produces a small but noticeable effect, no matter how small. On the principle that an ion engine has been advocated as useful for deep-space voyages even though its thrust is microscopic and its initial acceleration is measurable only in micro-gees, a very, very small generator of an acceleration ray will, in a sufficiently long time, produce a noticeable angular acceleration of a perfectly-balanced, frictionless flywheel, even if one must wait for "years" for the effect to become noticeable.

Moreover, if the ray persists for a sufficiently long time, the flywheel (assuming it is ideal, and will not fly apart) is capable of storing **ANY** amount of angular momentum and **rotational kinetic energy**, no matter how large, which grows as the **square of the time**, whereas **the averaged power** consumed by the ray generator grows only **linearly with time**; accordingly, **no matter how small is the acceleration effect**, there will be a finite time after which **the energy stored in the flywheel is greater than the energy used to power the beam generator**.

ANALYSIS

To see this more explicitly, suppose that the **averaged** power consumption of the beam generator [1, 2, 3] is given by k watts per unit time, where k is a constant. Let the flywheel consist of two masses of size M connected by lever arms of length L to the axis of rotation. Then the moment of inertia of the flywheel is given by $I = ML^2$. Let the acceleration to a mass M by the beam be denoted by a . Then the unbalanced **unidirectional** torque on the flywheel is given by $T = aML$, and so the angular acceleration of the flywheel is $T/I = a/L$; therefore, after t seconds the angular velocity will be at/L . Consequently, the kinetic energy of the flywheel after t seconds will be

$$E_f = (1/2) I (a t/L)^2 = (1/2) M a^2 t^2 = K t^2$$

where $K = (1/2) M a^2$ is a **constant**.

But at that time t , the total energy consumed by the beam generator will have been just $E_b = k t$. One concludes that the **ratio of energy consumed** in driving the flywheel versus **energy stored** in the flywheel, is $E_b/E_f = (k/K)/t$, which as t increases becomes **arbitrarily small!** Then the energy input is negligible in comparison to the usefully available energy output!

An alternative formulation is that $E_f > E_b$ as soon as $t > (k/K)$.

DISCUSSION

Where did the "excess energy" ($E_f - E_b$) come from? Presumably the SED theory of Puthoff to the effect that an accelerating charge can pick up energy from the background ZPF is correct, and so one is tapping into 10^{90} Joules [or more] per cm^3 that modern microphysics says, according to either QED or SED, is available for use but hitherto unexploited. For documentation, note the well-annotated study of several contemporaneously advocated inertial-mass-modification (i.e. anti-gravity!) experiments by R.L. Forward [4], which also contains a list of 28 "active researchers in **vacuum fluctuations**."

Consequently, the essentially zero-pollution rotary engine discussed above can, in principle, actually continuously produce more useful energy than is required to operate it! This startling result smacks of "perpetual motion," long rejected by the Establishment as *a priori* "impossible."

But if any of the new theories surveyed by Forward [4] turn out to be "correct" (in the sense that they make only verifiable predictions and make no **observably falsified** predictions), then they will be tentatively accepted by all true scientists as (provisionally) acceptable [true scientists regard ALL propositions as tentative!] But then the question arises, how to explain, e.g. by the Puthoff *et al.* ZPF theory, the persistence and quantization of **spin in QM** and QED? Puthoff has admitted to Bass in private E-mail messages that were later published in the *Cold Fusion Newsletter* that this is, and remains, the big unsolved mystery.

If indeed the Li-Torr idea [1] that the spinning of ions in a superconductor is the key to artificial acceleration rays is correct, then the question arises: where does the energy come from that keeps the ions spinning, despite the loss of energy to gravitational waves? It is not incumbent upon the present author to answer that question in fundamental physics in order to be entitled to point out that if the accidentally-discovered, strictly empirical Podkletnov Effect is authentic, then the excess energy must be coming from somewhere.

Regarding the competing "schools" of QM + QED versus SM + SED, i.e. versus Stochastic Mechanics (SM), as in Edward Nelson's work, plus Stochastic Electrodynamics (SED), as in the work by Puthoff *et al.* cited in [4], it is unknown whether QM + QED or SM + SED is the better theory. Therefore, the reader is at liberty to ascribe the unknown source of energy to the **paradoxically nonsensical Zero Point Energy (ZPE)** of the "virtual polarized vacuum" of QED **or** to the **real ZPE** of the "actual energetic vacuum" of SED, **or** to some **other** hitherto **unknown** source, such as an energetic aether.

CONCLUSION

Tapping a novel source of **near-infinite** (or **renewable**) **ambient energy**, hitherto untapped, does not constitute "impossible perpetual motion," nor a violation of Conservation of Energy; it just involves **extracting ambient energy** from the ZPE or ZPF, **whichever or whatever** it may be. (Orthodox physicists claim that there is enough energy in a vacuum whose volume could be contained between the reader's cupped hands to boil all of the oceans of the world!) With this vast ocean of untapped energy surrounding us at all times, the possibility remains that the non-polluting rotary engine discussed above is merely somehow tapping into something like the incredible reservoir of the little-understood vacuum-fluctuating ZPE/ZPF!

Accordingly, it is perfectly possible in principle to use such an acceleration-beam powered rotary engine, **once started**, to drive an auxiliary rotary electrical generator which drives the acceleration-ray generator which drives the primary rotary engine, and thereby to provide a **self-contained** rotary engine which (until it wears out from mechanical friction) produces limitless amounts of both mechanical and alternating-current electrical power without requirement of any external source of energy whatsoever!

REFERENCES

1. Frank Znidarsic, "The Zero Point Interaction," *J. New Energy*, vol 1, no 2, Summer 1996, pp 133-136, esp. Refs. 4a,b,c,d,e to papers by Li, Torr, Podkletnov, Modanese.
2. Otis Port, "Take That, Isaac Newton," *Business Week*, Sept. 30, 1996, p 42.
3. Chris Tinsley, "Table-Top Anti-Gravity?" *Infinite Energy*, vol 2, no 9, July-Aug. 1996, p 49.
4. Robert L. Forward, "Mass Modification Experiment Definition Study," *Infinite Energy*, vol 2, no 9, July-Aug. 1996, p 53-64.

EDITOR'S CHOICE

EXPERIMENTS OF UNDERWATER SPARK DISCHARGES
WITH PINCHED ELECTRODESTakaaki Matsumoto ¹

ABSTRACT

Experiments of sparking discharges were performed in ordinary water mixed with potassium carbonate. Here thin metal wires of palladium, nickel, titanium, iron, cadmium, molybdenum and tungsten were used as electrodes. In high voltages over 40 V, the surface of the electrode was pinched so that sparking appeared on the cathode or anode, and simultaneously extraordinary phenomena were observed. Especially, microscopic ring-clusters generated on the cathode caused tiny ball-lightning-like phenomena. The extraordinary phenomena was explained by The Nattoh Model.

INTRODUCTION

Recently many experiments of the electrolysis of heavy water have been performed since the cold fusion phenomena was published [1]. The studies have been mainly focussed to reproduce and enhance the excess heat, in which deuterium is charged into a metal to induce the cold fusion reactions. On the other hand, the author earlier proposed The Nattoh Model predicting that the cold fusion reactions can be induced in an extremely compressed hydrogen-cluster ("itonic" state) that can be easily generated by an electrical discharge [2], and showed that many extraordinary phenomena appeared associated with the cold fusion reactions in the experiments of the pulsed electrical discharge in water [3, 4].

This paper describes experiments of continuous discharges in ordinary water mixed with potassium carbonate, in which thin metal wires were used. Here the pinch effect of the current effectively worked to compress hydrogen-clusters on the cathode so that sparking appeared, associated with many extraordinary phenomena. Especially, many microscopic ring-clusters generated on the cathode caused tiny ball-lightning-like phenomena. The extraordinary phenomena were explained by The Nattoh Model.

EXPERIMENT

Experiments of the sparking discharge were performed using the DC continuous discharge in ordinary water. The experimental arrangement is shown in Fig. 1.

Thin wires of pure metals of palladium (99.95 %, 0.50 mm ϕ), nickel (99.7 %, 0.50 mm ϕ), titanium (99.9 %, 1.0 mm ϕ), iron (99.998 %, 1.0 mm ϕ), cadmium (99.9999 %, 1.0

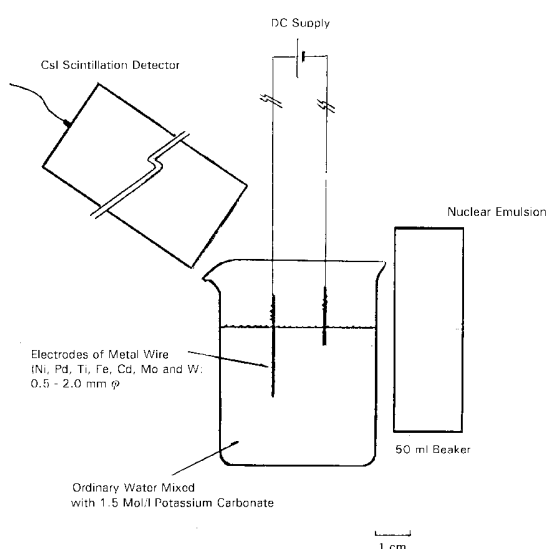


Fig. 1

¹ Dept. of Nuclear Engineering, Hokkaido Univ., Sapporo, 060 Japan

mm ϕ), molybdenum (99.95 %, 1.0 mm ϕ) and tungsten (99.95 %, 2.0 mm ϕ) were used as the electrodes. The wire electrodes were vertically immersed in ordinary water mixed with about 1.5 mol./l potassium carbonate, that was contained in a glass beaker (45 mm ϕ). The effective lengths of the cathode and anode that were inserted in the solution were about 3 mm and 15 mm long, respectively. On the shorter electrode, the current density could be increased such that the pinch effect of the current effectively worked to compress hydrogen molecules [2].

The DC discharge was continuously employed between the electrodes, in which the voltage was varied up to about 150 V under the constant voltage mode. The sparking that appeared on the surface of the electrode over 40 V was observed by a system of a micro telescope and a videotape recorder (VTR). The emission of radiation was monitored by a spectroscopy with a CsI(Tl) scintillation detector (12.5 mm x 12.5 mm x 20.0 mm). Furthermore, nuclear emulsions were located near the cathode. The nuclear emulsions (100 μ m x 50 mm x 50 mm, coated on both sides of 1 mm thick acrylic plate) were the same as those that were used in previous experiments [5, 6]. After the discharges, the electrodes were analyzed by an optical microscope (OM), a scanning electron microscope (SEM) with an energy dispersive X-ray spectroscopy (EDX), an electron probe microscope analyzer (EPMA) and a X-ray spectroscopy (XS).

RESULTS

A. Nonlinear Characteristics of I/V

The DC current was employed between the electrodes under the constant voltage mode. Fig. 2 shows the strong nonlinearity of the I/V characteristics in which the nickel wires were used for both the electrodes and the cathode was shorter. They were divided into three regions. In the lower voltage region, about 40 V, the current proportionally increased as the voltage increased. Here, the layer of the resolved hydrogen gas also was steadily increased on the cathode. In the intermediate voltage region between about 40 V and 60 V, the hydrogen gas seemed to burst and evolve from the cathode, and the current strongly fluctuated. In the higher voltage region, about 60 V, the pinch effect of the current effectively worked to suppress the gas evolution, and tiny sparks appeared on the surface of the cathode. They initially appeared on the bottom tip of the cathode and as the voltage increased, the number of the tiny sparks increased to eventually cover the whole surface of the cathode. Here, the current was strongly suppressed to a stable level of about 0.1 A.

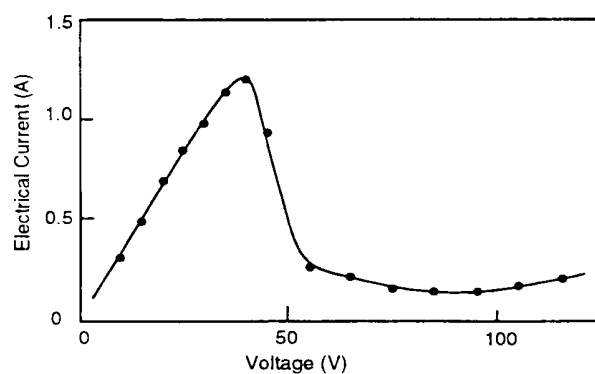


Fig. 2 Nonlinear I/V Curve

The I/V curve somewhat depended on the condition of the electrodes. Fig. 2 was obtained with new nickel electrodes. With old electrodes, impurity deposits on the surface, such as the electrolyte of potassium somewhat changed the I/V curve. However, the general aspect of the I/V curve showing three divided regions was maintained throughout the experiments.

B. VTR Observation of Microsparks

How the tiny sparks appeared depended on the kinds of electrode materials. Titanium was special among the metals used in these experiments. When the same metal wires were used for both of the electrodes, the tiny sparks appeared only on the anode of titanium, while with all the other metals, they initially appeared on the cathode and sequentially on the anode in the high voltage. With all the metals except titanium, it was also possible to generate the tiny sparks on the anode, but in that case, platinum was used as the cathode and simultaneously the voltage was required to increase higher than about 150 V. We made the tiny sparks appear on the cathode even with titanium, but the other metals, such as platinum, were used as the anode. This

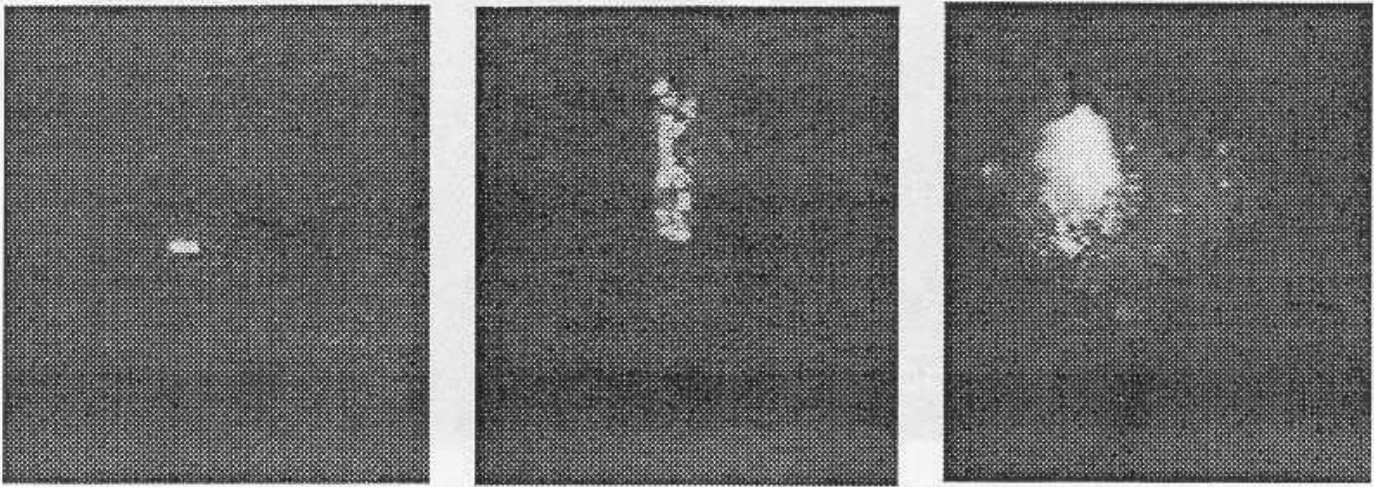


Fig. 3 Tiny sparks on the Palladium Cathode (x 10)
a) about 45 V, b) about 60 V, c) about 70 V.

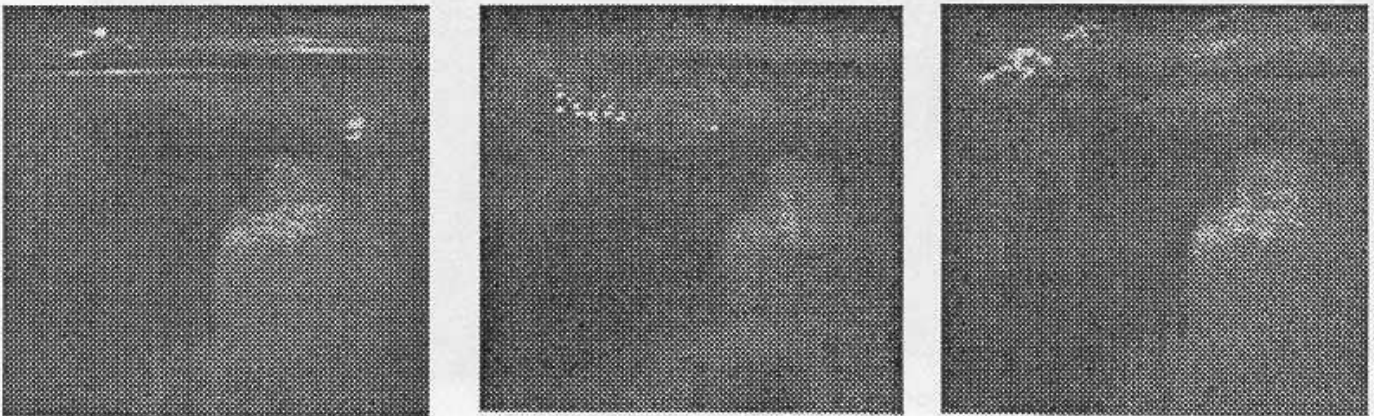
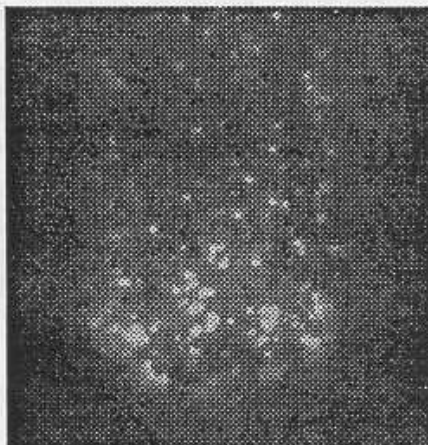


Fig. 4 Separated Tiny Sparks (time step 33 msec)



0.5 mm

Fig. 5
Microsparks on the Cadmium Cathode
(x 200)

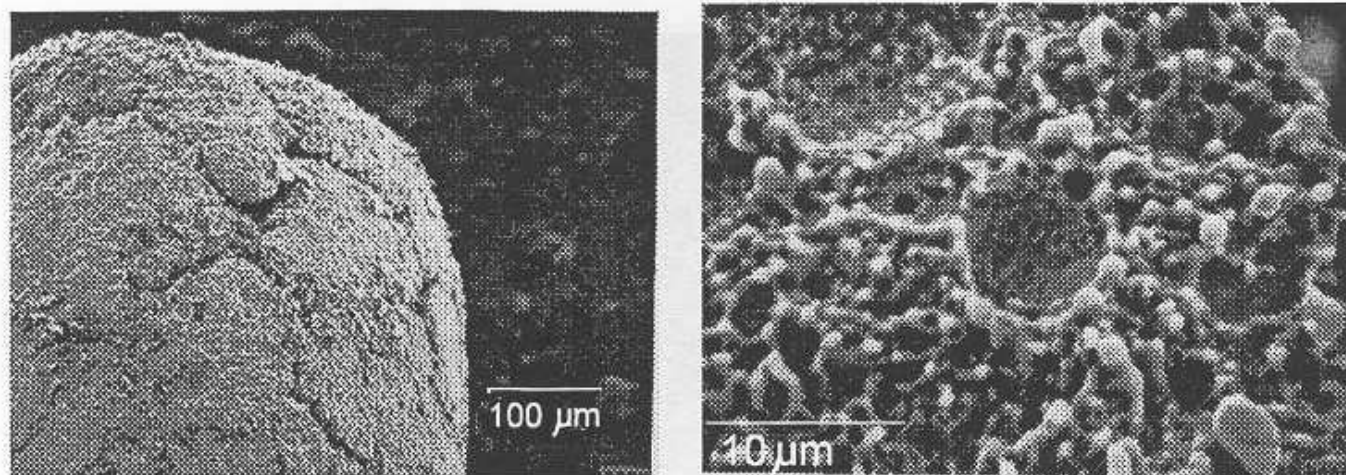


Fig. 7 Deposited Materials on the Ni Cathode (left) deposits with fracture, (right) tiny hole on deposits

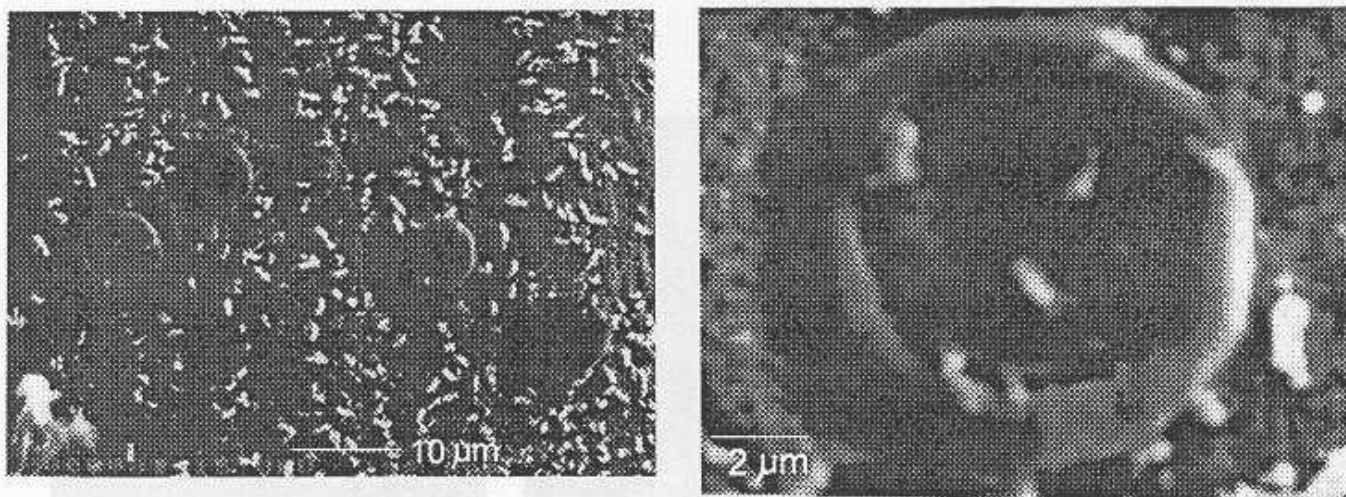


Fig. 8 Ring-Cluster on the Fe Cathode

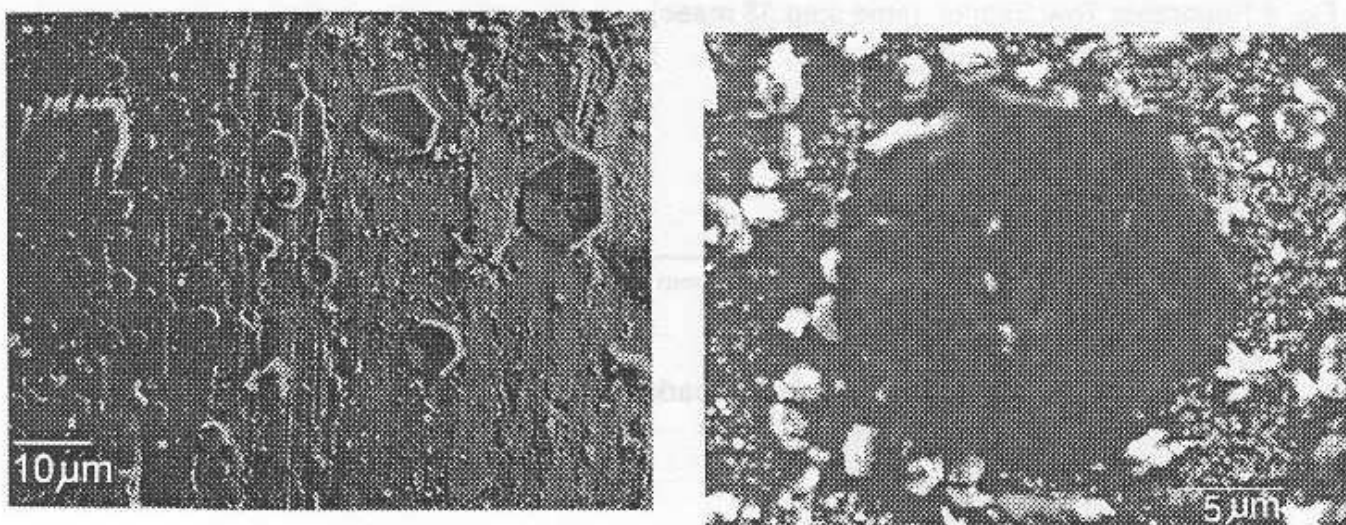


Fig. 9 Hexagonal Decay Products: (left) hexagonal plates, (right) intermediate stage of decay.

suggested that there might be different processes for sparking on the cathode or anode, and with titanium or the other metals.

The tiny sparks were observed *in situ* using the VTR system. Fig. 3 shows the tiny sparks appearing on the surface of the nickel wire cathode (with 10 times amplification of the VTR monitor). Figs. 3(b) and 3(c) show that the number of the tiny sparks increased as the voltage increased, but no sparks appeared on the anode.

Fig. 4 shows a sequence of pictures for the tiny sparks, in which they were accidentally separated from the surface of the palladium cathode by two explosions. The first small explosion took place in the gas atmosphere over the water level, which was triggered by the tiny sparks, as shown in Fig. 4(a). Due to mechanical shock from the explosion, a group of the tiny sparks were separated from the cathode, and were driven by the electrical potential towards the anode, as is shown in Fig. 4(b). The tiny sparks were decayed on the anode to trigger the second explosion, as shown in Fig. 4(c). These pictures showed that the tiny sparks were negatively charged and could exist in water solution as independent bodies.

The tiny sparks were observed in more detail using the VTR system with amplification of 200 times. Fig. 5 shows the expanded pictures of the tiny sparks appearing on the cadmium cathode. The tiny sparks were found to consist of a large number of microsparks, that were frequently created or broken. The microsparks sometimes formed ring-clusters with a diameter of about 100 μm and decayed to something like a black cloud that prevented the backside light from shining through. Furthermore, there were bright spots among the microsparks. A corona-like discharge was observed from the bright spot. The decay of the microsparks will be examined in more detail.

C. Emission of Radiation

The emission of radiations was monitored by the CsI(Tl) scintillation spectroscopy. Certain kinds of radiation were observed to be released through the wall of the glass beaker.

The CsI(Tl) scintillation detector was alternatively placed outside the glass beaker and over the water surface. The detector measured the emission of radiation in the high voltages in both cases. The energy spectrum of the radiations were continuous and monotonously declined as the energy increased. The typical spectra are shown in Fig. 6. The background was measured with no discharges. The counting rate was significantly higher than the background. As the voltage increased, the energy tail expanded more widely. The intensity of the radiation sharply dropped as the distance between the detector and the cathode increased. The radiation detected was neither gamma rays nor X-rays. The signals were generated by electromagnetic waves picked up with the electrical circuit. The emission of the electromagnetic waves will be discussed relating to the break-up of the ionic clusters.

D. Nuclear Transmutation

Discharge products deposited on the electrode surface were examined by SEM-EDX, EPMA and XS. Several kinds of the nuclear transmutation occurred.

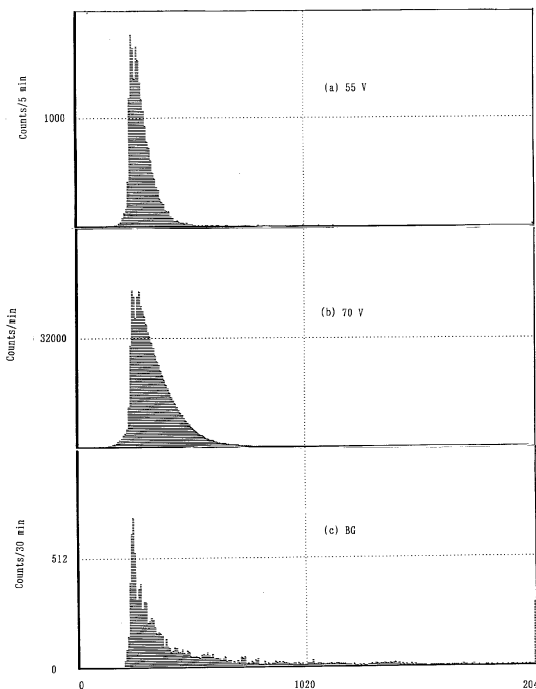


Fig. 6

Fig. 7 shows a SEM picture of the deposited materials on the cathode of the nickel wire. Thick layers including potassium were deposited **and there were many tiny holes (about 10 μm Φ)** over which the microsparks might be shining through [emphasis by Ed.].

Several elements were found by EPMA among the deposited materials on the anode of palladium wire: nickel, calcium, titanium, sodium, aluminum, chlorine, cadmium and iodine. They were not observed in a reference region of the palladium wire. Furthermore, nickel was clearly detected by XS. These elements could not be assigned to impurities but rather suggested to be transmuted during the electrical discharges associated with the microsparks. For example, chlorine, calcium and nickel could be transmuted by the capture of electrons, a proton and hydroxide with a potassium nucleus, respectively. On the other hand, cadmium and iodine could be transmuted by the capture of a proton and oxygen with a palladium nucleus, respectively. Such captures could occur in the highly compressed state of the hydrogen-cluster.

E. Microscopic Ring-Clusters

When the iron wires were used for the electrodes, tiny ring products were successfully caught on the surface of the cathode. The discharge was maintained with 70 V and 0.3 A for 27 min. and in the last period, there was a small explosion.

Many ring products could be observed with SEM around the zone on the surface of the cathode that touched the water level, as shown in Fig. 8. Simultaneously regular hexagonal products were observed in the same zone, as shown in Fig. 9. After a few days, the ring products all disappeared, and in place of them, only the hexagonal products remained. This suggests that the ring products decayed to the hexagonal plates. Fig. 9(b) shows the intermediate stage of the decay in which an inner circular zone still remained.

The ring and the hexagonal products were examined with EPMA. Fig. 10 shows dimensional distributions of the elements that were found near the products. Besides iron from the host metal and potassium from the electrolyte, some elements of calcium, sodium, chlorine and cadmium were both observed in the ring and the hexagonal products. Two circular zones, especially, could be seen for cadmium that were clearly separated from each other in the ring products, as shown in Fig. 10. Those observations suggest that the ring product could consist of a hydrogen-cluster and that the process of the nuclear transmutation took place in the clusters.

F. Nuclear Emulsions

Five plates of nuclear emulsions were placed to monitor particles that were emitted during the electrical discharges. Fig. 11 shows extraordinary rail-like traces observed on the surface of the first nuclear emulsion. Similar traces were not found in the other nuclear emulsions. Reference nuclear emulsions were located at 5 m distance from the cell in the same room, but similar traces were found neither in nor on the reference nuclear emulsions. The traces suggested that some particles walked around on the surface. Fig. 11(b) shows a ring product left with the rail-like trace. This clearly indicates that the extraordinary rail-like traces were generated by the ring products that escaped from the cell and walked around on the surface of the first nuclear emulsion. The diameter of the ring was about 10 μm , which was approximately the same as that of the ring products observed on the iron electrode. This observation suggests an extraordinary result that the ring product could penetrate through the glass wall of the beaker and the water solution. The curious behaviors of the ring product will be further discussed in Sec. 4.

G. Miscellaneous

The other extraordinary phenomena were observed during or after the discharge experiments.

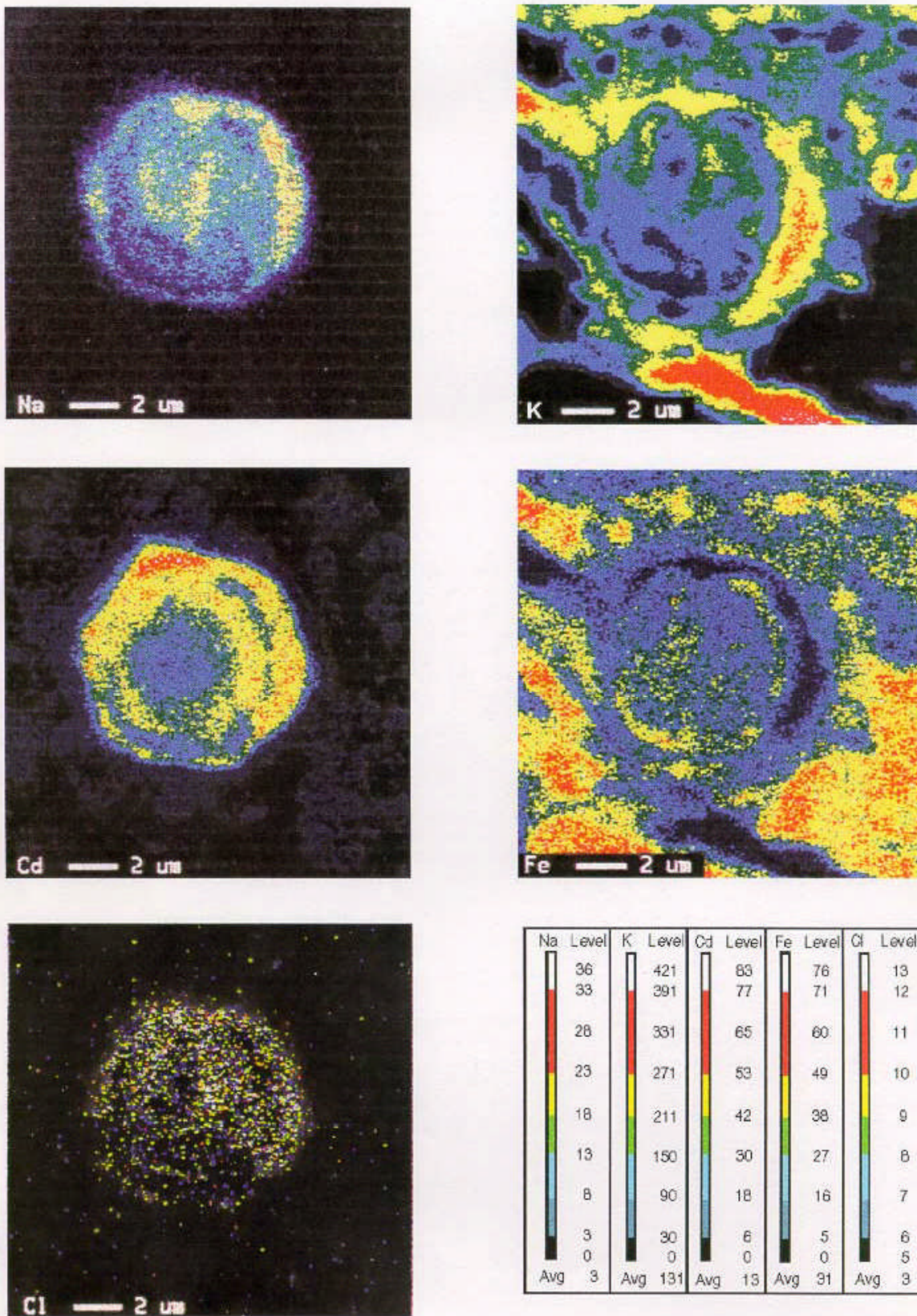


Fig. 10 EPMA Analysis of the Hexagonal Decay Product

BLANK

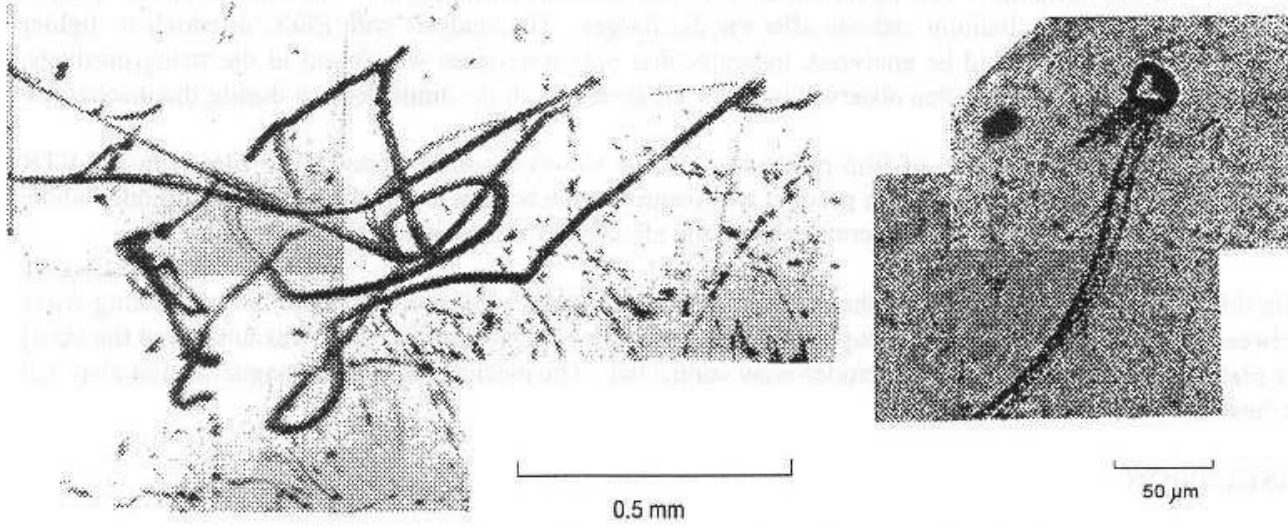


Fig. 11 Rail-like Traces: a) trace-like written with one stroke;

b) trace with ring-like product.

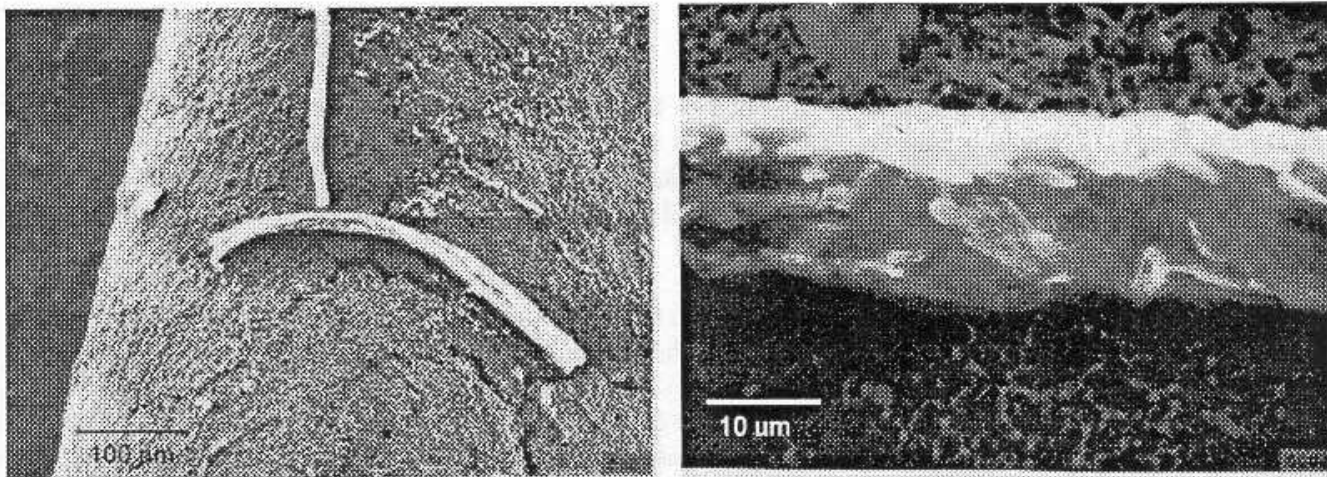


Fig. 12 String Product on the Pd Cathode

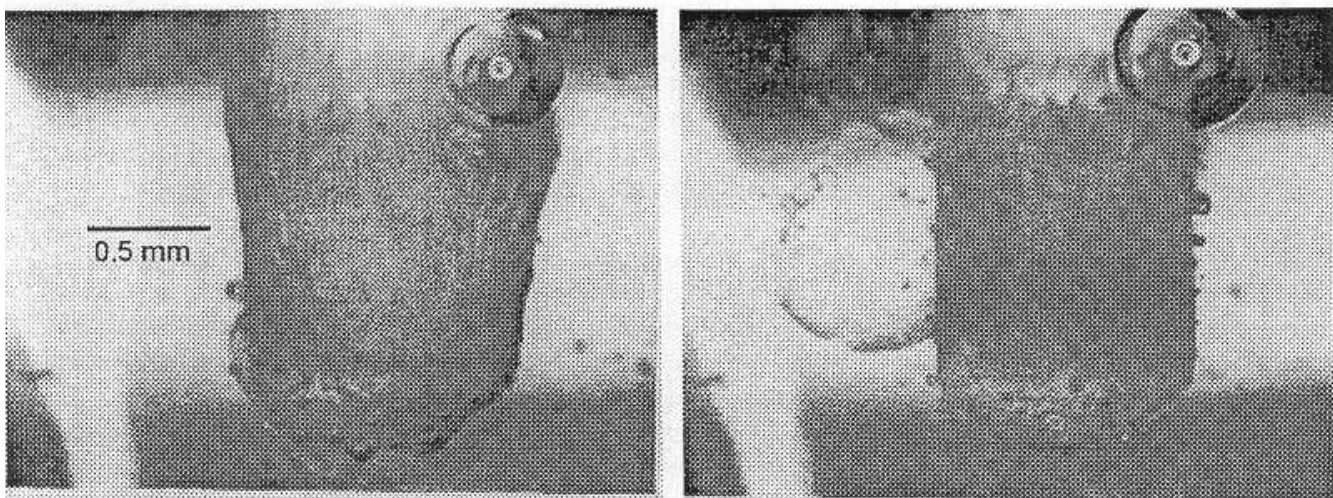


Fig. 13 Film Product on the Cd Cathode

The first was the formation of string products. Fig. 12 shows the string product that was observed by SEM on the surface of the palladium cathode after the discharges. The analysis with EDX, in which no lighter elements than sodium could be analyzed, indicates that only potassium was found in the string products. Similar string products were often observed by the VTR system with the amplification during the discharges.

The second was the formation of film products. Fig. 13 shows the production of the film with the VTR system (100 amplification). The film product was formed at the bottom top of the cadmium cathode, where the microsparks were frequently generated due to the effective compression of the hydrogens.

The third was the magnetization of the platinum wires (0.5 mm ϕ) that were used for the connecting wires between the wire electrode and the copper leading wire. The magnetization effect was noticed at the tip of the platinum wires, at which the electrodes were connected. The mechanisms of the magnetization also will be further discussed.

DISCUSSION

Many extraordinary phenomena were observed during the sparking underwater discharges. The mechanisms of some important phenomena are discussed here.

A. Formation of Microsparks

The first phenomena is concerned with the tiny sparks. The appearance of the tiny sparks somewhat depends on the kinds of the electrode materials. Titanium was special among the metals used in these experiments. With metals such as palladium and nickel, the tiny sparks initially appeared on the surface of the cathode, and as the voltage increased, they also appeared on the anode. These facts suggest that there were two processes for the formation of the tiny sparks.

On the pinched cathode, hydrogens were compressed to the high concentration on the surface of the electrode by the electrical potential, and simultaneously the high current density of the electrons were charged so that the itonic state of the hydrogen-clusters was formed [2]. The itonic hydrogen-clusters could emit the visible light from the microsparks because the itonic mesh was excited by the nuclear fusion reactions. On the other hand, on the anode, the hydroxyl radicals were compressed by the electrical potential. The itonic state of the hydroxyl radicals were also formed to emit the visible light. Here, since the heavy atoms of the oxygen were included, the higher voltage was required to generate the microsparks than on the cathode.

In the intermediate voltage region between about 40 V and 60 V, where the voltage was critical to the formation of the itonic hydrogen-clusters, the resulted clusters would sometimes breakup. This was a reason why the rapid evolution of the hydrogen gas seemed to occur on the cathode. On the contrary, the current was strongly suppressed by the appearance of the microsparks in the high voltage region. This was because the itonic hydrogen-clusters, negatively charged, covered the cathode to prevent the free flow of the current. Furthermore, the break up of the microsparks caused the spatial charge effects to reduce the current.

With titanium, different processes were suggested for the generation of the microsparks, that appeared on the anode in the low voltage region. The microsparks on the titanium anode were examined in a previous experiment of the AC discharges [7]. Here the microsparks appeared when the deposited materials were taken away and the local, but rapid, electrical discharges occurred. Fig. 14 shows a picture of the microspark products that were caught by a copper plate placed near the titanium electrode over the water level. The figure showed that the microspark products had the mesh structure. This means that the deposited materials were in the itonic state. Furthermore, inside the meshes, there were observed bright spots suggesting some nuclear reactions.

B. Extraordinary Ring-Cluster

The second concerns with the ring-cluster. It could easily penetrate materials like glass and eventually decayed to the almost hexagonal plates. There are two candidate models for mechanisms of forming the ring-cluster.

The first is the hydrogen ring-cluster with the closed current. When the compression of the hydrogen-cluster was proceeded on the pinched electrode in the high voltage region, some phase transition might have occurred in the hydrogen-clusters, because the hydrogens had no places to escape. The compression of the hydrogens was made two dimensionally on the surface of the pinched cathode so that the ring could have the minimum total energy. In the ring-cluster, closed electrical current could flow and it induced the magnetization effect. The ring-clusters could be negatively charged.

The second is a special kind of product represented by tiny white holes. The tiny white hole was early observed by the author in a previous Mills'- type experiment of electrolysis with light water and a nickel electrode [2]. There a lot of conic [sic] products were observed as evolved products resulted in the tiny white holes. In this experiment, especially with cadmium, the collapsed mass should be heavy so that evolved products might be curled up to form the ring structure.

It is remarkable to note that the ring-clusters could penetrate the regions such as glass, walk around on the surface of the nuclear emulsions and hop up and down between the nuclear emulsions [4]. These phenomena could be explained by charges associated with the ring-clusters. When the ring-cluster touched the material, a portion of the charges of the ring-cluster transferred to the material, and the repulsive force was generated between the ring-cluster and the material. This force could make the ring-cluster jump-up. When the ring-cluster penetrated through the material, the constituent atoms of the material could be sequentially absorbed into the ring-cluster. Then a microscopic hole having the similar diameter could be left in the solid state material.

However, the curious penetration of the ring-cluster cannot be explained by the first model. On the other hand, the second model seems to easily explain the penetration, because a tiny white hole is produced from a tiny black hole that should have the extremely small dimension compared with interatomic distance. Here the hexagonal plate generated from the decay of the ring-cluster should be explained as the crystallization of compressed materials included in the ring-cluster.

The magnetization effect was observed on the tip of the leading wires of platinum that were connected with the electrodes. The effect could be explained by the existence of the tiny magnets, i.e., the ring-clusters. Furthermore, when the decay proceeded further, corona-like discharge phenomena could be induced at the center of the ring-cluster, as observed *in situ* by the VTR system. Here the break-up of the ring-clusters could make the electromagnetic waves emit, as were detected by the CsI(Tl) scintillation detector. Similar radiation could also be emitted by the break-up of the itonic hydrogen-clusters.

The extraordinary behavior of the ring-clusters were very similar to those reported about the curious natural phenomena, ball-lightning [8, 9]. Ball-lightning is often born associated with a thunderstorm, that is, the electrical discharges on the large scale. It is reasonable to consider that during the thunderstorm, some products like the ring-cluster obtained in this experiment might be generated, move around and eventually explode, as were reported in the references [8, 9].

C. Nuclear Transmutation

The nuclear transmutation took place during the underwater spark discharges. The nuclear transmutation can take place in the itonic hydrogen-clusters, explained in Ref. [2]. Here, the hydrogens were so highly

compressed that various kinds of the nuclear transmutation became possible. The feasible schemes of the nuclear transmutation are described in an appendix for the case of the iron electrodes and the potassium electrolyte.

Furthermore, the analysis with EPMA showed that the nuclear transmutation was possible in the ring-cluster. This fact suggests that there might be another process for the nuclear transmutation, different from the nuclear transmutation in the itonic hydrogen-clusters. The ring-cluster showing the crystallization effect should have higher concentration of the atoms than the solid state. This makes the nuclear transmutation possible. In the appendix, the production of the cadmium element is explained by the fusion reaction between two iron nuclei.

CONCLUSIONS

In the experiments of the underwater discharges, the microsparks on the pinched electrodes were examined in detail. It was found that they were not normal sparks but consisted of the itonic hydrogen-clusters that were sometimes transformed to the ring-clusters. The itonic hydrogen-cluster and the ring-cluster could exist for a moment as an independent body. The ring-cluster can easily penetrate through the layers of glass or acrylic despite their heavy mass and charges, and hop up and down on the nonconductive materials such as nuclear emulsions. It is remarkable that the nuclear transmutation caused by the nuclear fusion reactions took place in the ring-cluster as well as in the itonic hydrogen-cluster. The ring-cluster was very similar to ball-lightning that was observed in the natural environment, although the scale was different. As the current density or voltage were increased, the ring-cluster with the larger dimension could even be produced in laboratory. The reproducibility of the underwater spark discharges method is so good that the property of ball-lightning should be examined in detail in laboratory.

Acknowledgments

The author is thankful to Mrs. N. Miyazaki and T. Suda for their help during the observation with the microscopies.

REFERENCES

1. See the proceedings of the International Cold Fusion Conference from 1 to 6, or related papers published in *Fusion Technology* in 1989 - 1996.
2. T. Matsumoto, "Mechanisms of Cold Fusion: Comprehensive Explanations by The Nattoh Model," *Memoirs of the Faculty of Engineering*, Hokkaido Univ., vol 19, no 2, p 201- 224 (1995).
3. T. Matsumoto, "Experiments of One-Point Cold Fusion," *Fusion Technology*, vol 24, no 3, p 332 (1993).
4. T. Matsumoto, "Extraordinary Traces Produced during Pulsed Discharges in Water," *Bulletin of the Faculty of Engineering*, Hokkaido Univ., no 175, p 73 - 86 (1995).
5. T. Matsumoto, "Observation of Quad-Neutrons and Gravity Decay During Cold Fusion," *Fusion Technology*, vol 19, no 4, p 2125 (1991).
6. T. Matsumoto, "Observation of Stars Produced During Cold Fusion," *Fusion Technology*, vol 22, p 518 (1992).
7. T. Matsumoto, "Experiments of Underwater Spark Discharges with Pinched Titanium Electrodes," to be published.
8. G. Elgey, The Mysterious Ball-Lightning, Japanese edition by Maruzen Co., Ltd., (c1990).
9. S. Silver, "Ball-Lightning," *Naturwissenschaften*, vol 67, p 332 (1980).

APPENDIX: Feasible Schemes of Nuclear Transmutation

Feasible schemes of the nuclear transmutation are discussed here by the Nattoh Model. The model predicted that a hydrogen-cluster is formed on the surface of the electrodes. Since the nuclear reactions take place under the multi-body interaction of the cluster constituents such as electrons, protons, oxygens and the heavy nuclei of the electrolyte and the host metals, there are various kinds of feasible schemes for the nuclear transmutation. The different kinds of nuclei produced by the nuclear transmutation depend on the applied voltage or the current density. As the voltage is increased, the higher order reactions could be enhanced. In this appendix, however, only the principal reactions will be considered here, taking an example of the iron electrode and the potassium electrolyte. The higher order reactions are straight forward.

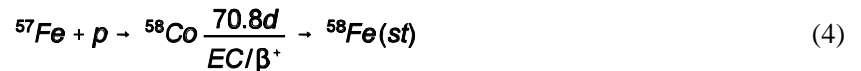
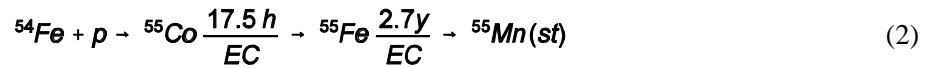
A. Iron electrode

Natural iron contains four stable isotopes: ^{54}Fe (5.84%), ^{56}Fe (91.68%), ^{57}Fe (2.17%) and ^{58}Fe (0.3%). The capture of an electron is not so effective for the nuclear transmutation of iron. Only the lightest isotope ^{54}Fe can be transformed by capturing an electron as follows:

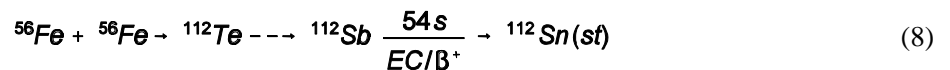
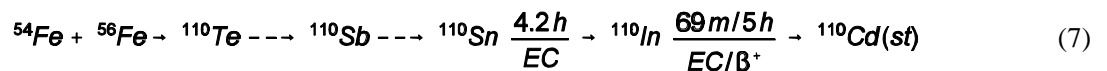
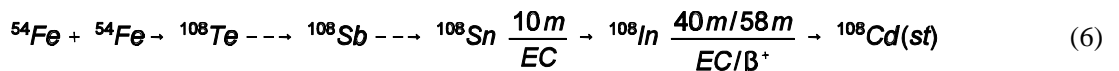


The other isotopes of iron cannot be transmuted by capturing an electron because the products of ^{56}Mn , ^{57}Mn and ^{58}Mn rapidly undergo the beta decay to return back to the original nuclei.

When the iron isotopes capture a proton, new elements and different iron isotopes can be produced,



where EC and β^+ indicate the capture of an electron and the emission of a positron, respectively. The half-life of EC or β^+ in the ionic state should be drastically shortened, because the electrons of the ionic state distribute very closely to the nucleus. Through Eqs. (3) and (4), the isotope ratio of the iron element should deviate from the natural value. Furthermore, the iron isotopes can fuse each other and heavy elements such as cadmium can be produced, for example,



B. Potassium Electrolyte

Natural potassium consists of three isotopes of ^{39}K (93.2 %), ^{40}K (0.01%) and ^{41}K (6.7 %). The feasible schemes can be derived similarly as for iron.

For the capture of one electron,



where ^{39}K and ^{41}K cannot transmute by the electron capture.

For the capture of one proton, the calcium element can be produced as follows,



It should be emphasized that during the nuclear transmutation in the hydrogen-clusters, neither energetic radiation nor activities could be generated. Even if the nuclei fuse each other to form an excited compound nucleus, the exciting energy could be transferred to the vibrational motion of the ionic mesh. Therefore, the nucleus could go to the ground state without emitting radiation. When the ionic mesh breaks up, however, the excited nucleus could emit high energy radiations as in the normal manner, and the activity also could somewhat persist.

Editor's Comments: This paper was not submitted for peer-review, however, the experimental data is timely and is an excellent addition to the papers published in this journal. See especially the paper by Jin et al., and the review paper by Bhadkamkar et al. in this issue, and the papers by Bass et al., Shoulders et al., and Fox et al. in the Fall 1996 issue of this journal. The adequacy of the Nattoh model is left for the future evaluation by peers. The author and the editor will welcome comments on both the experimental work and the author's Nattoh model.

EDITOR'S CHOICE**AN ALTERNATIVE SOLAR ENERGY SOURCE**

David R. Criswell and Philip R. Harris

Article originally appearing in *Earth Space Review*, vol 2, no 2, 1993

Space enterprises provide recognizable paybacks to the Earth's inhabitants. Communication, weather-monitoring, and defense satellites are indisputably valuable. Energy can be the next payback. Solar energy can be provided efficiently and safely at low cost from solar power bases on the moon. One alternative means of generating solar energy using the Moon is known as the Lunar Solar Power (LSP) system. It could establish a two-planet economy between the Earth and the Moon and both solve the Earth's impending natural energy resources shortage and act as a stepping stone for more extensive space exploration.

In 1980, 4.43 billion people used 10,300 gigawatts of power. This is approximately ten times more than can be extracted on a sustainable basis from the renewable biomaterials on Earth. On average, each person continually uses 2.33 thousand watts (kW) of thermal power. However, people in developed countries such as the US, Japan, and Western Europe use 90% of that power, at a rate of 6.3kW / person. Inhabitants of developing nations (Brazil or China, for example) use less than 1kW / person. Adequate and dependable supplies of low-cost and environmentally safe energy are critical to the economic development of these poorer regions and to sustaining the quality of life of the more developed sectors. By the year 2050, the estimated 10 billion population of Earth will require over 20,000 GW of electric power. This level of electric power can be functionally equivalent to over 60,000 GW of thermal power or six times the level of thermal power that is used today. At a time when coal and oil may be eliminated as a source of energy, and nuclear energy is considered dangerous by many, solar energy may be the best of possible alternatives. Using current photovoltaic technology, large tracts of year-round sunny land are required, and in many cases not necessarily available on a per country basis. Thus, an alternative which transcends geographical and political boundaries comes under consideration. Far-fetched to some, a potential savior to others, is the use of the Moon's surface to "harvest" solar energy.

Reaping the Sun's Benefits...On the Moon

The Lunar Solar Power concept was developed by Drs. David R. Criswell and Robert Waldron. LSP power bases are constructed in pairs on the opposite sides of the moon as seen from Earth. Each base consists of thousands of plots covered by large arrays of thin-film photovoltaics. They convert solar energy to electricity, in turn converted by electronic systems to low intensity beams of microwaves channeled to reflector antennas that look toward Earth. The plots are distributed about an elliptic area of the moon, near the lunar equator, so that the reflector antennas form a large diameter, synthetic lens that can project many separate power beams, each with less than 20% of the intensity of sunlight, back to receivers on Earth. Finally, the receivers on Earth feed the solar-derived power into the power distribution systems on Earth. Analyses reveal that LSP requires far less resources and land than arrays on Earth where the solar power is irregular and the arrays are massive and expensive.

The advantages of this 21st century system over conventional power have been summarized in Table 1. The last row highlights the case for lunar power by noting that it offers maximum useful power level of > 100,000 gigawatts (GW). Its only limiting factor appears to be stray microwaves. This system does not pollute (providing environmentally-sound means of accessing space are developed), and after an important initial investment, the studies show a cost decrease coupled with an increasing return on investments.

TABLE 1

LUNAR POWER SYSTEM
 Comparison of 21st Century Power Systems
 Goal: Establish 20,000 GigaWatts by 2040

| Power System | Maximum Output (GW*Yrs) | Maximum Useful Power Level (GW) | Time to Exhaust (Yrs) | Limiting Factors | Polluting Products | Long Term Cost Trend | Risks to Reach Goal |
|-------------------------|---------------------------|---|---|---|--|----------------------|---------------------|
| Bio-Resources | 100*Yrs | 1,000 | <10 | Mass Handling Nutrients Water Land Use | Co ₂ Biohazards Methane Disease | Up Not | Possible |
| Coal | <1,500,000 | 20,000 | 100 | Supply Pollution | Co ₂ Ash Acids Waste Heat | Up | Not Possible |
| Oil | <100,000 | 5,000 | <30 | Supply | Co ₂ Waste Heat | Up | Not Possible |
| Nuclear Fission | >500*Yrs | 500 Base load | 100s | Accidents and Terrorists Social Acceptance | Radioactive Spent Fuels Components Waste Heat | Up | High |
| Nuclear Fusion | >20,000*Yrs | >20,000 Base Load | 1000s (D-T) <100s (D-He ₃) | Engr. Demo First Wall Life (D-T) Power Balancing* | Radioactive Spent Fuels Waste Heat | Up | High |
| Hydro-Electric | 2,000*Yrs | 2,000 | 1000s | Sites & Fill-Up Rainfall Dam Failure | Sediment Flue Water | Up | High Possible |
| Ocean Thermal | <1,000,000 | <20,000 | <100 | Deep Cold Waters | Power Balancing | Up | Not Possible |
| Terrestrial Solar Power | >20,000*Yrs | >20,000 Not tied to peak or base load | >10 ⁸ | Clouds Power Storage Power Distribution Power Balancing* | Waste Heat Production Wastes | Down | Moderate |
| Solar Power Satellites | 2,000 *Yrs | 2,000 Base Load | >10 ⁹ | Orbital Debris Shadowing | Sky Lighting Orbital Debris | Down | Difficult |
| Lunar Power System | >>20,000*Yrs following | >100,000 Base & Load | >10 ⁹ | Stray Microwaves | None | Down | Low |

*Balancing Local and Inter-Hemispheric Heat Loads

We currently operate in a thermal economy where 15% of the gross world product is invested in energy sources that are continually at risk due to declining resources, increasing prices, political turmoil, and pollution. In a 1990 presentation to the first LSP coalition workshop, M. Peterson, professor emeritus of the Scripps Institution of Oceanography, emphasized that most concerns underlying earth observation (green-house gases, wastes and disposal, stratospheric ozone depletion) and relevant modeled predictions are directly related to energy needs. He sees the proposed LSP program as a solution to the problems outlined above by providing a major new source of energy that is dependable, economical, environmentally safe, available worldwide, and capable of growth.

Furthermore, preliminary analysis by the LSP inventors indicate that projected annual net revenue from a 20,000 LSP system could exceed \$15,000 billion dollars per year. This is 15×10^9 \$/yr. and approximately 60% of the present day gross product of the world. The estimate assumes that the energy is sold for 10 cents per kilowatt hour. This is approximately the cost of electric energy in the US today. The LSP strategy is timely and synergistic: (1) It fits within the NASA "Mission to the Planet Earth" program, while offering the Space Agency economic justification for the Space Exploration Initiative with plans for lunar return and industrialization; (2) It coincides with world needs to become less dependent upon petroleum and gas, and to halt the environmental damage of fossil fuels, especially depletion of the world's forest and ecological reserves; (3) It provides a transfer of military technology, scientists, engineers, resources, and investment to a "defense of the planet" that will foster advanced technology, research, and development; (4) It offers the Department of Energy an opportunity to join with the Environmental Protection Agency in solving environmentally-safe energy shortage problems; (5) It will not only renew existing industry, such as the corporations in aerospace and satellite communications, but will create "astro-businesses" from lunar construction to lunar law. Michael Duke, Deputy for Science with NASA's Lunar and Mars Exploration Program, stated in an August 10, 1990, letter to one of the authors (Harris) that "I have a feeling that it is a concept like the LSP that will get us back to the Moon and into space in a big way."

Energy Choices We Must Make

In the long term, there are severe limitations on the current means of producing electrical power. Energy options in space are promising and inexhaustible; be it the LSP, or the Solar Power Satellites (SPS) (as advocated by Peter Glaser, who originated the concept of solar power satellites in geosynchronous orbit). In the 21st Century, an isotope of helium, He^3 , that is unavailable on Earth, might be mined from lunar soils. It would be brought to Earth and used in nuclear reactors that could be cleaner burning, produce less total radioactivity, than other proposed fusion systems. He^3 could also power spacecraft and facilities in the distant parts of the Solar System.

Clean power from the LSP can be used to correct the major adverse effects on Earth of conventional power supplies. Afterwards, the technological feasibility for exploiting solar energy at lunar facilities is worth pursuing, particularly for its economic potential (observations confirmed by scientists and engineers in the 1989 task force report on the NASA Lunar Energy Enterprise Case Study, and the 1990 proceedings of the Lunar Power System Planning Workshop).

The majority of the project's investment will be for the construction and maintenance of the rectennas on Earth. These rectennas capture the microwaves, somewhat in the manner that a TV antenna captures radio waves, and convert them to electric power. The rectennas are projected to cost only 10% per unit of capacity of a similarly sized coal-fired electric plant. Integrating private and public sector contributions will be necessary to ensure the success of this macroproject and will require a cost-effective, primarily government-funded, space transportation system to the Moon and back. A technological venture of this scope would benefit from international participation, such as Canada, Japan, and Europe. The participation of the Commonwealth of Independent States (CIS) would also be valuable, since they have unique capabilities in lunar studies, heavy-lift launch systems and long-duration space living.

In July 1990 a significant planning workshop held in LaJolla, California, took the first step. Some twenty-five distinguished scientists, engineers, and other professionals established a Lunar Power System Coalition (LPSC) for interested individuals and institutions. As a result, research and proposals are being developed, while collaborators, sponsors and investors are being sought. It is hoped that LSP task forces will be established in many government agencies, aerospace, satellite communications and other high technology corporations. Foundations and governments, as well as the United Nations, could fund requisite R&D studies. The subject is appropriate for university investigations, especially interdisciplinary doctoral studies, and national laboratories' research.

Lunar Power Base and Communication Technology

LSP views the Moon as a natural platform uniquely suitable and available as a power station. Lunar solar power systems use lunar resources to construct large arrays of solar collectors on the surface of the Moon. The project may require establishing a lunar base for up to, eventually, 4,000 inhabitants and will necessitate a combination of public and private initiative. Advanced automation and robotics may reduce this workforce. To build facilities sufficient for hundreds, then thousands, of people to live and work safely on the Moon will tax the ingenuity of engineers and construction contractors. Biological and behavioral scientists will have to be involved in providing life support systems and determining human needs that reach beyond industrial engineering. This is not as easy as it appears: currently, the Earth-bound Biosphere II project, a self-contained, sealed, simulation of five different environments, still has difficulty regulating its gaseous mixture and providing enough food to sustain its eight inhabitants.

One critical element for the ongoing success of this project will be advanced communications. In a study for a preliminary supply base on the Moon, Criswell projected a communications and control center in the living area. Initially, the needs of the lunar crews would not be unlike those at scientific outposts in Antarctica or other extreme/polar regions. There will be a need for the lunar community to have both official and private communications with Earth. Also, privacy must be considered, which in turn incurs technical and legal implications, for once a lunar power industrial park is fully functioning, the message traffic between the lunar pioneers and the Earth will be substantial.

Communication Challenges

The development of LSP presents a two-fold challenge for communication specialists: first, to make the world aware of the need to supply the Earth with solar power harvested on the Moon; second, the communication requirements of an operational lunar power base. Efficient communications can provide quick growth rate, lower power costs, and higher energy capacity. To collect solar energy on the Moon and beam it to Earth is a macro-engineering project which calls for research demonstrations, an innovative space infrastructure, and major funding.

Communication technologists can help create public awareness of the need for LSP, particularly as a 21st century global power system that does not introduce new pollution into the biosphere, nor deplete existing organic resources. The worldwide technical community should be encouraged to initiate R&D in the field of space energy resources as the challenge moves beyond the realm of engineering and into those of finance, communication, sociology, law, and politics.

At the end of the first LSP workshop, Robert Waldron, from Rockwell International, provided the statement: "Global population trends coupled with legitimate aspirations for improved standard of living for current and future inhabitants of Earth will require a substantial increase in energy consumption well into the 21st Century." Waldron further affirmed that only a lunar power system can provide the required amount of energy in an affordable manner, while avoiding the environmental and ecological damage of existing power schemes. Any large-scale conversion to alternative energy sources will require the commitment and

investment of generations, which will most definitely be the case for LSP. The time has come for the technical community, particularly communication technologists, to lead in this change by including a concept such as LSP in their push for the use of alternative energy. People need to be made aware of the benefit of space resources, and planning must begin now for 21st century energy utilization.

David R. Criswell is Director, Institute for Space Systems Operations at the University of Houston in Texas, and co-founder of the LSP Coalition. (713)486-5019

Philip R. Harris is Senior Scientist at Netrologic Inc. of San Diego, and Associate Fellow of the American Institute of Aeronautics and Astronautics. A.M. only: (619)453-2271

Information on LSP is available by writing to the Lunar Power System Coalition's Executive Director, 6841 South Yosemite, Englewood, CO 80112, USA. 1-800-632-2828

Editor's Note: This Journal invites your comments on LSP.

EDITOR'S CHOICE

IN SEARCH OF A WARP DRIVE

Norman Silliman ¹

The story of man's effort of going to the stars has all the ups and downs of a soap opera plot:

- Man's incessant urge to overcome nature.
- Science triumphs, puts man on the moon .
- Realization of a dead end, Despair!
- Fighting back - Yankee ingenuity - search for a better way.
- A small group of dedicated individuals plot to out-perform the failed giant of science.
- Success, man lives happily ever after.

We are very sure of the first five segments of this twisting and turning plot. The sixth segment is unrealized and this sub-plot will have its own ups and downs of struggle and triumph.

So, what is needed to go to the stars? We need a "warp drive." We all know what a "warp drive" does, we just don't know how a "warp drive" works. For a **warp drive** to exist, Marc Millis explained, there must be two breakthroughs in physics – **control over gravity** and the ability to **exceed light speed** [1]. We need a source of power, but Millis is right about antimatter not being practical because of the \$100 billion per milligram cost.

A mission statement is very useful, since the problem is assumed to be very complex. It is also a key strategy in problem solving. If you don't know where you are going, how will you know when you get there? Another problem solving strategy is to break the problem into smaller segments: what subjects are part of the problem and what are part of the noise?

"The mission of the Interstellar Propulsion Society is to accelerate scientific and engineering advancements in space propulsion, leading to manned missions to other star systems at fractional light speeds, relativistic velocities and beyond. The Society's main function is to provide a medium for scientists and engineers, worldwide, to join in collaborative efforts to advance interstellar propulsion technology." [2]

Why is this declaration of intent from a special interest group needed? Conventional Physics has had 90 years to find, and use, tools for the advancement of the human race and has come up empty. Materials Science has given us transistors and jet/rocket engines, but Physics has given us the failure of hot fission and the absurdity of Quarks and neutrinos. General Relativity and Special Relativity have lead us up a blind alley. Not only has the "establishment" in physics failed to provide useful tools, they have defined the rules so no one will find useful solutions.

How big is the problem? One way to estimate the size of the problem is to compare the needed function to an existing similar function. What can possibly be compared to something as novel and important as a star drive?

We want a function that powers a **container** to travel from point "a" to point "b." We have several analogous devices. Sailing ships were first, steam ships were an improvement. Steam rail engines were first on land. Next came horseless carriages, and they were free ranging. Horse drawn vehicles don't count in this list as

¹ 315 Betty Lane, Pleasant Hill, CA 94523-2808; NLSilliman@AOL.com

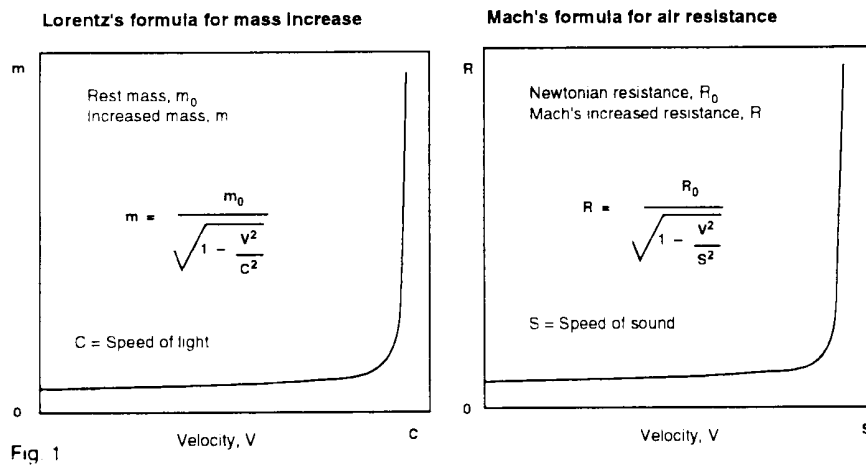
the horse cannot be defined as a machine. The next advance came in our very recent past with the heavier than air ships.

Airplanes are assumed to be the closest analogous device to a space ship. While they are slower and atmosphere bound, the function is the same: carry people and cargo from "a" to "b" in a timely manner. Submarines are a distant second for this purpose. The physical mechanism for accomplishing the move may be similar. Submarines point out the need for an enclosed environment more directly than do airplanes. In the comparison of air ships and star ships, the sub-functions required are:

1. Propulsion, movement through the medium;
2. Lift, movement away from the surface of the earth; and
3. Brakes, coming back to a stop at the end of the trip.

How are these functions handled by airplanes and submarines? By manipulating the medium. You say there is no analogy here! How are we to understand the implied relationships for a starship!

Airplanes move through the "air" by pushing the "air." Submarines move through the "water" by pushing the "water." Here is where the problem of understanding the analogy is located. The establishment physics has defined space as containing "nothing." Therefore, space ships have "nothing" to move through and "nothing" to push against! But for my analogy to work, space ships need to move through the "space" by **pushing** the "space."



Lets look at some historical evidence in regard to this comparison. Einstein (1905) gave us the light (speed) barrier by quoting Lorentz's formula. Later, Ernst Mach gave us the sound (speed) barrier which says the we cannot exceed the speed of sound with air vehicles. The engineers discovered if you use "air" propulsion devices, that is true. Propeller driven planes cannot exceed the speed of sound. That is because "the forward motion of the pressure waves are

completely arrested by the air stream velocity" [3]. See Fig. 1 for the problem [4].

You might notice the mathematical formulas describe similar **physical** functions. Water vehicles have a corresponding speed of water barrier, but no one talks about that.

Engineers don't believe what the "Scientists" say. As a result, we now have airplanes routinely traveling faster than the speed of sound. Aircraft engineers didn't have to put up with the silliness of the physicist's telling them that as the speed of the aeroplane approached the speed of sound, the mass of the aeroplane would increase to infinity. Two features are common to all "faster than sound" crafts: pointy noses and high power "thrust" engines.

How are these sub-functions handled for star ships? It seems they are possible only in science fiction. Heavy on the fiction!

Because of Einstein, we are not allowed to believe in the concept of an aether. That would be the medium we would have to manipulate. And since we are not allowed to believe in the aether, we have no idea of how to go about manipulating it. Worse, we have no examples from nature, like birds or fish, to copy.

We are stuck. We have no idea how to get a star ship to **cruise**. We have no idea how to provide large amounts of energy to power the ship. This is where "there must be two breakthroughs in physics" rears its ugly head. Well, maybe only one. I will show that "control over gravity" is not a breakthrough that is needed.

Of course, we have done the equivalent of the 'Kitty Hawk' biplane now. We have rocket boosters, so we have gone the equivalent of the 220 yards of the first flight. That is a start.

What is the physics involved in this problem/solution? If the problem is defined within the scope of General Relativity (time and space are coupled and space is curved by mass) or Special Relativity (the speed of light is a hard limit and everything depends on an observer), then we are doomed.

Luckily the real world does not correspond to the mind set of the "relativists." Maybe there is hope, so we will push on.

How do we determine if we are submerged within a fluid? For water it is easy, we can see the surface boundary. What about air? For many centuries, we were not "aware" we were emerged within a "sea" of air.

So, what questions can we ask to help with this determination? Birds and fish lead us to the easy questions. The wind and erosion effects lead us to the not so easy question.

1. Can we use (control) the media? Is there a resistance to movement through the fluid? Can we push against the fluid?
2. Is there any buoyancy?
3. Is there an effect of the flow of the fluid that is not answered in any other way?
4. How are disturbances in the media transmitted? When we drop a pebble in water, we get surface waves.

For air, the answers are "yes," "yes" and "yes." Wings on birds gave us this easy answer. Resistance to the fluid usually only shows up at higher velocities. Wind resistance is well known in the age of fast airplanes. Lighter-than-air-balloons are a fact of life for party goers. Tree leaves blowing in the wind are easy to notice, as well as fluffy clouds scooting across the sky, as examples of the fluid's invisible hand. Disturbances in the air are called sound waves, as obvious as it may seem.

For the aether, the answer is also "yes," "maybe," and "yes." We don't have evidence of wings or fins equivalence for the aether. The other evidence is more easily over looked, and in this case, badly mis-interpreted. The resistance to moving through the aether is the "relativistic mass increase" of subatomic particles pushed to near the speed of light.

We shouldn't be too hard on Einstein, as he perceived that the Lorentz equation seemed to describe the physical evidence. But since he already blinded himself by denying the existence of an aether, the only other way to make the equation work was to take the other solution for needing more energy: an increase in mass.

Well, the mathematics works fine under that assumption, too. It made a plausible explanation for the physicists of the time (1905). The fact that no one cared/understood what the terms in the equation corresponded to gave strength to the mathematicians to plow ahead with prettier equations that didn't correspond to reality for the next 90 years.

Buoyancy in regard to the aether is a probable "no," unless we can invent the equivalent of a Mylar sheet. There does not seem to be a way to contain aether. So antigravity is out for the near term. Disturbances in the aether are called light waves or radio waves.

For the invisible effects of aether, the "yes" answer is easier to support. We have two sets of closely related phenomenon that show promise. Magnetic and static electrical effects both cause movement in other materials that defy conventional explanations.

These two effects are the subject on an earlier paper (1994), *Physicist's Dilemma: Action at a Distance* [5]. Magnetism makes sense if the effect is interpreted as a flow of structured aether.

In my paper, I suggest the "lines of force" that appear to come from both ends of a magnet are really "vortex tube" flows. For that to work with no net motion, the flow from one end has to match the flow from the other end. This flow is always symmetrical under normal conditions. And, since the "north" flow acts differently than the "south" flow, I postulate one end is "right-handed" twisting vortex and the other end is "left-handed" twisting vortex.

Since magnetism is the **vortex flow** of aether (as I suggest in my paper), then we have a way of manipulating the aether. The reason we want to manipulate the aether is to influence inertia/momentum.² The trick to building a warp drive is to figure a way to get the flow to be non-symmetrical: one sided.

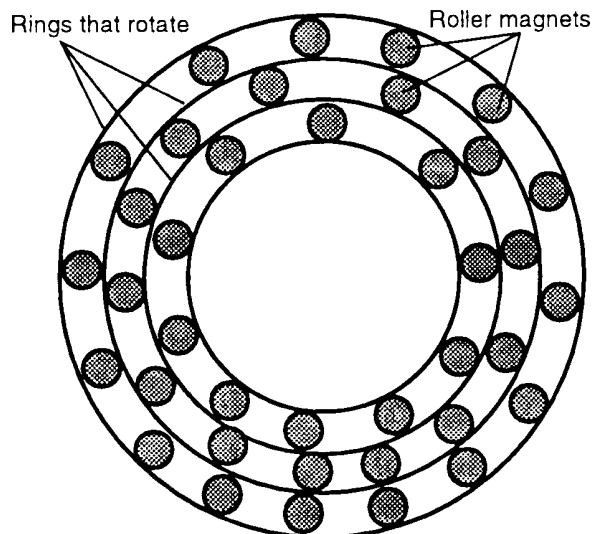


Fig. 2 Roller-ring assembly for Searle Disk

One of the exciting things about working on understanding the mechanics of magnetism and static electricity is the possibility of useful inventions.

A device that would "drill a hole" in the aether would have the affect of making an empty place that an object could move into with a small force, bypassing Newton's 3rd law of motion.

If the "drilled hole" was vertical, then the appearance of anti-gravity would be displayed. While the effect would be an upward thrust, the appearance would look like anti-gravity. Just like airplanes don't need the function of "anti-gravity," space ships don't, technically speaking, need "anti-gravity" either.

Since a single magnet shows no signs of doing anything useful in this manner, how about a ring of magnets in a circle, rotating in the same direction as the vortex spins. This makes a two-stage vortex. That may not be enough.

There have been isolated hints of this effect for several years. But no one connected dots.

I received issues of *Electric Spacecraft Journal* and *Extraordinary Science* magazines in the spring of 1995. They have similar write-ups describing John Searl's levity disk. Searl describes his disk as containing

²Readers are reminded of the **Aspden Effect** (rotational inertia), *New Energy News*, Feb. 1995, p 1.

concentric rings with magnetic "rollers" circling them (the action seems to be magnets moving around the circumference of the rings, "rolling" or rotating as they move) [6]. This would make a three-stage vortex and that would make some drill, which might even provide a rationale for the reports of UFOs making high speed 90 degrees turns. UFOs can't be believed now, as there is no scientific theory that allows such behavior.

In my studies of magnetism, I noticed static electrical effects are in exact parallel to the magnetic effects.

Table #1 [7] summarizes all we know about "action at a distance," for magnetic and static electrical effects, and points out the holes in our current information.

When the problem of getting magnetic devices to produce non-symmetrical flows is resolved, then we can substitute the less powerful (but cheaper to run) static devices that do the same thing.

Table 1. Magnetic / static comparison table

| Function | Electron/Proton | Molecular |
|---|--|---|
| Force or action | Electrostatic Negative / Positive | Magnetic North / South Poles |
| Primary effect | Like charges repel, opposite charges attract | Like poles repel, opposite poles attract |
| Range, practical maximum | Inverse square law, a few centimeters | Inverse square law, a few meters |
| Secondary effect | Moving / changing static field causes static fluid flow | Moving / changing magnet field causes electric current |
| Reciprocal effect | Moving static fluid flow causes static field | Moving electric current causes magnetic field |
| Link between 2nd effect and reciprocal | Moving static fluid "Static Current" | Moving electrons - electric current |
| Preferred path | Non-conductors | Conductors, Ferrites |
| Causative Agent | Static Field, Atom / electron size mini-tube of power | Magnetic Field, Molecular size "tube of power" |
| Mode | Surface effect, seems to result from mobile electrons | Bulk effect, seems to require iron size molecules |
| Examples | Amber, spider web, hair, scotch tape | Lodestone, permanent magnet |

Interestingly, the problem of a stand-alone power supply is being answered. The alternative energy literature has been having a hay day reporting new, non-traditional, advances in the generation of power. Some of these reports have devices that are described as "over-unity," meaning once you get the process started, the power out is greater than the power in.

Hal Fox, editor of *New Energy News*, reports on five of the most important news items for the first half of 1996:

- (1) The Patterson Power Cell™ recently produced thermal power over 16 times greater than input electrical power.

- (2) Experiments by Kenneth Shoulders demonstrate high-density electron clusters can amplify input electrical power by ten times (or more) in the production of output electrical power.
- (3) The stabilization of water-soluble radioactive metallic compounds is accomplished by low-temperature nuclear reactors achieved by a specially-designed electrically-powered reactor.
- (4) The use of a super magnet in both the rotor and stator of the Takahashi motor has provided mechanical and electrical energy with over 300% efficiency.
- (5) The Aspden Effect shows that a magnetic rotor retains rotational inertia for many seconds [8].

The March/April issue of *Infinite Energy* (vol 2, no 7, 1996) has a lead article about Dr. Paulo Correa and his patented plasma generator for commercial-grade electricity, the (Pulsed Abnormal Glow Discharge) PAGD Reactor [9].

While power sources available today (fuel cells, rockets, fission reactors) are rather inefficient, the possibility of new sources appear to be showing up at the right time in history to power our new space drive.

Dr. Robert Forward describes for us the linear thinking that has been circulating in the space community for the last 20 years in the lead article of the Interstellar Propulsion Society's October 1995 newsletter [10]. He lists the "just beyond our reach" devices that have made enough sense that people have looked closely at them. He lists:

1. Nuclear Electric Rocket, studied by Jet Propulsion Laboratory
2. Nuclear Pulse Rocket, Proposed by Stanislaw Ulam at the Los Alamos Laboratory
3. Antimatter Rockets
4. Rocketless Rocketry
5. Interstellar Ramjet, invented by Robert Bussard
6. Beamed Power Spaceships
7. Microwave-Pushed Starships, invented by Robert Forward
8. Laser-Pushed Starships, designed by Jet Propulsion Labs. and the World Space Federation of the USA.

I liked all of these suggested devices when I read about them, starting back in the 1960's. But they all have attributes of being engineering intense and needing increasingly more expensive infrastructure. Worse, they all assume we have an "off earth" presence available, a place to assemble the ship.

So, the new promise of small, modular, power sources of the 1990's and the new avenue of search for an "action" engine lightens my spirits and leads the way for the sixth segment in our soap opera to unfold in a fun, exciting and successful manner.

REFERENCES

1. Marc G. Millis, Interstellar Propulsion Society Home Page, www.tyrian.com/IPS/ (1996).
2. ---, Interstellar Propulsion Society Home Page, Mission Statement, www.tyrian.com/IPS/ (1996).
3. Steven Rado, "Aethro-Kinematics", Laser Disk, Lib. Cong. Cat. #Txu628-060, pp 257-258 (1996).
4. Steven Rado, "Aethro-Kinematics", Laser Disk, Lib. Cong. Cat. #Txu628-060, p 261 (1996).
5. Norman Silliman, "Physicist's Dilemma: Action at a Distance," Proc. of the International Symp. on New Energy, pp 609-620 (1994).
6. Modified from Charles A. Yost, "A Talk with John Searl," *Electric Spacecraft Journal*, issue 12, Oct/Nov/Dec, p 8 (1994).
7. Norman Silliman, "Physicist's Dilemma: Action at a Distance," Proc. of the International Symp. on New Energy, p 617, 618 (1994).

8. Hal Fox, "Five New Discoveries Best Explained by an Energetic Aether," Presented at the Southwestern and Rocky Mountain division of the American Association for the Advancement of Sciences, June 1996.
9. Dr. Paulo and Alexandra Correa, "New Energy Electric Power - Now," *Infinite Energy*, March/April issue, vol 2, no 7, pp 18-21 (1996).
10. Dr. Robert Forward, "Going to the Stars...," Newsletter of *The Interstellar Propulsion Society*, vol 1, no 2, Oct. 1995.

LETTERS TO THE EDITOR

From Wingate A. Lambertson, Ph.D.,
Fall 1996

UNEMPLOYMENT GIVES ONE TIME TO THINK

A report on the Seventh Annual Energy Efficiency Forum was given by Hal Fox in the July 1996 issue of *New Energy News*, vol 4, no 3, pp 5-7. The forum addressed three topics: "What Policies Should the Federal Government Pursue in Changing Energy Markets," "Global Energy Efficiency, Who Will Pay for It?" and "Impacts of Deregulation on Efficiency in a Changing Electric Industry." Hal concluded that there was "an almost complete lack of information about the most dramatic energy changes in the history of the world," and "None of the presenters made any reference to cold fusion, solid-state energy devices, or super motors."

Many of the investor-owned public utilities around the world belong to the Edison Electric Institute which conducts an annual conference for their top executives. The 1996 conference was held in Dallas, Texas, with Colin Powell as its keynote speaker. There was no mention in the entire program of any alternative energy activity.

Both of the above meetings were directed towards the top management of the energy industry and it is assumed that they were attended primarily by the second echelons of management, vice presidents, and executive vice presidents. These executives could not possibly return to their presidents and recommend that they get involved in a alternative energy effort. The conference program directors either did not know about the new energy field or deliberately left it off the program. The purpose of this paper is to explore what this lack of information can mean to these corporate presidents and vice presidents within the next five years. New energy technology is going to take-off within five years and it is not going to take a generation to develop.

Subsidy of hydroelectric power is going to be terminated and the public electric utility companies will be divided into their three functions of generation, transmission and delivery of electric power. This change is now taking place and is where executive attention is being focused.

About 10 years ago I met with the research director of a large investor-owned public utility and talked with him about my work on zero-point energy conversion. He made the observation that no matter what new energy source developed, they would still have to transmit and deliver that energy. He could give up generation and still keep his job. He just did not understand – generation, transmission and delivery are all going to be replaced. They will be replaced by a home or factory energy collector which sits beside the home or in the attic the same as the air conditioner. After an energy unit is installed, the supplier can expect to make only one call a year to service that unit.

Picture yourself as president of a large investor-owned public utility. Over the past five years you have borrowed one to five billion dollars for new peaking units and scrubbers. Suddenly and without warning, you find that you are having trouble servicing those bonds because small, free energy units have taken most of your high-rate paying loads. How long do you think you will hold your job when your board members ask you why you did not invest in new energy technology early, when inventions were cheap? Your first step may be to call in your vice presidents who attended these conventions and forums and ask them why they did not keep you informed. Your second step will probably be to fire them before you get fired.

The transportation energy industry is changing as oil companies go into mini-markets and the fast food business. Imagine yourself as president of a large oil company. Over the past five years you have been spending \$81 billion a year in exploration for new oil reserves. Suddenly, the total fuel market begins dropping with the greatest drop occurring in your most profitable markets. You set up an executive committee or hire a consulting organization to study the problem and recommend solutions. They come back with the report that people are installing new energy power supplies in their vehicles and that they are either filling their tanks with water at home or they are just having a few 12 volt batteries replaced every three years. In another 10 years your energy market is going to disappear.

The board of directors call you on the carpet and ask you WHY you have been spending \$1 billion a year for a raw material which has no market? After you call your vice presidents in for an accounting, you fire them all and hope in so doing, to hang on until retirement. Keep in mind that this accounting requirement is coming and is only five years away.

The good news is that you will have lots of time to think about what you wish you had done after you lose your job.

If I were the director of any of these high level energy forums and conventions and valued my job, I would make sure that an overview of the new energy technology activities would be featured next year.

Editor's Note: In a recent discussion with a member of the board of directors of an electric utility company, he said, "They do not believe that there are any new energy technologies that will impact their business **before they retire.**"

From Ernest Criddle, Canada
January 1997

I understand that the *Journal of New Energy*, vol 1, no 1 is out of print. Please use the remainder of my subscription to *Fusion Facts* to advance the reprint date of this issue. An earlier date for reprinting will be a sufficient reward.

Since I now possess the entire set of *Fusion Facts*, let me nominate Hal Fox and his Fusion Information Center as a pivotal force in "Cold Fusion." Your consistent and dedicated efforts have provided a focus for discussion and a landmark example of positive thinking to this community. Thank you all for enriching the effectiveness of efforts in this field.

FUSIONfacts

FORMERLY A MONTHLY NEWSLETTER FROM JULY 1989 TO DECEMBER 1996

WE DIDN'T DIE, WE JUST CHANGED OUR LOCATION

FUSION FACTS to continue reporting on papers published in other venues

HYDROGEN EVOLUTION REACTION

R. Notoya (Hokkaido University, Catalysis Research Center, Sapporo, Japan), "Cold Fusion Arising from Hydrogen Evolution Reaction on Active Metals in Alkali Metallic Ionic Solutions," *Environmental Research Forum*, vols 1-2 (1996), pp 127-140, 13 refs, 7 figs, 2 tables.

AUTHOR'S ABSTRACT

It was experimentally confirmed that the hydrogen evolution reaction on porous nickel and platinized platinum in 0.5 mol/l potassium and sodium carbonate solutions and 0.1 mol/l cesium sulfate solution was causative of some nuclear reactions. These solutions of light and heavy water in the thermally open cells were electrolyzed for a given period galvanostatically. Analysis of the electrolytes by use of ICP-MS, a flame photo-spectrometer, liquid scintillation spectrometer, and a germanium γ -ray spectrometer, revealed that the some products of nuclear changes were generated during electrolysis. For example, from potassium and proton to calcium, from cesium-133 and neutron, proton and so forth, to some species of mass numbers of 132 to 140 amu, from sodium-23 and neutron to sodium-24, as well as tritium, which were accompanied by an extraordinarily large heat evolution. The reaction mechanism for the cold fusion caused by electrolysis was proposed, in which the intermetallic compounds between alkali metals and cathode materials played an important role, on the basis of the mechanism for the hydrogen evolution reaction in alkaline solutions on active metals.

TRANSMUTATION PRODUCTS IN MICROSPHERES

G.H. Miley, G. Name, M.J. Williams (Fusion Studies Lab., U. of IL), J.A. Patterson, J. Nix, D. Cravens (Clean Energy Technol. Inc., Dallas, TX), and H. Hora (Univ. of New South Wales, Australia), "Quantitative Observation of Transmutation Products Occurring in Thin-Film Coated

Microspheres during Electrolysis," pre-print from ICCF-6 Proceedings. Also *Cold Fusion*, issue 20, Dec. 1996, pp 71-84, 14 refs, 5 figs, 3 tables.

AUTHOR'S ABSTRACT

Several research groups previously identified new elements in electrodes that appeared to be transmutation products (Bockris et al., 1996a; 1996b). However, due to the low concentrations involved, the distinction from possible impurities has been difficult. Now, by using a unique thin-film electrode configuration to isolate the transmutation region, plus measurements based on neutron activation analysis, the authors have achieved, for the first time, a quantitative measure of the yield of transmutation products. Results from a thin-film (500-3000Å) nickel coating on 1-mm microspheres in a packed-bed type cell with 1-molar LiSO₄-H₂O electrolyte were reported recently at the Second International Conference on Low-Energy Nuclear Reactions (Miley and Patterson, 1996). Key new results are now presented for thin-film Pd and for multiple Pd/Ni layers. The transmutation products in all cases characteristically divide into four major groups with atomic number $Z \approx$ 6-18; 22-35; 44-54; 75-85. Yields of ~1 mg of key elements were obtained in a cell containing ~1000 microspheres (~1/2 cc). In several cases over 40 atom % of the metal film consisted of these products after two weeks operation.

CONCLUSION

The use of thin-film electrodes has been shown to provide a unique and important method to study nuclear transmutations in electrolytic cells. By localizing the reaction, these films, combined with NAA and SIMS analyses, allow for the first time quantitative measurements of yields. As demonstrated by duplicate nickel-film runs, good reproducibility appears possible. However, as the authors stressed earlier (M-P 96), others are invited (and strongly encouraged) to investigate this new technique to provide full proof of reproducibility.

The most striking and unexpected result is the characteristic four-peak yield curve that appeared in all runs, but with various differences in numbers of products in various regions around the peaks. This curve, containing high-Z materials in the higher peaks, inescapably implies that multi-body reactions must occur. Since there is still debate about how deuteron ions can overcome the Coulombic barrier in "conventional" experiments, the implication that multi-body high-Z reactions occur greatly stretches the understanding of this phenomena. Various collective effects appear to be involved, although the initiation could still proceed via swimming electron layer screening at interfaces. Theoretical studies are urgently needed to shed light on this amazing phenomenon, assuming that experimental reproducibility is confirmed by others.

BIPHASIC NATURE OF HEAT GENERATION

Mitchell R. Swartz (JET Energy Technology, Inc., Wellesley Hills, MA), "**Consistency of the Biphasic Nature of Excess Enthalpy in Solid-State Anomalous Phenomena with the Quasi-One-Dimensional Model of Isotope Loading into a Material,**" *Fusion Technology*, vol 31, no 1, Jan 1997, pp 63-74, 36 refs, 6 figs.

AUTHOR'S ABSTRACT

Electrochemical experiments, using nickel cathodes in light water solutions, were used to examine the enthalpy generated by electrically driving each electrode pair compared with ohmic controls contained within the same solution. For nickel wire cathodes, the peak power amplification (π_{Ni}) was in the range of $1.44^{\pm 0.58}$. For spiral-wound nickel cathodes with platinum foil anodes, π_{Ni} was $2.27^{\pm 1.02}$. By contrast, neither iron nor aluminum cathodes demonstrated excess heat.

Driving these nickel samples beyond several volts, however, produced an exponential falloff of the power gain. This biphasic response to increasing input power may be consistent with the quasi-one-dimensional model of isotope loading and may contribute to the difficulty of reproducing these phenomena.

SUMMARY AND CONCLUSION

This paper reports comparison tests of nickel versus aluminum and iron cathodes with platinum used as the anode in light water (H_2O) solutions. Several sources of erroneous false positive excess heat, which can occur under uncontrolled conditions, including nickel colloid generation, recombination, and analytic errors, have been ruled out. When careful observation is made of some samples of nickel under controlled low-to-moderate current density cathodic conditions, excess heat is observed. When nickel wire was used as the cathode, there was power amplification in the range of $1.44^{\pm 0.58}$.

When cold worked nickel spiral cathodes with platinum foil anodes were used, the power amplification was in the range of $2.27^{\pm 1.02}$. Neither iron nor aluminum demonstrated excess heat.

A notch or plateau is observed in the curve of power gain versus power input and is important because it may account for some of the wide-spread difficulties in observing the phenomena. The exponential falloff of the output with increasing electric potential may be consistent with the Q1D model of isotope loading. Although the Q1D model of isotope loading does not explain exactly the nature of these reactions, it – and the observed π -notch – begin to explain when these reactions will not occur.

LETTERS TO THE EDITOR

of *FUSION TECHNOLOGY*, vol 31, no 1, Jan. '97.

Alexandre E. Pozwolski (Education Nationale, Paris, France), "Comments on Composite Electrolytes and Cold Fusion," pg 120, 4 refs, 1 fig.

A.V. Nedospasov (Scientific Assoc. "IVTAN", Moscow, Russia), E.V. Mudretskaya (Scientific Prod. Ctr. 'Elé', Moscow, Russia), "Comments on the Possible Nature of 'Cold Fusion' Phenomena," pg 121-122, 5 refs.

FROM *FUSION TECHNOLOGY*:

PREFACE TWELFTH TOPICAL MEETING ON THE TECHNOLOGY OF FUSION ENERGY

Carl D. Henning and John Perkins (Lawrence Livermore National Lab., Livermore, CA)

This Twelfth Topical Meeting on the Technology of Fusion Energy was held in Reno, Nevada, during the American Nuclear Society (ANS) national summer meeting. The meeting was sponsored by the Fusion Energy Division of ANS and cosponsored by the Atomic Energy Society of Japan, Fusion Engineering Division, and by the U.S. Department of Energy, Office of Research and Inertial Fusion. The fusion topical had **18 oral sessions** plus a large poster session and two town meetings. **About 265 abstracts were submitted for presentation**; this represented a substantial increase from the previous topical meeting in 1994, despite declining budgets in magnetic fusion in the United States.

Comments from George H. Miley, the Editor of *Fusion Technology*.

Fusion Technology (FT) traditionally publishes reviewed papers for the long-standing series of American Nuclear Society (ANS) topical meetings on the technology of fusion energy. Reviewed proceeding began with the Fifth Topical (Knoxville, Tennessee, April 1983), which was contained in *Nuclear Technology/Fusion*, Vol. 4, No. 2, Parts 2 and 3 (1983). *Nuclear Technology/Fusion* became *FT* in 1984, and the first topical to be covered by *FT* was the Sixth Topical (San Francisco, CA, March 1985). [And has continued ever since. – Ed]

From the Proceeding of the Twelfth Topical Meeting on the Technology of Fusion Energy, Reno, NV. June 16-20, 1996:

LIST OF THE SESSION TITLES

PART 2A

National Ignition Facility
 Inertial Fusion Drivers and Targets
 International Thermonuclear Experimental Reactor
 Recent Results from Inertial and Magnetic Confinement Experiments
 Divertor Design and Experiments
 Plasma-Facing Components: Analysis and Technology
 Plasma Fueling and Heating, Control and Current Drive
 Fuel Cycle and Tritium Technology
 Fusion Materials
 Fusion Blanket and Shield Technology

PART 2B

Neutronics Experiments and Analyses
 Neutron Sources for Fusion Technology Testing
 Status of Fusion Nuclear Data
 Fusion Magnet Systems
 Steady-State and Long-Pulse Machine Studies
 Power Plane Design and Technology
 Innovative Approaches to Fusion Energy
 Safety and Environment
 Fusion Power Plants and Economics
 Nonelectric Applications of Fusion

**ABSTRACTS FROM THE CONFERENCE,
 PAPERS PUBLISHED IN *FUSION TECHNOLOGY*
 Vol 30, No 3, Parts 2A -2B.**

R. Aymar (ITER San Diego Joint Worksite), "**The International Thermonuclear Experimental Reactor,**" pp 397–403.

AUTHOR'S ABSTRACT

The International Thermonuclear Experimental Reactor (ITER) is a joint project of the European Union, Japan, the Russian Federation and the United States with the objective to design, construct and operate a tokamak burning plasma experiment. The present phase of the project, the six year Engineering Design Activity (EDA), is nearing completion of the fourth year. The major features of ITER are now well defined. The development of detailed engineering designs for the components, plans for the machine assembly, the support facilities, the site requirements construction plans, schedule and costs and a safety assessment are well along and will be completed by the end of the Engineering Design Activity in July, 1998, when construction can begin if the ITER partners approve the construction phase.

E.T. Chang and R.J. Cerbone (TSI Research, Inc., Solana Beach, CA), "**Prospect of Nuclear Waste Transmutation and Power Production in Fusion Reactors,**" pp 1654-1658.

AUTHORS' ABSTRACT

A small tokamak-based fusion reactor can be attractive for actinide waste transmutation. Equilibrium concentrations of transuranium isotopes were estimated in a molten-salt based fusion transmutation reactor. Nuclear performance parameters were derived for two types of fusion-driven transmutation reactors: Pu-assisted and minor actinides-only systems. The minor actinide-only burning system appears to be the ultimate fusion transmutation reactor. Because such a transmutation system can destroy the minor actinides generated in 35 LWRs, each of which produces the same thermal power as the transmutation reactor. However, a Pu-assisted transmutation reactor may achieve the same thermal power at a lower fusion power because of the higher energy multiplication in the blanket. It can therefore be developed as a shorter-term technology to demonstrate the viable long-term solution to nuclear waste.

[Reduces toxicity from millennia to only a few hundred years. --Ed]

David H. Candall (Dir. Office of Inertial Fusion and the NIF Defense Programs, DOE, Washington, DC), "**The Need for the National Ignition Facility,**" pp 391-396.

AUTHOR'S ABSTRACT

This paper has an attitude – that the National Ignition Facility (NIF) is needed. The NIF will be unique in its ability to address high energy density physics and to test fusion ignition in the laboratory. This is a major scientific step and has high appeal to scientists and engineers. The reason for taking this step now is the importance of high energy density physics for US policy on nuclear weapons. The fact that the same capability and experiments give the most fundamental information on the potential of inertial fusion for commercial energy, and have value for applications in astrophysics, further supports the case for proceeding with this facility.

G.L. Kulcinski (Fusion Technol. Inst., Univ. Wisconsin-Madison, WI), "**Near-Term Commercial Opportunities from Long Range Fusion Research,**" pp 411-421.

AUTHOR'S ABSTRACT

An alternate approach to the development of safe, clean, and economical fusion energy for the 21st Century is presented. Instead of continuing exclusively on the path of larger and more costly magnetic confinement fusion reactors based on the DT cycle, it is proposed that near term commercial opportunities using fusion plasmas be identified and pursued. Specific examples of such opportunities are given in the areas of the detection of explosives, the production of medical isotopes, and the destruction of long lived fission product isotopes. It is also suggested that a more profitable path to the goal of fusion electricity might be to concentrate on small, simple devices that eventually can burn the more advanced fusion fuels that emits few if any neutrons. Such devices could gain back the public confidence and counter the "fusion is always 50 years away" syndrome.

Mitsuru Ohta (Naka Fusion Research Est., Japan Atomic Energy Research Inst., Japan), "**Status of Japanese Fusion Technology,**" pp 404-410.

AUTHOR'S ABSTRACT

The Japanese fusion program is based on the 3rd phase basic program of fusion research and development enacted in June 1992. The main objectives of the program are to achieve the self-ignition condition and to produce a long-burning plasma by constructing a fusion experimental reactor, which corresponds to ITER at present. In addition, the program aims at developing the basic fusion technology needed for constructing the prototype fusion reactor. Much effort is devoted to the ITER project to achieve the above-mentioned objectives.

Most of the technologies needed for constructing a fusion reactor will be developed during the engineering design

activity, the construction, operation and shutdown of ITER. Fusion material usable under 100dpa, some safety issues, cost-saving technology and some other technologies will remain to be solved.

Next-step fusion research should be directed to the study of how a commercial fusion reactor could become less expensive and environmentally safer, on the basis of plasma physics and technology established in the ITER project.

From COLD FUSION Magazine

Issue 20, December 1996

Papers published this issue:

Mark Goldes (Magnetic Power Inc., Sebastopol, CA), "A Creative Solution to the Heat-to-Electric Dilemma," p 4.

Hideo Kozima (Dept. Phys., Fac. Sci., Shizuoka Univ., Japan), "The 3rd Symposium (1996) - Basic Research Group of the Japanese NHE Project," a brief report, pp 37 - 41.

Chuck Bennett (Sacramento, CA), "Nuclear Shear," pp 42-43.

Chuck Bennett (Sacramento, CA), "A Quantized Aether," pg 44.

Hideo Kozima (Dept. Phys., Fac. Sci., Shizuoka Univ., Japan), "ICCF6 Report," pp 48-52.

Richard T. Murray (Room For All, Santa Fe, NM), "A Critique of George Miley's Recent Preprints," pp 59-70.

ABSTRACTS from this issue of Cold Fusion

Hideo Kozima (Dept. Phys., Fac. of Sci., Shizuoka Univ., Japan), "**On the Existence of Trapped Thermal Neutrons in Cold Fusion Materials,**" p 5-11, 48 refs, 1 table.

AUTHOR'S ABSTRACT

The stable existence of the thermal neutron assumed in the TNCF model has been discussed in this paper on the basis of the interaction of the neutron and the nuclei on the lattice points in crystal. If an optimum shape of a boundary is formed stochastically, neutrons could be trapped in a crystal region surrounded by the boundary. The trapped neutron can form the neutron Cooper pair lowering its energy interacting each other through the phonon. The stabilized neutron, then, will not decay spontaneously and also not be

captured by one of the lattice nuclei. To specify the stability of a neutron in a crystal, a new concept "neutron affinity of a nucleus" was introduced. Trapped neutron destabilized by a large perturbation can induce a trigger and succeeding breeding reactions resulting in the cold fusion phenomenon.

Hideo Kozima, Masahiro Nomura, Katsuhiko Hiroe and Masayuki Ohta (Dept. of Phys., Fac. of Sci., Shizuoka Univ., Japan), "**Nuclear Transmutation in Cold Fusion**," pp 16-20, 8 refs, 1 fig.

AUTHORS' ABSTRACT

Nuclear transmutation in chemical and biological systems is investigated with use of Trapped Neutron Catalyzed Fusion Model (TNCF Model). In the TNCF model, it is possible to analyze experimental data consistently and quantitatively. We present the investigation of experimental results in cold fusion systems with various materials and methods in this paper.

Hideo Kozima, Masayuki Ohta, Masahiro Nomura, Katsuhiko Hiroe (Dept. of Phys., Fac. of Sci., Shizuoka Univ., Japan), "**Analysis of Nickel-Hydrogen Isotope System Using the TNCF Model**," pp 21-25, 13 refs.

AUTHORS' ABSTRACT

Experimental results obtained in the Ni-H and Pd-H systems generating the excess heat and/or with transmuted nuclei (NT) were investigated on the Trapped Neutron Catalyzed Fusion (TNCF) model proposed by one of the authors (H.K).

Experimental results, which are not able to be explained by d-d or p-p reaction, are explained by n-p or n-⁶Li and the following breeding reactions on TNCF model, assuming the existence of the trapped thermal neutron. The trapped neutron works also as a key particle to transmute elements in the system. The same as the excess heat, it is difficult to understand the NT without thermal neutrons.

Using the TNCF model, the excellent experiment data showing excess heat and NT in the Ni-H and Pd-H systems are explained consistently and quantitatively.

Masayuki Ohta, Masahiro Nomura, Katsuhiko Hiroe, Hideo Kozima (Phys. Dept., Sci. Fac., Shizuoka Univ., Japan), "**Cold Fusion in an Ni-H System (II)**," pp 25-27, 8 refs.

AUTHORS' ABSTRACT

The excess heat production in the Ni-H system of gas phase was investigated again. In a previous paper, a qualitative explanation of the experiment was reported. A quantitative analysis of excess heat production in Ni-H system is given in this paper.

There is a coincidence in the order of magnitude with another experiment in a Ni-H system. The successful analysis using the TNCF model shows the reality of trapped thermal neutrons in a crystal lattice.

Hideo Kozima (Dept. of Phys., Fac. of Sci., Shizuoka Univ., Japan), "**Tritium Generation in Mo/D Cathode in Glow Discharge with D₂ Gas**," pp 28-31, 12 refs.

AUTHOR'S ABSTRACT

The trapped neutron catalyzed model for cold fusion (TNCF model) was used to analyze experimental data showing tritium generation in a glow discharge system with Mo cathode and D₂ gas. The density of the trapped thermal n_n in the Mo cathode was determined from the production rate of tritium of 10¹⁵ s⁻¹ observed in the gas where deuteron density was 10²⁰ cm⁻³ and a path length of tritium in the cathode was assumed as 10⁻² cm:

$$n_n = 10^7 \text{ cm}^{-3}.$$

Hideo Kozima (Dept. of Phys., Fac. of Sci., Shizuoka Univ., Japan), "**Cold Fusion Phenomenon Explained by using the TNCF Model**," pp 31-36, 29 refs.

AUTHOR'S ABSTRACT

A model based on the stable existence of thermal neutrons in crystals was used to analyze experimental data obtained in electrolytic cold fusion experiments in these seven years. The density of the trapped thermal neutrons n_n in samples was determined by using the experimental results of excess heat helium 4 (⁴He), tritium, neutrons and/or nuclear transmutation (TN). The values of the density n_n determined by the experimental data were 10⁵ ~ 10¹⁵ cm⁻³. Other quantities we could determine from experimental data were the ratio of events generating tritium and neutrons t/n and the ratio of events generating the excess heat and tritium (and ⁴He) N_Q/N_t which had been controversial quantities to reconcile with the existing common sense of physics. The values determined on our model were t/n ~ 10⁵ and N_Q/N_t ~ 10, substantially consistent with experimental data to one order of magnitude.

Hideo Kozima, Masahiro Nomura, Katsuhiko Hiroe and Masayuki Ohta (Dept. of Phys., Fac. of Sci., Shizuoka Univ., Japan), "**Consistent Explanation of Experimental Data Obtained from SRI International and EPRI**," pp 45-48, 8 refs.

AUTHORS' ABSTRACTS

Experimental data on the isotope ratio changes (^{10}B and Pd) in a PdD_x/Li cathode which produced the excess heat were analyzed on the TNCF model. A quantitative changes of the isotope ^{10}B and the amount of the excess heat generated in the cathode were consistently explained using a single adjustable parameter n_n , density of the trapped thermal neutron, the value of which was determined as $\sim 10^9 \text{ cm}^{-3}$ when the experimental time was assumed to be a week ($6 \times 10^5 \text{ s}$).

Evan L. Ragland (The Boiler Works, Diamondhead, MS), "**Triode Cell Experiments for Controlled Fleischmann-Pons Effect**," pp 53-58, 7 refs, 6 figs. Also in *Infinite Energy*, vol 2, no 10, Sept./Oct. 1996, pp 22-24, 7 refs, 6 figs.

AUTHOR'S ABSTRACT

Experimental research and evaluation of three electrode (triode) cold fusion electrolysis cells is reported herein. Apparatus development began, after patent application, 05 June 1995. The triode apparatus introduces controlled loading and operation of Fleischmann/Pons-type (F/P) cells. In August 1995, excess heat generation was observed in

initial triode apparatus experiments conducted by Dr. Dennis Cravens in his New Mexico laboratory. In November 1995, the Boiler Works laboratory in Diamondhead began experimental evaluation of the triode apparatus. A series of experiments in December, January and February led to development of a functioning triode fusion reactor. The reactor was put into operation 20 March 1996 and operated continuously until 23 August 1996. Over the five months of operation of the reactor, several experiments were performed and over 65,000 data points were recorded. This data base is being applied in further triode apparatus developments.

A second reactor test bed for "quick change" cathode specimen evaluation is in operation. Thin film cathode specimens prepared by the Materials Science and Engineering Lab. of the Univ. of Alabama in Birmingham are presently being evaluated. These include Pd film on Ag, Al, Cu, and quartz substrates and Pt films on Si bead specimens. Engineering design of a 2 KW reactor cell is underway.

Details of triode apparatus operation, control, and experimental results are reported. The general design approach to the 2KW reactor is described. It is concluded that sufficient experimental and theoretical understanding of cold fusion exists for engineering design and development of water heating appliances.

ERRATA

Journal of New Energy, volume 1, number 4

Due to some software problems, some of our superscripts (- or +) printed out wrong in this issue. Others are typographical errors. Please change the following:

p. 7, Eq. 9, change end of eq. to read: $\ln \Lambda T_e^{-3/2} (eV) \text{sec}^{-1}$ (superscript reads: - 3/2)

p. 14 , next to last line on page, the correction should be: J_z instead of J_θ , i.e.,

induces an axial self-magnetic field $B_z(r)$ and the axial current $J_z(r) = neu_z(r) e_z$ generally induces azimuthal

p. 15, Eq. 58 should end with the corrected phrase $\left(1 - \frac{u_z^2(r)}{c^2}\right) r dr$, adding the subscript u_z^2 .

p. 16, the paragraph below Eq. 61 should read: (most changes are superscript errors)

where ω_{re}^+ (ω_{re}) corresponds to a fast (slow) rotation of the electron fluid. In the uniform density profile the rotational velocity ω_{re}^+ or ω_{re}^- are constant, i.e. the electron fluid will make a rigid rotation around the symmetric axis. Using Eq. (54) we have $\omega_{ce} = eB_0/m_e = 7.4 \times 10^{16}$ rad/sec. Substituting the ω_{ce} and Eq. (4) for ω_{pe} to the Eq. (61) gives $2\omega_{pe}^2/\omega_{ce}^2 = 0.77$, $\omega_{re}^+ = 0.74 \omega_{ce} = 5.5 \times 10^{16}$ rad/sec and $\omega_{re}^- = 0.26 \omega_{ce} = 1.9 \times 10^{16}$ rad/sec. (With relativistic treatment, we will have $\omega_{re}^\pm \sim 10^{13}$ rad/sec.) These are super high speed rotations.

p. 16, Eqs. 63 a + b should be corrected to end in "meter/sec²"

p. 17, Eq. 64, center section should read: $\left[1 - (1 \text{ replace "plus" sign with "minus" sign})\right]$

p. 18, two superscript changes in next to last line, above the equation: <frequencies ω_{re}^+ and ω_{re}^- defined>

p. 19, the copy below Eq. 69 should read: (all changes are superscript errors)

where $T = L/v_z$ is the length of time that the electron is in the interaction region; k_z is the wave number and Ω^\pm is defined by

$$\Omega^\pm \equiv \omega - k_z v_z - \omega_{re}^\pm. \tag{70}$$

We see that the electron cyclotron emission spectrum $\eta(\omega)$ has two maxima located at $\Omega^+ = 0$ and $\Omega^- = 0$, or equivalently

$$\omega - k_z v_z \approx \omega_{re}^\pm = \frac{1}{2} \omega_{ce} \left[1 \pm \left(1 - \frac{2\omega_{pe}^2}{\omega_{ce}^2}\right)^{1/2} \right]. \tag{71}$$

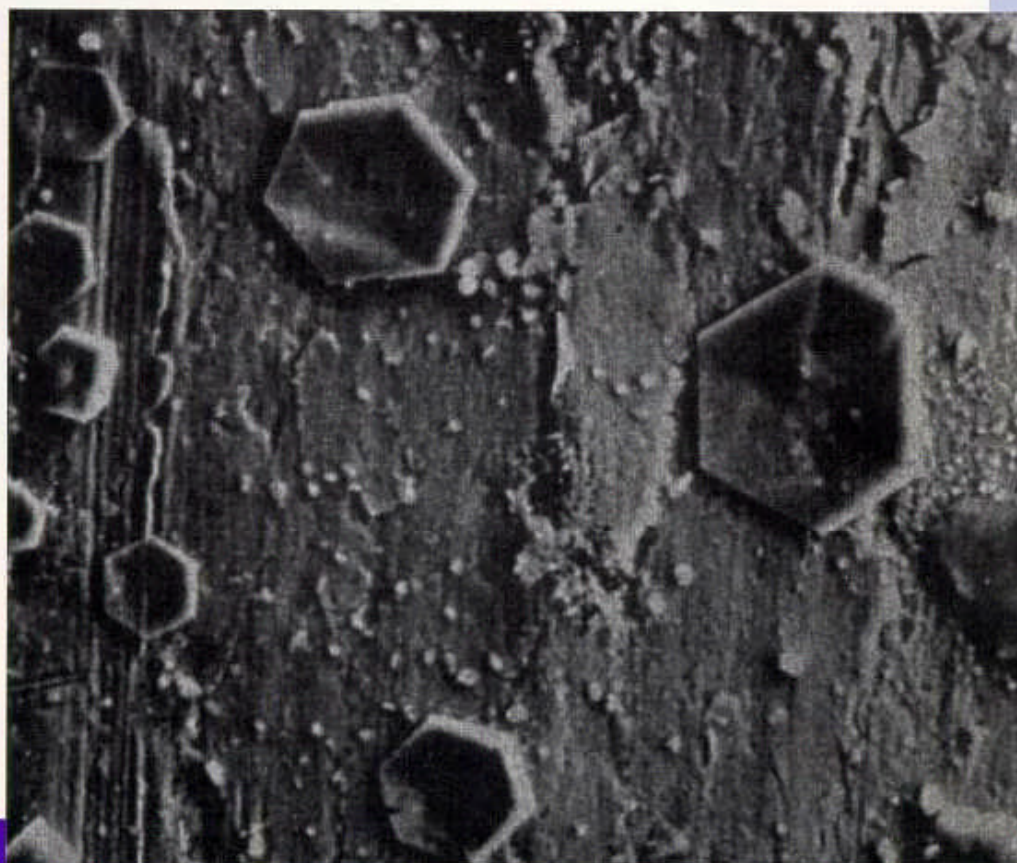
For $2\omega_{pe}^2/\omega_{ce}^2 \rightarrow 0$, the Eq. (71) gives $\omega_{re}^+ \rightarrow \omega_{ce}$ and $\omega_{re}^- \rightarrow 0$. As the $2\omega_{pe}^2/\omega_{ce}^2$ increase, ω_{re}^+ shifts downward and ω_{re}^- shifts upward. Therefore, from measuring the cyclotron emission from the EV, we may determine the parameter $2\omega_{pe}^2/\omega_{ce}^2$ or n/B_0^2 . If we know n (or B_0), then we can determine the value of B_0 (or n) for the EV.

p. 21, Eq. 3, = changes to +, i.e., $n + \frac{A+1}{Z} M = \frac{A+2}{Z} M$

JOURNAL OF NEW ENERGY

An International Journal of New Energy Systems

Vol. 1, No. 4, 1996



Matsumoto - SEM view of hexagonal decay products on Fe cathode.



Winter 1996

ISSN 1086-8259



JOURNAL OF NEW ENERGY

An International Journal of New Energy Systems

Instructions to Authors:

The Journal of New Energy is published quarterly by Fusion Information Center, Inc., with offices at the University of Utah Research Park, Salt Lake City, Utah.

ISSN: 1086-8259

Mailing address:

Journal of New Energy

P.O. Box 58639

Salt Lake City, Utah 84158-0639

(801) 583-6232 FAX: (801) 583-2963

JNE Staff:

Hal Fox, Editor

Dineh Torres, Publications Dir., Graphics

Robyn Harris, Circulation Mgr.

Editorial Advisory Board

Petar K. Anastasovski

Robert W. Bass

John O'M. Bockris

Robert T. Bush

Peter Glück

Shang-Xian Jin

Carlos Sanchez

Mahadeva Srinivasan

Mitchell R. Swartz

Professional papers on cold fusion and other enhanced energy systems are solicited from scientists, engineers, inventors, and students. Papers from recognized professionals may be published immediately with an accompanying invitation for peer-review comments. Other papers will be submitted for peer review. Names and addresses of any reviewers will be sent to authors with reviewers' comments.

The Journal of New Energy (JNE) is devoted to publishing professional papers with experimental results that may not conform to the currently-accepted scientific models. The topics to be covered in this journal include cold nuclear fusion, low-energy nuclear reactions, high-density charge cluster technology (including some plasma circuits where enhanced energy is produced), high-efficiency motors or generators, solid-state circuits that appear to provide anomalous amounts of output energy, and other new energy devices. Papers with experimental data are preferred over theoretical papers. Standard alternative energy topics such as hydrogen fuel, wind power, solar power, tidal power, and geothermal power are not solicited.

Authors should submit abstracts. If the abstracts are favorably considered for publication, the author will be sent an author's kit of instructions for the preparation of the paper. The editor and the editorial advisory board are responsible for making publication decisions.

Authors or their employers will be invoiced for production costs sufficient to cover the cost of publication in excess of subscription funds received. The JNE will try to match donors with authors from developing countries so that all acceptable manuscripts can be published. Donors are requested to contact the JNE and they will be specially honored in the Journal.

© Fusion Information Center, Inc. Copying not allowed without written permission. All rights reserved.

Printed in the U.S.A

Editor Hal Fox is the leading founder of the Fusion Information Center which publishes both *Fusion Facts*, a monthly technical newsletter designed to keep subscribers informed of the latest developments in cold fusion and energy research, and *New Energy News*, a monthly newsletter covering all areas of new energy research for members of the Institute for New Energy and other worldwide subscribers.

Infinite Energy

Cold Fusion and New Energy Technology

INFINITE ENERGY is an international technical magazine with outreach to the general public as well. It is written at the technical level of *Scientific American* or *Science News*. To maintain the highest editorial standards, it is written and edited by scientists, engineers, and expert journalists. It is aimed at pioneering scientists, engineers, industrialists, and investors who are entering an exciting new R&D area. This technology continues to grow explosively, with significant involvement by corporations and institutions in the U.S., Japan, France, Italy, India, Russia, and China. New technology developments and scientific discoveries are being made monthly and reported in the peer-reviewed, scientific literature. **INFINITE ENERGY** reports on the latest information that is now pouring in from research centers and correspondents around the globe.

The **highly affordable** subscription price of this six-issues per year publication of general *and* technical interest is \$29.95 for residents of the U.S. and Canada. (To cover first-class air mail for other countries, the annual foreign subscription price is \$49.95.)

To subscribe to **INFINITE ENERGY**, please send a check or money order, or Credit Card information to Cold Fusion Technology.

Name: _____
Address: _____
Address: _____
City: _____ State: _____ Postal Code/Zip: _____
Country: _____ Phone: _____ Fax: _____
If using Credit Card: Check one: Master Card _____ VISA _____ American Express _____
Card Number: _____ Expiration Date: _____
Signature: _____ **Optional:** E-Mail address: _____

**Cold Fusion Technology
P.O. Box 2816
Concord, NH 03302-2816
USA**

✓ **INVENTORS**

Are you looking for a proven team who will help protect and develop your cold fusion inventions?

✓ **MANUFACTURERS**

Do you need information on cold fusion inventions and processes that are available for commercialization?

Contact **ENECO**

We are an intellectual property clearinghouse serving the interests of both cold fusion inventors and commercial developers throughout the world. Our staff is actively perfecting U.S. and international patents in most areas of cold fusion and other new energy inventions, including the original, pioneering work of Pons and Fleischmann.

Call us to discuss our development and licensing programs: Phone: (801) 583-2000, or Fax: (801) 583-6245.

ENECO

391-B Chipeta Way
Salt Lake City, Utah 84108

FUSION INFORMATION CENTER

The *Fusion Information Center, Inc.* (FIC) is a Utah Corporation founded in April 1989, with the goal of being a part of the new and exciting technology of cold fusion. The current president, Hal Fox, was the director of the first research laboratory at the University of Utah Research Park, Salt Lake City, Utah.

FIC is best known for its publication of two newsletters: *Fusion Facts* (monthly since July 1989) and *New Energy News* (monthly since May 1993). In addition to its publishing activities, FIC has been helping many inventors, scientists and authors with information and in some cases with funding.

Projected programs will expand FIC's scope of publishing and the commercialization of a few selected new-energy research & development projects. We continue to review new research as it appears.

FIC has the world's most complete collection of cold fusion papers and one of the best collections of new-energy papers and publications. We welcome the visit of authors, inventors, and scientists to our office in the University of Utah Research Park.

In some cases, we can help you find funding for your projects. Please call on us if you are involved in the development of new energy devices or systems.

Fusion Information Center, Inc.
P.O. Box 58639, Salt Lake City, UT 84158-0639
(801) 583-6232 FAX: (801) 583-2963

INSTITUTE FOR NEW ENERGY

The **Institute for New Energy** is an international organization to promote new and renewable energy sources. Its monthly newsletter is *New Energy News*, reporting worldwide on all facets of new and enhanced energy.

The Institute for New Energy

P.O. Box 58639
Salt Lake City, UT 84158-0639
Phone: 801-583-6232
FAX: 801-583-2963
E-mail: inc@padrak.com
Web Site: www.padrak.com/ine/

New Energy News

New Energy News (NEN) is the monthly newsletter for the Institute for New Energy, containing 20 to 30 pages per issue. It is *FREE* with your membership.

Membership

- Membership to the INE is \$35.00 per year for individuals in the U.S.A.
- \$40.00 for Canada, and Mexico
- \$50.00 for all other countries, *and*
- \$60.00 per year for Corporations and Institutions

Call the INE for additional information at the above address, *or*
Contact the INE President: Dr. Patrick G. Bailey — inc@padrak.com